Optimum Design Parameters and Mechanical Properties of Polymeric Nanocomposites Using NSGA-II Optimization Method

M.S Rabothata

A dissertation submitted to the Faculty of Engineering and the Built Environment, University of the Witwatersrand, Johannesburg, in fulfilment of the requirements for the degree of Master of Science in Engineering.

Johannesburg, June 2018

Declaration

I declare that this dissertation is my own, unaided work, except where otherwise acknowledged. It is being submitted for the degree of Master of Science in Engineering in the University of the Witwatersrand, Johannesburg. It has not been submitted before for any degree or examination at any other university.

Signed this 27th day of June 2018

M.S Rabothata

To my parents Mr and Mrs, Masilo and Sewela Rabothata. Ditlou.

Acknowledgements

- I would like to thank Department of Science and Technology (DST), Council for Scientific and Industrial Research (CSIR) and SITA for sponsoring my research program and made it possible for the completion of this dissertation.
- Thanks to my parents, Masilo and Sewela Rabothata and to my beloved siblings, Mokhutlwane and Nthabiseng for their unconditional love, encouragement and support throughout the most challenging times of my research tenure.
- I would like to express my deep appreciation to Prof J. Muthu, my supervisor for his patient guidance, useful advise and encouragement during my research work. Without his encouraging presence and insightful knowledge this work would not have been possible.
- I would like to thank my colleagues and friends for being there throughout.
- Lastly, I would like to thank everyone who contributed to my completion of this work in one way or the other.

Abstract

The aim of this work was to develop a method for optimizing both design parameters and mechanical properties of polymer based nanocomposites using numerical multi-objective optimization (MOO) methods. The main objective was to simultaneously maximize the elastic modulus and the tensile strength of nanocomposites. The rationale behind focusing on these particular properties is that they play a significant role in designing of materials for structural applications. Ji and Zare models of determining the elastic modulus and tensile strengths of polymeric nanocomposite materials were respectively used for the formation of the objective functions for numerical optimization. The design variables (i.e major factors affecting the given mechanical properties) were identified as the diameter of nanofillers, thickness of the interphase region, nanofillers loading as weight fraction, elastic modulus of the interphase, interfacial shear stress and the orientation factor of the nanofillers. The Fast Non-dominated Sorting Genetic Algorithm (NSGA-II) approach in MATLAB was used to maximize the objective functions by obtaining the optimum solutions of the given design variables. The optimization model was able to successfully find optimum solutions of the design variables. Furthermore, the overall optimization results were found to be in good agreement with the available experimental results from literature. The proposed optimization model was found to be significantly accurate in finding the optimum values of the design variables for improving the mechanical properties of nanocomposites. The optimum values of the design variables were determined to be 2.12 – 2.96 nm for the thickness of the interphase, 5.41 – 7.01 nm for the diameter of the nanofillers, 2.95 – 4.69 wt.% for the nanofillers loading, and 1 for the nanofillers orientation factor. In addition, the results further showed that nano-reinforcements such as multi-wall carbon nanotubes (MWCNTs) yields high elastic modulus of the interphase and interfacial shear stress.

Contents

Declaration i

Acknowledgements iii

Abstract iv

Contents v

List of Figures ix

List of Tables xiv

List of Symbols xvi

List of Acronyms xviii

1 Introduction 1

1.1 Background and Motivation 1

1.2 Research Problem 5

1.3 Purpose of Study 7

1.4 Objectives 7

1.5 Overview and Research Approach 8

1.6 Thesis Outline 8

2 Literature Survey **10**

2.1 Nanocomposite materials optimization 10

2.1.1 Factors affecting mechanical properties of nanocomposites . . . 11

2.2 Numerical optimization methods 15

2.3 Multi-Objective Stochastic Search Techniques 17

2.3.1 Genetic Algorithm (GA) 18

2.3.2 Simulated Annealing (SA) 21

2.3.3 Particle Swarm Optimization (PSO) 25

2.3.4 Ant Colony Optimization(ACO) 26

2.4 Application of Stochastic Search Methods to Nanocomposites Design . 28

2.4.1 Comparison of Stochastic Multi-Objective Techniques 31

2.5 Multi-Objective Optimization (Multi-Objective Optimization (MOO)) Problems 33

2.5.1 Application of Genetic Algorithm (GA) to MOO Problems . . . 36

2.6 Modeling the Mechanical Properties 37

2.6.1 Modeling the Elastic Modulus 38

2.6.2 Modeling the Tensile Strength 41

2.7 Summary of the models for mechanical properties of polymer nanocomposites 44

3 Methodology **46**

3.1 Nanocomposite Design Optimization Problem 47

3.1.1 First objective function (f_1) 49

3.1.2 Second objective function (f_2) 52

3.1.3 Determination of effects of dispersion 56

3.1.4 The numerical optimization problem 58

3.2 NSGA-II for MOO in MATLAB 60

4 Results and Discussion **64**

4.1 Overall results of MOO model 65

4.1.1 Variation of Overall Optimization Results 70

4.2 Effects of the design variables on the mechanical properties 72

4.2.1 Effects of nanofiller loading on the mechanical properties 73

4.2.2 Effects of interphase properties 81

4.2.3 Effects of dispersion on the tensile strength 98

5 Conclusions and Recommendations **103**

5.1 Conclusions 103

5.2 Recommendations 106

Bibliography **107**

A Nanocomposite Design Optimization **118**

A.1 MATLAB Setup 118

A.1.1 Objective Function 118

A.1.2 Optimization Toolbox 119

A.2 Descriptive Statistical Analysis of Data 122

A.2.1 Measures of variation of data 123

A.2.1.1 Interpretation of box and whisker plot 124

A.3 Analysis of MOO Results 126

A.3.1 Mean Analysis of Optimization model results 126

A.3.2 Median Analysis of Optimization model results 126

A.3.2.1 Objective functions 127

A.3.2.1.1 Elastic modulus 127

A.3.2.1.2 Tensile strength 128

A.3.2.2 Nanofillers thickness 129

A.3.2.3 Thickness of the interphase 129

A.3.2.4 Nanofillers loading 130

A.3.2.5 Interphase modulus 131

A.3.2.6 Interfacial shear stress 132

A.3.2.7 Dispersion Parameter, B 133

List of Figures

1.1 Applications of composite materials 1

1.2 Schematic of major factors affecting properties of nanocomposites . . . 3

1.3 Different length scales in composite materials design 5

2.1 Possible dispersions of nanofillers within polymer matrix, (a): Uniform dispersion. (b): Dispersion with agglomerations 12

2.2 Experimental vs. theoretical results of Pa66/$CaCO_3$ and (PP/$CaCO_3$) polymer nanocomposite materials. (A) Without the interphase properties and (B) With consideration of the interphase region [39]. 14

2.3 Illustration of global vs. local minimum 16

2.4 Different types of optimization techniques [40] 16

2.5 Schematic of the selection of the individuals and the application of an objective function in a GA operation. 19

2.6 Schematic of the crossover and mutation processes of a GA procedure of binary digit individuals [46]. 20

2.7 Illustration of a simple Simulated Annealing (SA) optimization process [50]. 22

2.8 Schematic of a basic SA process [49]. 23

2.9 Representation of Particle Swarm Optimization (PSO) algorithm: (a) Initialization (b) Particles movement towards solution which is given by the grey circle [54]. 25

2.10 Schematic of the basic PSO algorithm. 27

2.11 Behavior of real ants in search of food [56] 28

2.12 Pareto-front for two-objective optimization problem in objective space . 35

2.13 Schematic of a nanocomposite illustrating the three-phases of the material 45

3.1 Flow chart of the optimization of mechanical properties of nanocomposites 48

3.2 Representation of Ji model and the responses to applied load with 'm', 'f' and 'i' denoting respectively the matrix phase, filler phase and interphase regions. 49

3.3 Schematic of tensile load and the development of interfacial shear stress along a nanofiller in polymer nanocomposite [101]. 52

3.4 Relationship between the objective functions and the design variables . 59

3.5 MATLAB's Fast Non-dominated Sorting Genetic Algorithm (NSGA-II) optimization procedure for maximizing mechanical properties of nanocomposites 62

4.1 Optimum normalized elastic modulus of MOO model vs. normalized elastic modulus (E_R) of the experimental data. 69

4.2 Percentage increase in normalized elastic modulus for both mean and median analysis. 69

4.3 Box and whisker plot for the normalized elastic modulus 71

4.4 Box and whisker plot for the normalized tensile strength 72

4.5 Normalized elastic modulus (E_R) vs. nanofiller loading (θ_f) for Nylon-Montmorillonite (MMT). 74

4.6 Normalized elastic modulus (E_R) vs. nanofiller loading (θ_f) for Polyamide (Pa)-Calcium Carbonate ($CaCO_3$). 75

4.7 Normalized elastic modulus (E_R) vs. nanofiller loading (θ_f) for SBR-Multi-wall Carbon Nanotubes (MWCNTs). 75

4.8 Normalized elastic modulus (E_R) vs. nanofiller loading (θ_f) for iPP-MWCNTs. 76

4.9 Box and whisker plot for nanofillers loading 77

4.10 Normalized tensile strength (σ_R) vs. nanofiller loading (θ_f) for Nylon-MMT. 78

4.11 Normalized tensile strength (σ_R) vs. nanofiller loading (θ_f) for Pa-$CaCO_3$. 79

4.12 Normalized tensile strength (σ_R) vs. nanofiller loading (θ_f) for SBR-MWCNTs. 79

4.13 Normalized tensile strength (σ_R) vs. nanofiller loading (θ_f) for iPP-MWCNTs. 80

4.14 Effect of interphase thickness on the normalized elastic modulus for Nylon-MMT. 82

4.15 Effect of interphase thickness on the normalized elastic modulus for Pa-$CaCO_3$. 83

4.16 Effect of interphase thickness on the normalized elastic modulus for SBR-MWCNTs. 83

4.17 Effect of interphase thickness on the normalized elastic modulus for iPP-MWCNTs. 84

4.18 Effect of interphase thickness on the normalized tensile strength for Nylon-MMT. 85

4.19 Effect of interphase thickness on the normalized tensile strength for Pa-$CaCO_3$. 85

4.20 Effect of interphase thickness on the normalized tensile strength for SBR-MWCNTs. 86

4.21 Effect of interphase thickness on the normalized tensile strength for iPP-MWCNTs. 86

4.22 Box and whisker plot for thickness of the interphase 87

4.23 Effect of interphase modulus on the normalized elastic modulus for Nylon-MMT. 89

4.24 Effect of interphase modulus on the normalized elastic modulus for Pa-$CaCO_3$. 89

4.25 Effect of interphase modulus on the normalized elastic modulus for SBR-MWCNTs. 90

4.26 Effect of interphase modulus on the normalized elastic modulus for iPP-MWCNTs. 90

4.27 Box and whisker plot for the elastic modulus of the interphase 91

4.28 Comparison of elastic modulus of nanocomposites constituent for mean analysis. 93

4.29 Comparison of elastic modulus of nanocomposites constituent for median analysis. 93

4.30 Percentage difference between the elastic modulus of the nanofiller and the interphase 94

4.31 Effect of interfacial shear strength on the normalized tensile strength for Nylon-MMT. 96

4.32 Effect of interfacial shear strength on the normalized tensile strength for Pa-$CaCO_3$. 96

4.33 Effect of interfacial shear strength on the normalized tensile strength for SBR-MWCNTs. 97

4.34 Effect of interfacial shear strength on the normalized tensile strength for iPP-MWCNTs. 97

4.35 Box and whisker plot for interfacial shear stress 98

4.36 Effect of interfacial shear strength on the normalized tensile strength for Nylon-MMT. 99

4.37 Effect of interfacial shear strength on the normalized tensile strength for Pa-$CaCO_3$. 100

4.38 Effect of interfacial shear strength on the normalized tensile strength for SBR-MWCNTs. 100

4.39 Effect of interfacial shear strength on the normalized tensile strength for iPP-MWCNTs. 101

4.40 Box and whisker plot for the parameter B 101

A.1 MATLAB m-file script for the objective function 118

A.2 Problem setup 119

A.3 'Options' part 1 120

A.4 'Options' part 2 121

A.5 Steps for statistics analysis of data 122

A.6 Generic box and whisker plot 126

List of Tables

2.1 Comparison of Optimization methods [41] 32

3.1 Optimization design variables and constraints 58

3.2 Materials used for numerical optimization 60

4.1 Optimized mean design variables and the corresponding normalized mechanical properties. 67

4.2 Optimized median design variables and the corresponding normalized mechanical properties. 67

4.3 Experimental results of the normalized elastic modulus (E_R). 67

4.4 Experimental results of the tensile strength (σ_R). 68

4.5 Standard deviations of the normalized elastic modulus and the tensile strength. 70

A.1 Standard deviations of the overall optimization results. 127

A.2 Summary variables for the normalized elastic modulus. 127

A.3 Comparison of the mean and the median of the normalized elastic modulus. 128

A.4 Summary variables for the normalized tensile strength. 128

A.5 Comparison of the mean and the median of the normalized tensile strength. 128

A.6 Summary variables for thickness of nanofillers. 129

A.7 Comparison of the mean and the median of the nanofillers thickness. . 129

A.8 Summary variables for the interphase thickness. 130

A.9 Comparison of the mean and the median of the interphase thickness. . 130

A.10 Summary variables for nanofillers loading. 130

A.11 Comparison of the mean and the median of the nanofiller loading. . . . 131

A.12 Summary variables for the interphase modulus. 131

A.13 Comparison of the mean and the median of the interphase modulus. . . 131

A.14 Summary variables for the interfacial shear stress. 132

A.15 Comparison of the mean and the median of the interfacial shear stress. 132

A.16 Summary variables for the dispersion parameter. 133

A.17 Comparison of the mean and the median of the parameter B. 133

List of Symbols

The units of quantities defined by a symbol are indicated in square brackets following the description of the symbol. Quantities with no indicated units may be assumed to be dimensionless.

A Specific surface area of nanofillers.

a Ratio of interphase-to-matrix elastic modulus.

α Aspect ratio of the nanofiller.

B Dispersion Parameter.

β Function of nanofiller loading in Ji Model.

E Elastic modulus [GPa].

η Nanofiller orientation factor.

L Length of nanofiller [nm].

λ Function of the thickness of the interphase, thickness of the nanofiller and the nanofiller loading in Ji Model.

m Mass of nanofillers [kg].

r Radius of the nanofillers [nm].

ρ Nanofiller density.

σ Tensile strength [MPa].

t Thickness [nm].

τ Interfacial shear stress [MPa].

θ Nanofiller loading.

$\mathbf{V}$ Total volume of nanofillers.

List of Acronyms

ACO Ant Colony Optimization.

$CaCO_3$ Calcium Carbonate.

CCD Central Composite Design.

CNTs Carbon Nanotubes.

FE Finite Element.

GA Genetic Algorithm.

IQR Interquartile Range.

MMT Montmorillonite.

MOGA Multi-Objective Genetic Algorithm.

MOO Multi-Objective Optimization.

MOSA Multi-Objective Simulated Annealing.

MWCNTs Multi-wall Carbon Nanotubes.

NGSA Non-dominated Sorting Genetic Algorithm.

NSGA-II Fast Non-dominated Sorting Genetic Algorithm.

Pa Polyamide.

PE Polyethylene.

PESA Pareto Envelope-based Selection Algorithm.

POM Polyformaldehyde.

PSO Particle Swarm Optimization.

RBDO Reliability Based Design Optimization.

ROM Rule of Mixtures.

RSM Response Surface Method.

SA Simulated Annealing.

VEGA Vector Evaluated Genetic Algorithm.

Chapter 1 Introduction

1.1 Background and Motivation

In recent decades, composite materials, particularly polymer based composites have seen an increased demand in numerous engineering applications such as maintenance and replacement of components, wing to fuselage fairings, flame retardant panels, car engine covers, tires and bumpers, radiation resistance, electrical insulation materials and etc. [1, 2, 3, 4]. Figure 1.1 shows some of the applications of composite materials.

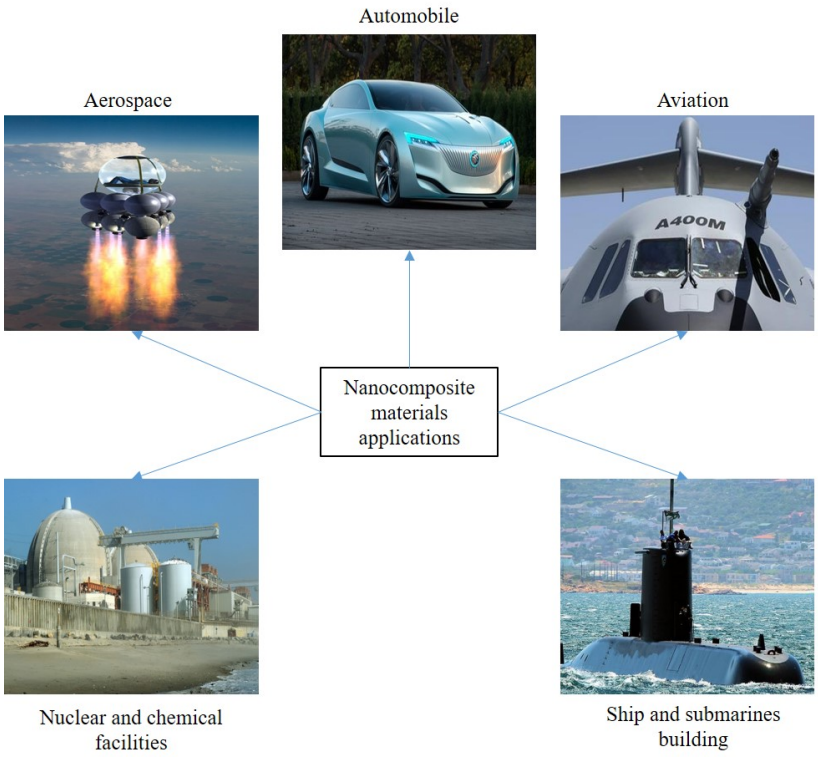

Figure 1.1: Applications of composite materials

A composite material is basically synthesized of two or more materials, known as a matrix and a reinforcement. The most popular matrix materials are polymers such as thermoplastics and thermosets. Fiberglass, carbon fibre, aramid, silica and aluminum on the other hand are mostly used as reinforcements in composite materials design. The most attractive attribute of composites is that they can be tailored to a specific application. This has resulted in the demand and growth for these materials and further prompted researchers globally to learn how to design them for different applications.

More recently, the field of composite materials sciences and design has witnessed the emergence of nanomaterials (or nanocomposite materials) and these materials have since attracted much attention due to their significant improvement in the physical, mechanical and thermal properties [5]. Nanocomposites are materials made of a combination of a matrix and some form of reinforcements or fillers in nanoscale (i.e. less than 100 nm). The development of these materials has been on the rise for several years. Their implementation however, continues to be limited by lack of understanding of the basic physical relationships that exist between the material structural parameters at a nanoscale and the material properties at a macroscale.

Major applications of nanocomposites in many engineering applications requires structures with a high strength-to-weight ratio, high stiffness, fatigue durability (i.e. the ability to withstand wear or damage), corrosion resistance, etc. These enable nanocomposites to replace most conventional or traditional composite materials. Research has shown that the physical, mechanical and thermal properties of nanocomposite materials are mainly influenced by the following parameters [6, 7, 8, 9, 10]:

(i) Size (diameter) and loading of nanofillers (i.e. the content of nanofillers within the polymer matrix).

(ii) Interphase (i.e. region where the surface of the nanofillers interact with the polymer matrix) and the strength of the bond between the nanofillers and the polymer matrix.

(iii) Alignment of nanofillers.

(iv) Dispersion of nanofillers within the polymer matrix.

Figure 1.2 shows a schematic of major factors affecting properties of nanocomposites.

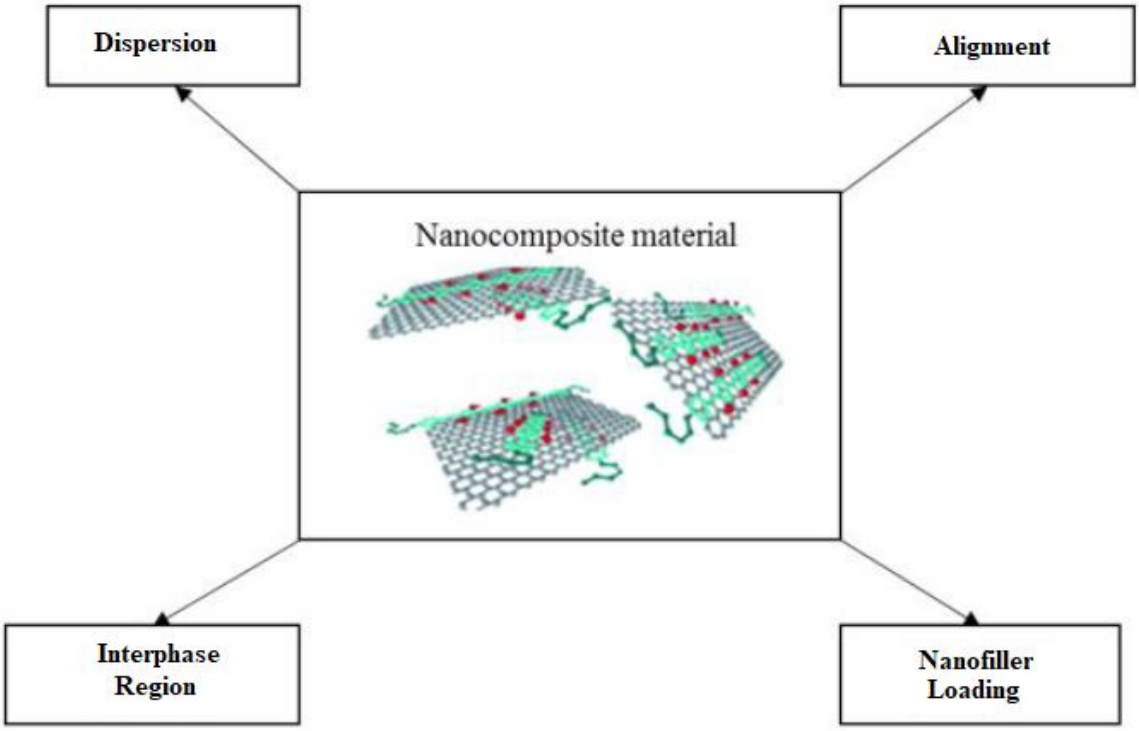

Figure 1.2: Schematic of major factors affecting properties of nanocomposites

It has been widely reported that increasing nanoparticle loading enhances mechanical properties of polymer nanocomposites. However, it has also been frequently observed that loading beyond certain percentages can be detrimental to the properties due to the emergence of significant nanofillers agglomerations [10, 11]. Numerous reviews have also cited nanofiller dispersion as a major challenge in the advancement of polymer nanocomposite technology [12, 13].

Furthermore, it is globally conceived that optimal nanocomposite materials' properties will be reached if nanofillers are dispersed uniformly within the polymer matrix [14]. Significant improvements on mechanical properties of nanocomposites have been achieved through proper alignment of nanofillers in a polymer matrix. For example, the fully aligned nanofillers produce more desirable properties such as high elastic modulus, tensile strength, fracture toughness compared to the randomly oriented nanofillers. It is worth noting however that, controlling of the nanofillers' orientations and proper alignment of nanofillers remains one of the major challenges within nanocomposite manufacturing [15, 16, 17, 18, 7].

Interfacial adhesion refers to the bond between the polymer matrix and the nanofillers. The interfacial region or the interphase is the area of interaction between the nanofillers and the matrix. This region has distinct properties from the different constituents of the nanocomposite material and therefore it is highly critical to the performance of the entire material. The strength of adhesion at the interface determines the efficiency of load transfer between the nanofillers and the polymer matrix, and ultimately the mechanical properties of the material. This means that any insufficient adhesion at the interphase will cause degradation of the materials' properties [19].

Therefore, effective design of nanocomposite materials is dependent on accurate prediction and characterization of optimum parameters affecting their properties. Over the years, numerical optimization techniques have been used for solving many complex real engineering problems and to this day, optimization process remains critical to the design process. Design problems associated with nanocomposites are known to be multi-objective optimization problems. This is due to the fact that nanocomposites are usually designed to meet more than one objective, i.e. minimizing of weight and cost of manufacturing whilst maximizing mechanical properties such as strength, durability, resistance, etc.

Numerical optimization methods have been used for design of traditional or composite materials [21, 22]. However those design problems were mostly focused on obtaining optimum design parameters such as volume fractions, fiber orientations, plies' stacking sequence, fabrication procedure and etc. to optimize composite materials (i.e. minimize cost, minimize weight or maximize strength) . In addition, it should be noted that the traditional optimization of composite material design only focused at micro and macro scales. Figure 1.3 shows the different scales that exist in composite materials design.

Research also indicates that the use of numerical optimization techniques on composites was only used for fiber reinforced based composites [20, 21, 23]. Hence, the development of composite materials and the discovery of nanoscopic materials (polymer-based nanocomposites in particular) justifies the need to use the optimization techniques during the preliminary design phase. Again, as mentioned before, the development of polymer based nanocomposite materials and or the understanding of the most important design parameters of nanocomposite materials is still under-researched.

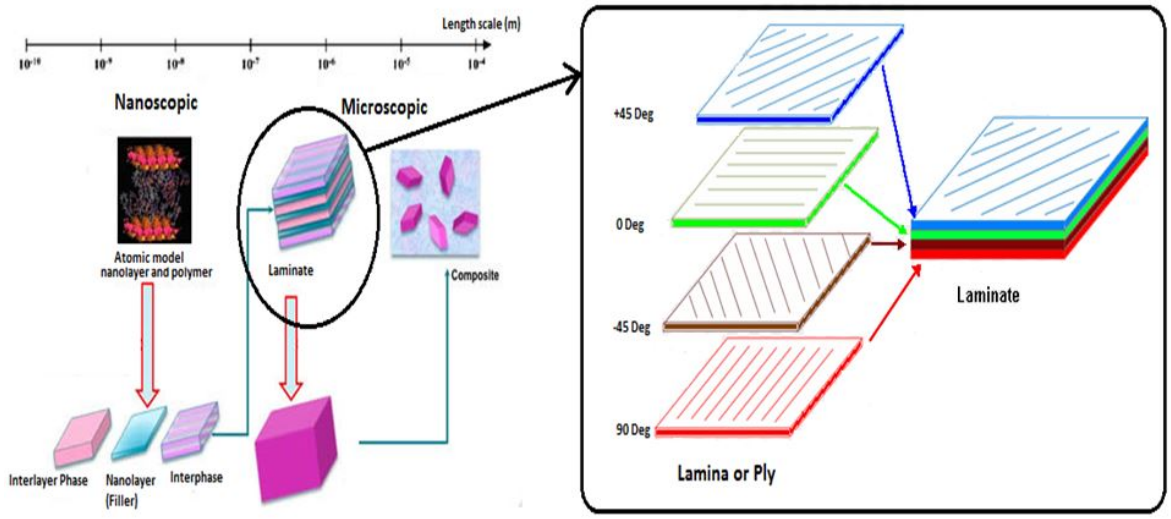

Figure 1.3: Different length scales in composite materials design

Thus, until now, very limited research has been carried out to numerically optimize mechanical properties of nanocomposites based on parameters such as dispersion, alignment, weight fraction or nanofiller loading and interfacial adhesion which are said to be the 'major factors' influencing the mechanical properties of nanocomposite material. Hence the current work focuses on using numerical optimization techniques to design and optimize the mechanical properties of nanocomposite materials based on the given parameters.

1.2 Research Problem

Even though there has been numerous research studies on optimum design and development of nanocomposites materials, there still lacks comprehensive work on using numerical optimization methods during the design processes. In fact, currently there is no known work that focus on using numerical optimization techniques to optimize the mechanical properties of nanocomposites [24, 25]. This can be attributed to the fact that the development of nanocomposite materials is largely empirical (i.e. based on observation and experience) and a higher degree of control of their properties is still difficult to achieve [26].

Real engineering design problems often require many iterations to obtain optimum parameters. As a result, the process of physical experimental optimization has proven to be oftentimes lengthy to reach desired outcomes, especially if more than one conflicting design objectives are to be met. Furthermore, in general, physical experimentation is very expensive and time consuming due to the fact that the experiments are run without a prior knowledge of the optimum results. The iterations therefore have to be tested time and again before obtaining on the optimum values of the design parameters. Due to this, researchers and designers run the risk of depleting resources and therefore incurring more costs.

Numerical experimentation on the other hand has the ability to predict the results of experiments that had not yet been carried out. This makes it as one of the most important approaches in the design process [27]. Hence, over the past several decades, numerical experimentation and computational techniques have been playing an ever increasing role in the design process of many engineering applications. The fact that with this approach, the optimum results can be predicted before hand makes numerical experimentation a way of saving time and costs during the design process.

It is worth noting however, that the simulations which are run during numerical experimentation are imperfect models for the physical reality and can only be trusted so far as they demonstrate agreement without any bias with physical experimental results. This means that validation process is of significant importance as it is used to test the correctness and completeness of the models.

The need for numerical optimization in nanocomposites design is therefore justified through to the following:

- There is limited literature on the usage of numerical optimization methods to design and improve nanocomposite materials properties based on dispersion, interfacial adhesion, alignment and nanofiller loading
- Nanocomposite design process is very complex due to multiple design variables (i.e. more than one variable is optimized) and therefore best or optima properties can be obtained without laboratory's experimental trial and error methods which can be very tedious
- Numerical optimization techniques may save designers a lot of time and costs.

1.3 Purpose of Study

Based on the above discussions coupled with the increased interest in using nanocomposites for numerous structural applications, it would be highly beneficial to perform numerical optimization during the design phase of the nanocomposite materials. This is done so as to ensure that the designed materials are as effective as possible and that the desired properties are optimized by knowing the optimum parameters and conditions which can yield those properties.

Hence, the main objective of the current study is to use numerical multi-objective optimization techniques to optimize the elastic modulus and tensile strength of polymer nanocomposite materials by finding the optimum values of the design parameters. By simultaneously considering the effects of the design parameters, the overall properties of nanocomposites are expected to be improved. The reason for focusing on these particular properties is due to the fact that they play a significant role in designing of materials for many structural applications. In addition, significant findings regarding the effects of the above mentioned design parameters on the mechanical properties will be highlighted, analyzed and discussed. Furthermore, the obtained results and findings will be validated through the use of experimental results from previous studies on mechanical properties of composite materials with similar design parameters.

1.4 Objectives

The main objective of the current study is to use multi objective optimization (MOO) techniques (Genetic Algorithm (GA) in particular) to optimize the nanocomposite mechanical properties based on the respective design parameters (i.e. dispersion, nanofiller loading, alignment and interphase) of those properties. The objectives of this study are outlined as follows:

- Develop an approach for optimizing mechanical properties of polymer nanocomposites materials using GA techniques for solving MOO problems
- Obtain optimum design parameters for maximizing the elastic modulus and the tensile strength of polymer nanocomposites

- Validate the method and the optimized results with experimental data from previous studies

1.5 Overview and Research Approach

Firstly, historical data describing the mechanical properties behavior of nanocomposites are obtained from the literature. The collected data is then used to identify the design parameters of nanocomposite materials which are further investigated and discussed. This is done to determine the most important aspects and characteristics of the design parameters. In addition, the constraints (or limitations) of the design parameters with respect to the design of the nanocomposites are also outlined. This is followed by the introduction of optimization methods, their applications to multi-objective optimization problems, the comparison and selection of the most suitable method for the current study.

A nanocomposite design problem is then converted to a MOO problem based on the given design parameters. Furthermore, theoretical mechanics models for determining the mechanical properties of composite materials are used to establish the objective functions to be optimized. Lastly, Non-dominated Sorting Genetic Algorithm (NSGA-II) is then used for solving the nanocomposite design MOO problem for maximizing the mechanical properties. Finally, the characterization, validation and discussion of the results together with conclusions and directions for future work will be presented.

1.6 Thesis Outline

This thesis is organized as follows:

- Chapter 1 gives the introduction of nanocomposite materials and the factors (design parameters) that affects the mechanical properties of nanocomposites. The chapter further provides the need for numerical optimization of the mentioned design parameters. In addition, the motivation and the rationale for the current study together with the objectives are outlined.

- Chapter 2 gives an overview of published studies on factors that influence the mechanical properties of nanocomposites. An introduction to numerical optimization methods for solving MOO problems is also given and briefly discussed. The chapter further discusses the types of numerical optimization methods, their applications and advantages and disadvantages in their approach to solving problems. Lastly, the chapter discusses the modeling of mechanical properties of nanocomposites (i.e. the analytical models and theories used for the prediction of the mechanical properties of nanocomposite materials).

- Chapter 3 gives a procedure and methodology for analysis of MOO for design of nanocomposite materials properties.

- Chapter 4 presents the results of the different design parameters and the mechanical properties obtained from the suggested numerical optimization model. The chapter further discusses and validate the obtained results. Additionally, the chapter also discusses how the given design parameters influence the mechanical properties.

- Finally, chapter 5 gives a summary of the findings of the current work and briefly discusses future directions of work in this field based on the results presented here.

Chapter 2 Literature Survey

This chapter gives a brief overview of published studies on the factors that influence the mechanical properties of nanocomposite materials and an introduction to numerical optimization methods for solving multi-objective design problems. The chapter further discusses the modeling of the mechanical properties of nanocomposites (i.e. the analytical models and theories used for the estimation of the properties).

2.1 Nanocomposite materials optimization

Generally, in composite materials, designers seek the best possible design that consumes the least amount of resources whilst maximizing the materials' properties depending on the application. This requires a proper understanding of the properties of all the constituent materials such as the reinforcements and the polymer matrix. When designing wing to fuselage fairings for aircrafts applications for example, one may wish to design the components in such a way that they have high strength with the minimum amount of weight.

The use of nanofillers as reinforcements in polymer based nanocomposite materials has been under studies as early as the 1950s [28], however significant interest in these materials within both the academic and industrial arena came nearly forty years later [29]. To date, nanofillers continue to play a promising role in composite materials design and manufacturing. Hence there is still immense research interest in the development of composite materials, especially polymer based composites for structural applications.

As mentioned in the preceding section, the understanding of the properties of nanocomposites' constituents (i.e. polymer matrix and nanofillers) at different length scales remains a huge challenge. It should be noted that this understanding is integral to the determination, characterization and design of the properties of nanocomposites [30, 31]. Thus, it would be highly beneficial for nanocomposite materials designers and manufacturers to have a deeper understanding of the parameters that influence or affect the materials' mechanical properties.

The requirements of nanocomposite materials are usually outlined according to the specific application. Thus engineers need to fully comprehend the properties together with the applications so as to design the materials that will meet these requirements. It is worth noting that the general process of design of materials is usually complex, tedious and time consuming as it involves large numbers of iterations in the quest for finding the 'best' or optimum design. As a result, mathematical optimization has appeared to be a powerful tool for design and in many cases, it has helped design engineers to avoid repeating iterations prior to finding optimum designs to problems. In addition, the process of numerical optimization may also save the costs associated with raw materials that would normally be used through traditional trial and error methods.

2.1.1 Factors affecting mechanical properties of nanocomposites

Recent work by Islam et al. [6] on the effects of nanoparticles loading on the mechanical behavior of silica-epoxy nanocomposites concluded that the elastic modulus, tensile stress, and yield stress of most nanocomposites increase with increasing nanofiller loading. While this has been reported to be generally the case with nanocomposite materials, it has been frequently observed that beyond certain nanofiller loadings, the properties degrade significantly [32]. Khare et al. [10] reported that optimum nanofiller loading often coincides with the emergence of significant nanofiller agglomerations which implies non-uniform distribution or dispersion of the nanofillers within the polymer matrix.

Hence it is important to ensure a balance between optimum nanofiller loading and the avoidance of agglomeration of nanofillers. Poorshjouy et al. [33] investigated the effects of Carbon Nanotubes (CNTs) loading and dispersion on the mechanical properties of nanocomposites. The authors revealed that evenly distributed or uniform dispersion was obtained at nanofiller loading of lower than 5 wt.%. Their results, indicated that increasing of nanofiller loading beyond 5 wt.% leads to agglomerations [i] and poor dispersion resulting in a decrease of the mechanical properties of the nanocomposite material. Figure 2.1 shows the possible dispersions of nanofillers that could be achieved in nanocomposite materials.

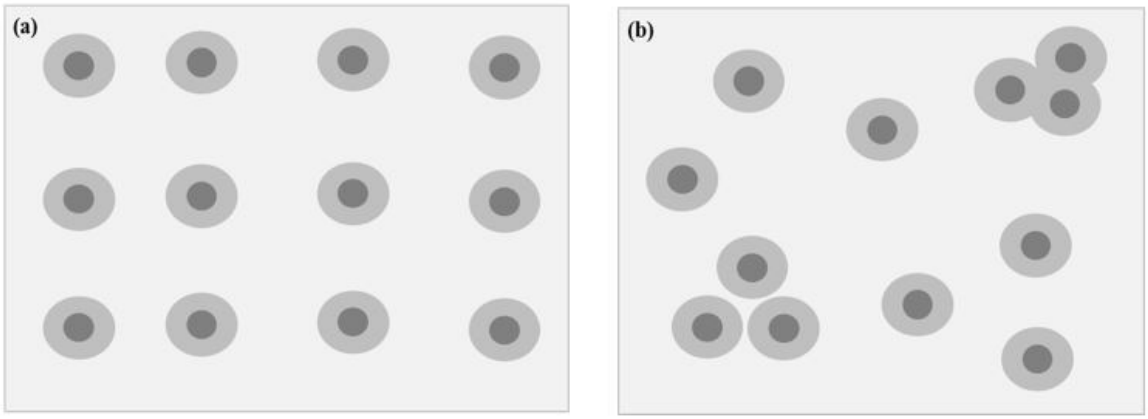

Figure 2.1: Possible dispersions of nanofillers within polymer matrix, (a): Uniform dispersion. (b): Dispersion with agglomerations

Independent research works of Deng et al. [34], and Cheng et al. [17] have showed that significant improvements on mechanical properties of nanocomposites can be achieved through proper alignment of nanofillers within the polymer matrix. Furthermore, Shankar et al. [15] recorded a higher elastic modulus for aligned nanofillers compared to those which are randomly oriented.

Mirjalili et al. [35] modeled and experimentally verified the effects of aligned and randomly oriented CNTs with respect to crack growth plane on the fracture toughness of polymers using Elastic Plastic Fracture Mechanics. Both the experimental and the numerical results indicated that there is no significant improvement in toughness for randomly dispersed nanotubes with nanofiller loading of lower than 2 wt.%. The results however, showed that aligning of 3 wt.% CNTs loading in epoxy normal to the crack growth plane improved the toughness of the nanocomposite by up to 400%.

[i] Agglomerations refers to the clustering of the nanofillers

Joshi et al. [36] analyzed the effect of various alignments of Multi-Wall Carbon Nanotubes (MWCNTs) in nanocomposites. In their work, the highest values of the elastic modulus were obtained for cases where the MWCNTs were aligned in the direction of the applied loads. In addition, the authors further concluded that the moduli of composites behave non-linearly with respect to nanofillers loading due to effects of agglomerations.

Hua et al. [8] investigated both the roles of interphase-matrix adhesion and the interphase property on the mechanical behavior of silica/epoxy resin nanocomposites. Their results suggested that the interphase modulus and the interfacial adhesion conditions have a significant influence on the overall stiffness of nanocomposites. Furthermore, they concluded that an interphase with higher stiffness has a higher load-sharing capacity and that there was uniform stress distribution within the material. Zakaria et al. [37] also investigated the effects of interphase characteristics on the tensile properties of Polyformaldehyde (POM) reinforced with $CaCO_3$. Their study concluded that increasing of the adhesion between nanofillers and polymer matrix increases the elastic modulus and strength of the nanocomposite material.

Wongpajan et al. [38] investigated the effects of the interfacial shear strength on the tensile strength of glass fiber reinforced polymer nanocomposites (GFRP). From their results, the authors observed that the tensile strength of their sampled materials increased with increasing fiber content. Their work also investigated the effect of fiber orientation on the tensile strength and it was established from the results that the tensile strength shows a declination trend for non-uniform orientation of fibers. In addition, the authors further reported that the interfacial shear strength also increases with the increasing fiber content.

Zare Yasser [39] developed a modified model based on the Mori-Tanaka theory for determining the Young's modulus of polymer nanocomposites with the consideration of the interphase region. The author found that the original Mori-Tanaka theory underestimated the mechanical properties of polymer nanocomposites containing spherical nanofillers and attributed this to the disregarding of the interfacial interaction between the polymer and the nanofillers.

The calculations from the modified model completely agreed with the experimental results. In addition, the model predicted that a high-content, thick and strong interphase creates a high modulus in polymer nanocomposites. Figure 2.2 shows the comparison of the experimental and theoretical results of Polyamide-66/Calcium Carbonate (Pa66/$CaCO_3$) and Polypropylene/Calcium Carbonate (PP/$CaCO_3$) polymer nanocomposite materials.

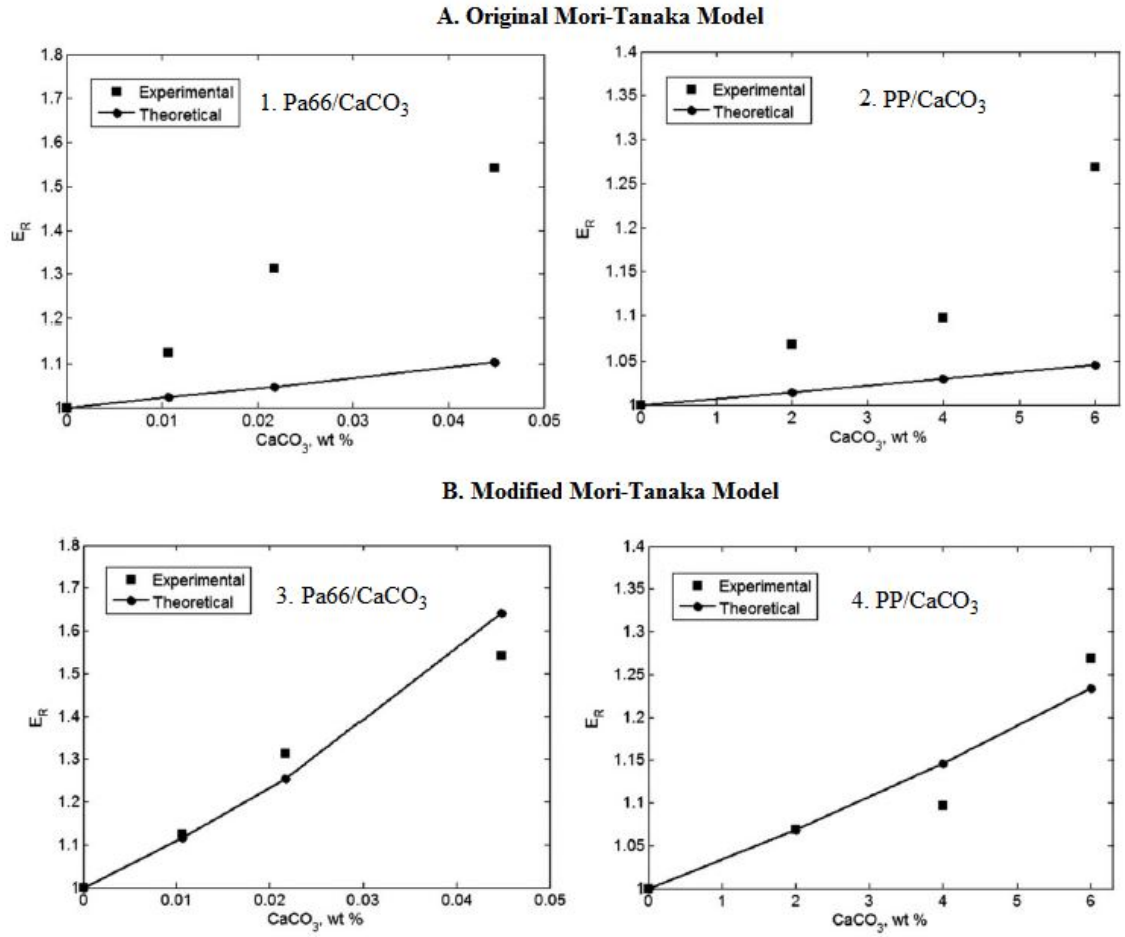

Figure 2.2: Experimental vs. theoretical results of Pa66/$CaCO_3$ and (PP/$CaCO_3$) polymer nanocomposite materials. (A) Without the interphase properties and (B) With consideration of the interphase region [39].

i). Section summary: Factors affecting the mechanical properties

From the above review, it can be seen that nanofiller loading, dispersion, alignment and the interfacial adhesion all play a very important role on the mechanical properties of polymer nanocomposites. Furthermore, it can be understood that these factors cannot be considered in isolation as they simultaneously affect the properties. Thus, it is of critical importance to ensure that all these factors are accounted for when designing polymer based nanocomposite materials.

2.2 Numerical optimization methods

Optimization is defined as a numerical search method that is used to find and determine the best possible solution for a given problem using sets of mathematical statements and equations. The methods can be categorized as either global or local optimization methods. Local optimization methods are those that will always reach the same locally optimal solution from the same starting whereas global optimization methods are those that are less dependent on the initial position(s). This means that during computation, local methods will only target nearby local optima whereas on the other hand, global methods should be able to locate (local) optima anywhere in the search space.

It should be noted that optima refers to either maxima or minima depending on whether the the problem of interest is a maximization or a minimization problem respectively. Figure 2.3 is an illustration of the difference between global minimum and local minimum. Global optimization methods are known to outperform local methods when solving problems. Thus they are usually preferred over local methods.

In general, optimization and search techniques can be divided into the following three main groups:

1. Calculus or gradient-based techniques
2. Enumerative techniques
3. Stochastic or guided random techniques

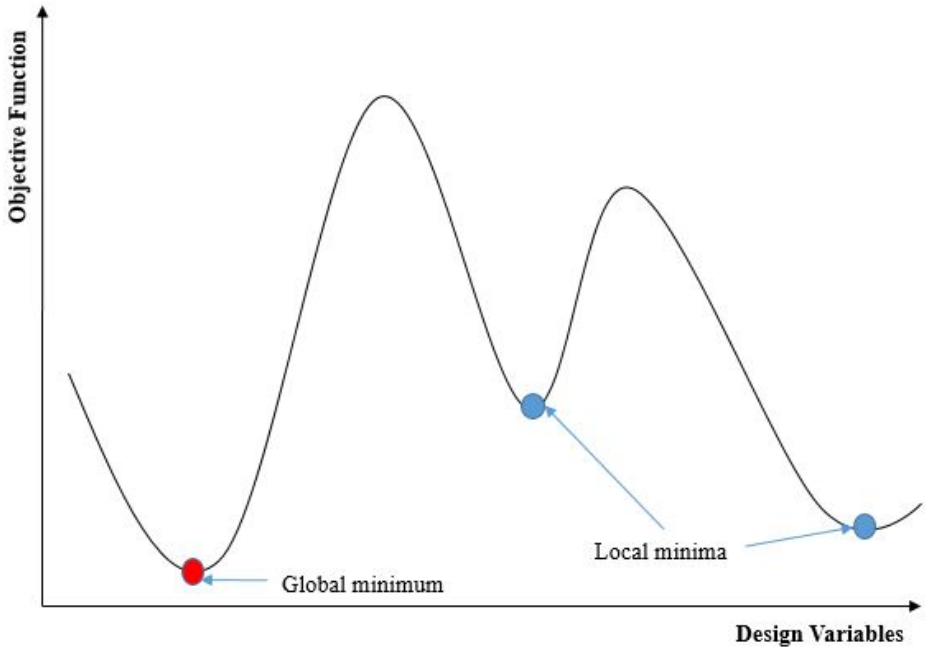

Figure 2.3: Illustration of global vs. local minimum

Figure 2.4 shows the different types of search and optimization techniques [40]

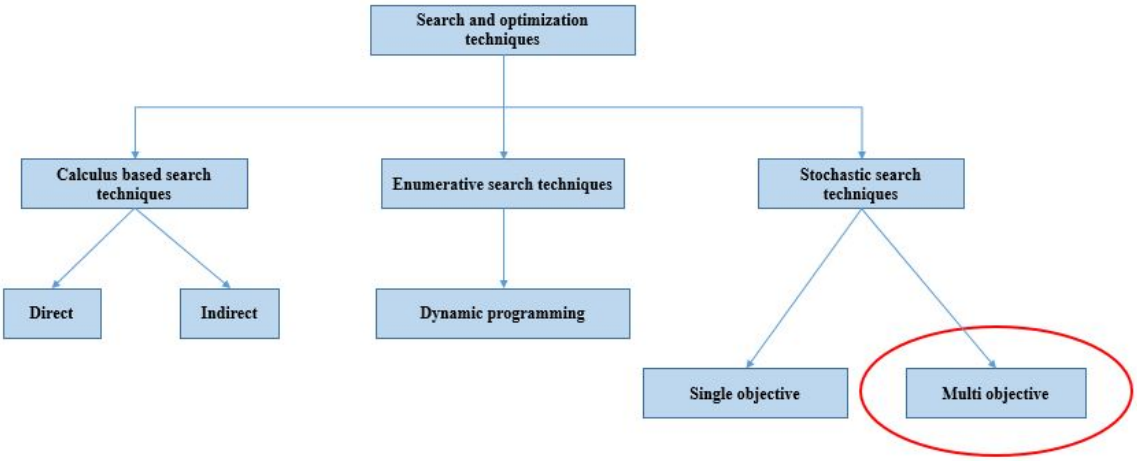

Figure 2.4: Different types of optimization techniques [40]

Calculus or gradient based techniques uses knowledge of derivative information to locate the optimum point. This type of optimization can further be divided into two categories, viz. direct and indirect methods. Furthermore, the method is local in scope and it assumes the existence of derivatives when solving problems. This results in restrictions regarding the application of the technique to many real life problems [40].

Enumerative techniques obtain optimum solutions to problems by evaluating all the points of the finite or discretized infinite search space. A well-known example of this type of a search technique is dynamic programming which is an optimization approach that obtains an optimum solution by converting a given problem into a sequence of simpler problems. Enumerative techniques usually break down on problems of high levels of complexity and size as it becomes impossible to search all the points in the space [40].

Stochastic techniques deal with optimization problems that are described by random or probabilistic variables rather than deterministic. These techniques are classified into two categories i.e. single- and multiple-objective search methods. Most real world optimization problems are solved by stochastic techniques. This is because the methods are capable of obtaining global optimum for problems that involve discrete variables, continuous or mixed variables, multi-variate or multi-objective functions, non-continuous functions, non-differentiable functions, etc. [40].

The current study deals with the designing of polymer based nanocomposite materials which is multi-objective in nature i.e. this study aims to find the optimum parameters for the maximization of both elastic and tensile properties of nanocomposite materials. Thus the focus in the current work will be placed on the stochastic search techniques, especially multi-objective search/optimization technique as indicated in Figure 2.4.

2.3 Multi-Objective Stochastic Search Techniques

This section gives a description and the architect of the popular multi-objective optimization algorithms. The algorithms are then compared and the best suited algorithm for solving the current study's design problem is selected. There are many stochastic search optimization techniques that have been developed over the years for real engineering problems. However, for the current study only the following four most popular techniques will be focused on [40, 41]:

- Genetic Algorithms (GA)
- Simulated Annealing (SA)
- Particle Swarm Optimization (PSO)
- Ant Colony Optimization (ACO).

2.3.1 Genetic Algorithm (GA)

The concept of Genetic Algorithm was developed by Holland et al. [42, 43] in the 1960s and 1970s. GA is described as a heuristic, stochastic optimization and search technique that is based on the principles of genetics and natural selection [44]. It is one of the most popular evolutionary algorithms (i.e. algorithms that mimic the mechanics of natural genetics for artificial systems). Thus, in nature, weak and unfit species within a particular environment are faced with extinction by natural selection whereas the strong ones have a greater opportunity to pass their genes to future generations through a process of reproduction.

After a while, only the species carrying the correct combination in their genes become dominant in their population. Sometimes, during the slow process of evolution, random changes may occur in the genes. If these additional changes are beneficial in the challenge for survival, the new species evolve from the old ones. Unsuccessful changes are eliminated by natural selection [45].

The algorithm starts by generating random initial population through an iterative process. The population in each iteration is called a generation and it is composed of potential solution points to a problem. The solution points are called individuals or chromosomes. These individuals are made of genes whose purpose is to control features that distinguish one individual to the other. The original implementation of GA used binary digits as genes [42]. However, in recent years, various types of genes such as vectors, individual rank or crowding distance have been introduced to the implementation of the algorithms. GA individuals corresponds to a unique solution points in the solution space. The solution points for every individual are evaluated against the fitness or (objective) function (i.e. the function that the algorithm is trying to optimize).

The value of the objective function obtained through each individual is called *fitness* and it measures how 'good' an individual is compared to the other individuals in the population. This means that the individual is selected on the basis of how well it solves the problem at hand. Figure 2.5 shows a schematic of the process of individual selection from the population through the use of an objective function.

Consider Figure 2.5:

1. From the population , individuals I_1, I_2 and I_3 are,
2. Evaluated using the objective function,
3. To obtain solutions, $F(I_1)$, $F(I_2)$ and $F(I_3)$ in the optimization solution space.

For a minimization problem of two objectives, 'good' individuals would be those individuals that gives the minimum fitness values in the solutions space. This means that the obtained solutions of $F(I_{1,2,3})$ on the dashed line in Figure 2.5 can be regarded as the best optima solutions for the given problem.

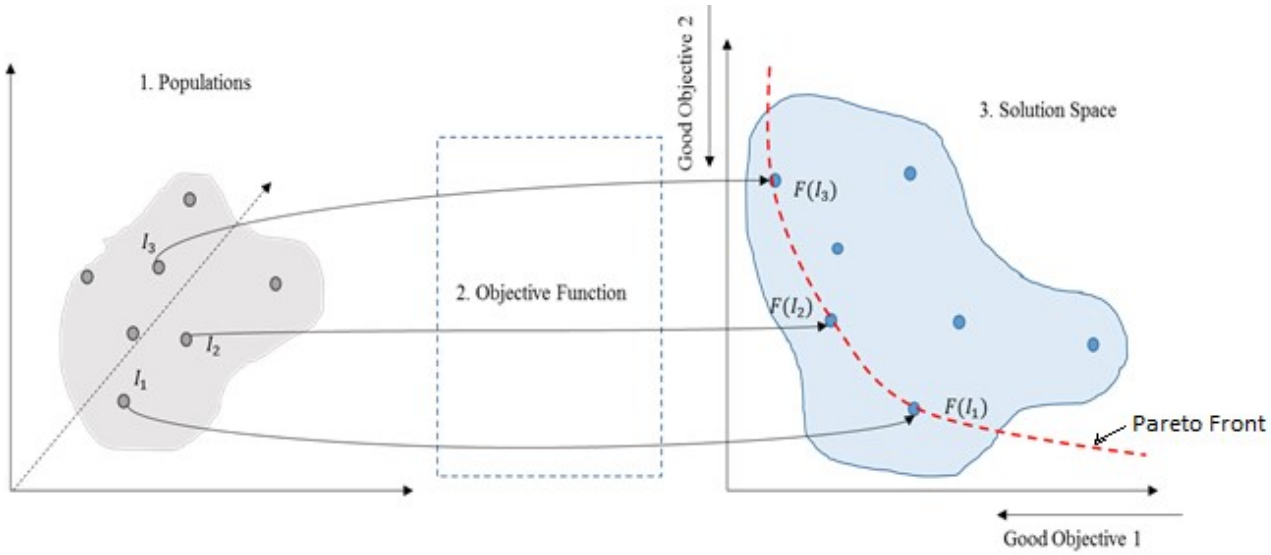

Figure 2.5: Schematic of the selection of the individuals and the application of an objective function in a GA operation.

The process of selecting the best individual is similar to that of natural selection (i.e. survival of the fittest) whereby individuals are selected depending on their fitness (dominance). Strong individuals (non-dominated) survive and the weakest ones (dominated) die off [44]. There are different selection procedures for selecting individuals in GA and this depends on how the fitness values are used. The most popular selection procedures are proportional selection, ranking and tournament selection.

The process of generating new individuals from the existing ones is composed of two processes i.e. crossover and mutation. Crossover is regarded as the most critical process of GA. Crossover generally involves combining of two individuals called parents together to form new individuals called offspring. The parents are selected among existing individuals in the population with preference towards fitness so that the offspring is expected to inherit good genes. Crossover is an iterative process and thus it helps in ensuring that the genes of good individuals appear frequently in the population, and will eventually lead to convergence to an overall good solution.

In addition, individuals in each generation stand a small chance of slightly changing through a process of mutation. The role of mutation is to ensure that there is diversity in the population and that the probability of obtaining any point in the search space never goes to zero. Furthermore, mutation prevents GA from converging to one local optimal solution prematurely [44, 41]. After mutation, the procedure is repeated until an appropriate stopping condition is reached. Figure 2.6 shows the basic procedure of a GA's crossover and mutation processes of binary digit individuals.

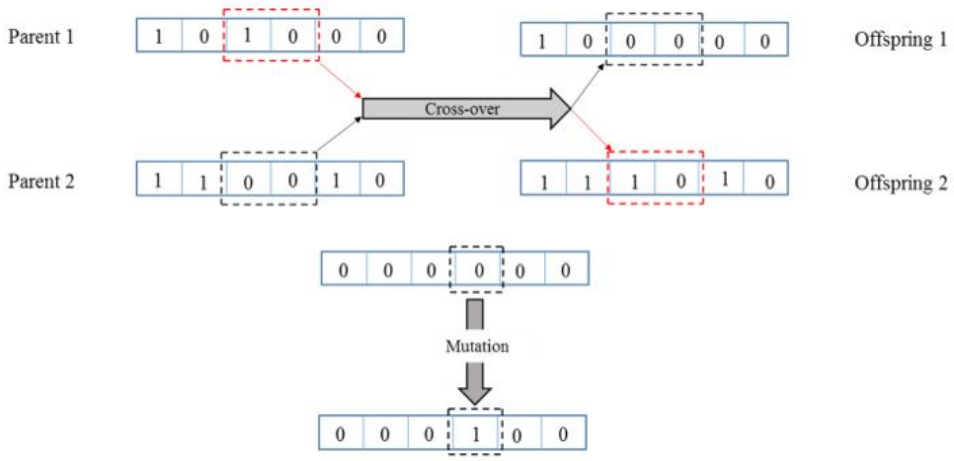

Figure 2.6: Schematic of the crossover and mutation processes of a GA procedure of binary digit individuals [46].

2.3.2 Simulated Annealing (SA)

Simulated Annealing (SA) is considered to be the most popular optimization method after GA. The method is inspired by a process of annealing of materials. The algorithm its name from the fact that it emulates the physical annealing process in metallurgy. During annealing, the temperature of a solid material is raised to a melting point where the atoms can randomly move around freely in a high energy state, and then slowly cooled down to allow an ordered rearrangement of the atoms to a lower energy state [47]. The material reaches equilibrium at every temperature level. The atoms get closer and closer to lower energy state as the temperature decreases. The process takes place until the lowest possible temperature is achieved.

The analogy and relations of the physical process of SA with the optimization procedure are given as follows [48]:

- The physical material state correspond to the problem solutions
- The energy of a state corresponds to the cost of a solution (or the objective function)
- The temperature corresponds to a control parameter (or the problem variable)

The approach of SA algorithm to numerical optimization problems consists of two stochastic processes i.e. one is responsible for the generation of solutions and the other is responsible for the acceptance of generated solutions. The two processes are usually controlled by two temperature values (i.e. the current state temperature and the accepted temperature) which are similar to the physical annealing process and follows a given annealing schedule [49].

When solving a problem, the SA algorithm starts every iteration by generation a new random point (current temperature, (T)) which is then systematically updated until a stopping criteria (optimum condition) is satisfied. Starting with the new randomly generated point, the algorithm uses perturbation and evaluation functions to perform a stochastic search of the design space. Updating of the points is also an iterative procedure that is based on a probability distribution parameter with a scale that is proportional to the temperature (T).

For a minimization problem, the algorithm accepts all the new points that decreases the objective or cost function (i.e. energy state in the physical annealing process) and vice versa for a maximization problem. The new points that increase the objective function are accepted with a probability of Boltzmann distribution. The determination of this probability is dependent on T. During computation, T is kept constant and only reduced after a number of iterations. This therefore, slows down the rate of temperature reduction, and ensures that the algorithm avoids being trapped in a local minima in the early iterations and that it is also able to search globally for better solutions [40].

The optimal solution of the algorithm correspond to the lowest energy state. Just as the atoms move randomly to find an ordered arrangement, the global optimum of the algorithm is also reached through a search within randomly generated configurations [47]. Figure 2.7 illustrates a simple SA optimization problem [50]. From the figure, at stage 1, the atoms have high temperature and are at a high energy state. The temperature is then decreased to a lower energy state in stage 2. Lastly, the atoms return to the lowest energy state at 3 after a complete process of cooling.

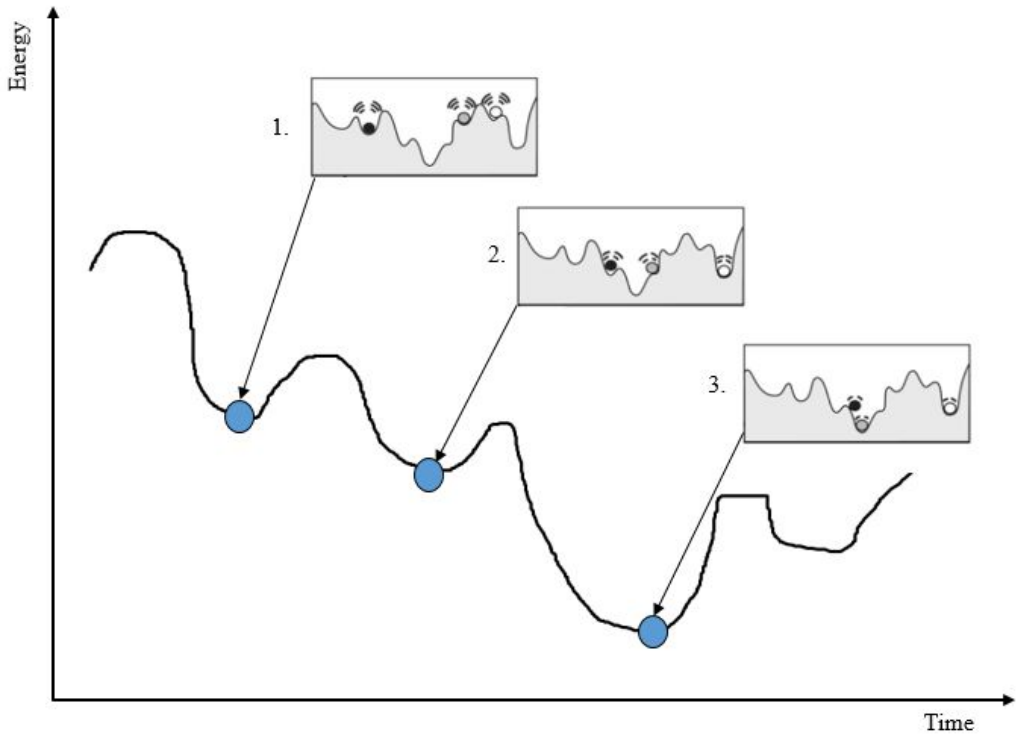

Figure 2.7: Illustration of a simple SA optimization process [50].

Figure 2.8 shows a schematic of a basic SA optimization process. It is worth noting from the figure that the temperatures are only updated once the equilibrium criteria is satisfied. This is done to ensure that the there are enough iterations until there is little or no variation in the energy of the accepted solutions, thus, the equilibrium would have been reached.

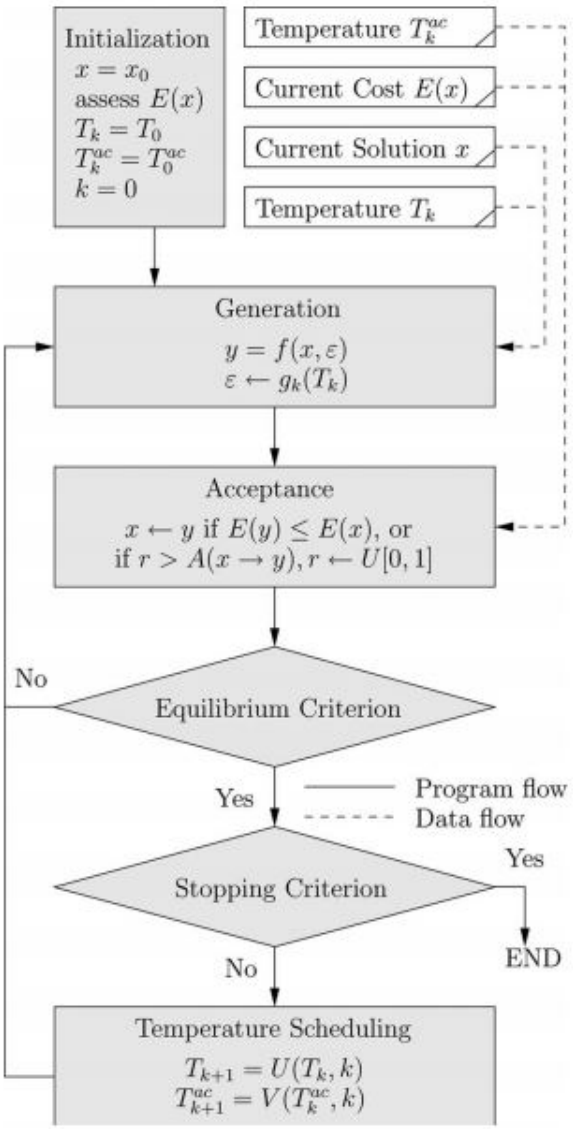

Figure 2.8: Schematic of a basic SA process [49].

From the figure above, the solid lines represent the program flow, whereas dashed lines represent the data flow. The current solution is denoted by x, with T_k and T_k^{ac} denoting the generation and the acceptance temperatures at iteration k, and T_0 and T_0^{ac} denoting the respective initial temperatures. E is the energy function, and $U(T_k, k)$ and $V(T_k^{ac}, k)$ are the generation and acceptance temperature schedules respectively.

The SA procedure given by Figure 2.8 can also be characterized as follows:

- Step 1 - *Initialization*: A random initial solution is assigned to x. The cost function $E(x)$ is the assessed. Initial temperatures $T_k = T_0$ and $T_k^{ac} = T_0^{ac}$ are set, an the time index is set at $k = 0$.
- Step 2 - *Generate*: A probing solution of y given by $y = x + \epsilon$ is generated. ϵ represents a random variable that was sampled using the distribution, $g(\epsilon, T_k)$. This is followed by the assessment of the cost function for the new probing solution $E(y)$.
- Step 3 - *Accept*: Solution y is accepted with a probability of 1 if $E(y) \leq E(x)$; else, it is accepted with probability $A(x \rightarrow y)$, i.e. make $x = y$ only if $A > r$. r here represents a random variable sampled for a uniform distribution $[0, 1]$. Return to step 2 until the number of inner iterations N (specified by the user) is reached i.e. when the *equilibrium criterion* is satisfied.
- Step 4 - *Decrease temperatures*: The temperatures are reduced according to the schedules $U(T_k, k)$ and $V(T_k^{ac}, k)$, and the time index k is incremented.
- Step 5 - *Stopping*: Finally, the algorithm will stop as soon as the stopping criteria is met. Otherwise, it will return to step 2.

2.3.3 Particle Swarm Optimization (PSO)

Like GA, PSO is also a population based stochastic optimization search technique. The algorithm however, has no complicated evolutionary operators such as crossover, selection and mutation and thus, it has the ability to converge faster as compared to the other evolutionary methods [51]. It is called a behaviorally-inspired algorithm as opposed to GAs which are called evolution-based algorithms [52]. This is due to the fact that, the PSO algorithm is based on the social behavior of living things such as a swarm of insects like bees, ants and wasps, a flock of birds, or a school of fish [41, 53, 52]. The algorithm simulates the behavior of swarms and uses the swarm intelligence concepts whereby multi-agent systems such as bees or wasps share information during the search to benefit all. The performance of each individual agents (particles) is measured using a fitness or an objective function just like evolutionary algorithms.

In PSO, a swarm consists of a set of volume-less particles (a point) moving in a multi-dimensional search space, each representing a potential solution. Each particle occupies a particular position and flies or moves with an adaptable velocity within the search space. The position and the velocity of each particle can be adjusted according to (or relative to) its own movement as well as that of its companions. The particles remember their past and best positions ever attained and this helps the algorithm to search the multi-dimensional space faster. Figure 2.9 shows the concept of the movement of particles of PSO within a search space and Figure 2.10 gives schematic illustrating the basic PSO algorithm.

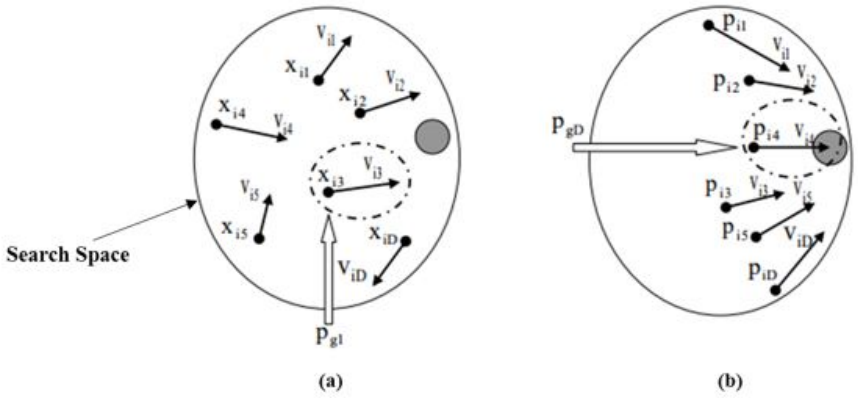

Figure 2.9: Representation of PSO algorithm: (a) Initialization (b) Particles movement towards solution which is given by the grey circle [54].

The parameters of the PSO algorithm in the figure above are described as follows [54]:

- The i^{th} particles are represented by the vector: $X_i = [x_{i1}, x_{i2}, ..., x_{id}, ..., x_{iD}]$.
- The best fitness value (or the best value of the objective function) of the i^{th} particle is given by the best previous position of the particle which is represented as $P_i = [p_{i1}, p_{i2}, ..., p_{id}, ..., p_{iD}]$.
- $P_g = [p_{g1}, p_{g2}, ..., p_{gd}, ..., p_{gD}]$ represents the global best particle in the swarm i.e. the particle which is closest to the solution relative to all particles in the search space.
- The velocity or rate of change of the position of the i^{th} particle is represented by $V_i = [V_{i1}, V_{i2}, ..., V_{id}, ..., V_{iD}]$.

2.3.4 Ant Colony Optimization(ACO)

An ACO algorithm is a swarm intelligence based multi-point search method in which a colony of artificial ants cooperates in finding solutions (i.e. food in real life). The simulation of the algorithm was developed based on the communication and coordination of real ants called stigmergy [55], which is defined as an indirect coordination between agents or actions, where the trace left in the environment by an agent stimulates the performance of a subsequent agent (agents in this instance refers to ants).

When traveling to and from the food source, ants deposit a chemical substance that forms trails called pheromone. The ants are then guided by the quantity of the pheromone on the trails to find the food source. Figure 2.11 shows the behavior of real ants seeking a path to and from their nest and the food source. From the figure; A. Ants follow a path between the nest and a source; B. An obstacle is placed on the path and the ants can choose whether to turn left or right with equal probability; C. Pheromone is deposited more quickly on the shorter path; D. All the ants end up choosing the shorter path.

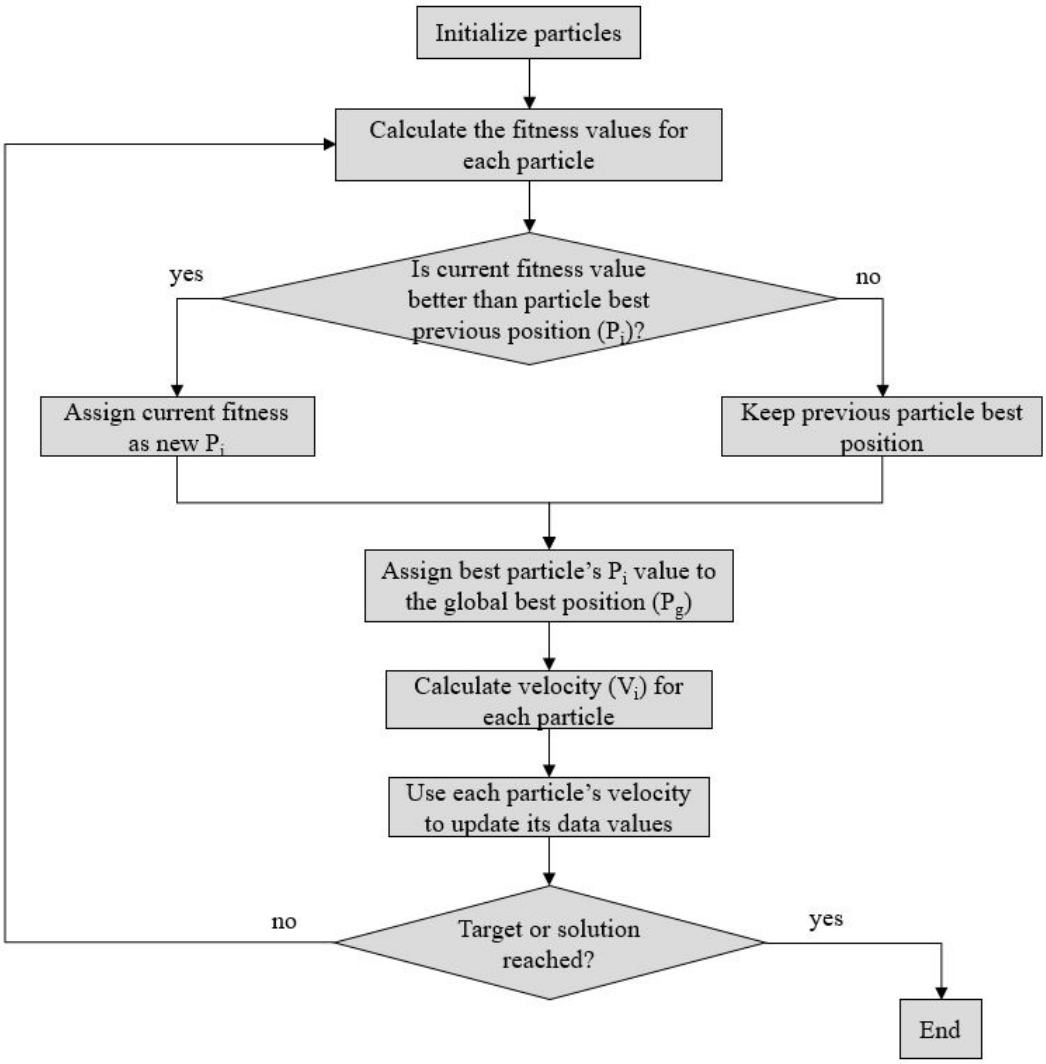

Figure 2.10: Schematic of the basic PSO algorithm.

The artificial ants in ACO algorithm also simulate pheromone deposition and use it to solve problems. This is achieved by modifying appropriate pheromone variables associated with the problem states they visit while trying to construct solutions to the optimization problem [57]. The ACO has been used successfully to solve numerous optimization problems. In most cases, however, the algorithm has been found not as powerful as other heuristic search methods [58].

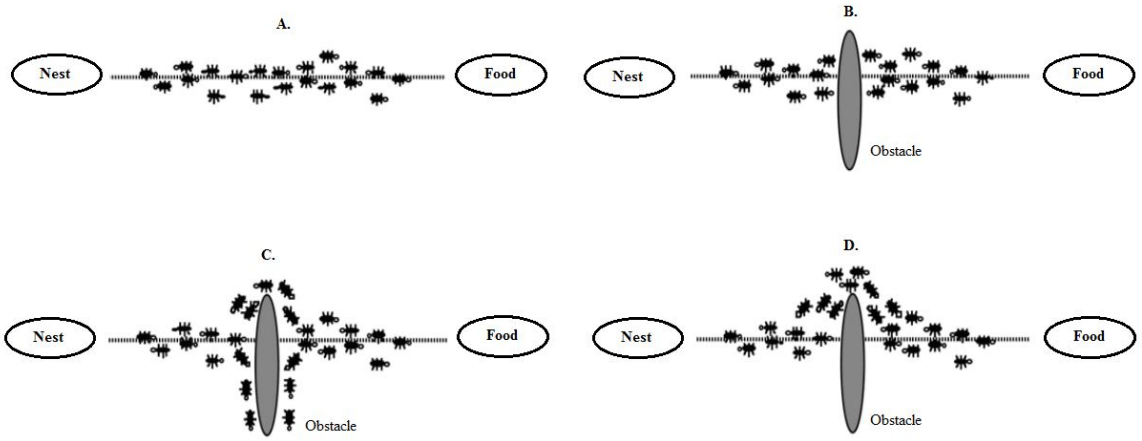

Figure 2.11: Behavior of real ants in search of food [56]

2.4 Application of Stochastic Search Methods to Nanocomposites Design

This section discusses the applications of the stochastic search techniques that have been used over the years to solve composite materials optimization problems. As mentioned before, there is not enough work on the use of optimization methods to optimize the properties of nanocomposite materials. In addition, there is no work on the optimization of nanocomposites using the four major factors that the author of the current study know of. Therefore, this section will only present literature that is based on obtaining optimum solutions for design parameters such as volume fractions, fiber orientations, plies' stacking sequence, fabrication procedure, etc. for the optimization of both traditional composite materials and nanocomposite materials.

Khandan et al. [21] used SA to develop a new methodology that could be used for minimizing the thickness of laminated composite plates by optimizing the fiber orientations for different load cases. Their study focused on the effects of transverse shear forces experienced by the plate. The optimization algorithm proved to be reliable as it was able to locate global optimum points of the laminate design regardless of the initial points given to it. The obtained numerical results were found to be in agreement with the experimental results. To validate the methodology, the numerical results were further compared to the results of the previous research with specific loading cases.

Ertas and Sonmez [23] also used a variant of SA to obtain optimum fiber orientation to maximize the fatigue life of composite materials subjected to various in-plane loads. The objective function used for the optimization was based on the fatigue-life prediction model proposed by Fawaz and Ellyin [59] and the design variables were taken to be fiber angle, biaxial loading and the ratio of the minimum and maximum stresses experienced by the material. The algorithm was given random initial conditions for a number of runs and in almost all the runs, the algorithm obtained similar design variables results. Thus, the algorithm was consistent in obtaining the optimum designs and therefore proving its reliability in solving optimization problems.

Awad et al. [60] used Multi-Objective Simulated Annealing (MOSA) together with Finite Element (FE) to find the optimum fibre orientations for minimizing the cost and the structural panel weight of a two-way fibre-reinforced composite sandwich panel. The optimized panel was found to have an acceptable safety factor and its service deflection was within the allowable limit. Thus, the proposed approach managed to successfully reduce the cost and the weight of the sandwich panel.

Rostamiyan et al. [61] applied a combination of Central Composite Design (CCD) model based objective functions and the GA to maximize the compressive strength, the tensile strength and the fracture toughness of epoxy/high-impact-polystyrene nanocomposites by finding the optimum content of the different constituents of the nanocomposite material. The optimization results showed a significant increase in the targeted mechanical properties of the material.

Moghri et al. [46] proposed a methodology for finding optimal materials and processing parameters (i.e. melt temperature, nanoclays content, feed rate and screw speed) to maximize tensile modulus and tensile strength of injection-molded Pa-6/clay nanocomposites. The two objectives were maximized by using GA code implemented in MATLAB and the Response Surface Method (RSM) based objective function. The authors observed an acceptable agreement between the values of the process parameters predicted by the optimization algorithm and those that were obtained through experiments. The study showed that the GA can be used with the RSM to effectively find the optimum process variables for maximizing tensile properties of polymer/clay nanocomposites.

Vo-Duy et al. [62] used a variant of GA called the Fast Non-dominated Sorting Genetic Algorithm (NSGA-II) to minimize the weight of laminated composite beams whilst maximizing their natural frequency by simultaneously finding the optimum values of the design variables; fiber volume fractions, thickness and fiber orientation angles of the laminates. The fiber volume fraction was taken to be a continuous design variable subject to a constraint on the manufacturing process while the thickness and the fiber orientation angles were taken to be discrete variables. Results from three numerical examples were compared to results from previous studies to demonstrate the reliability and effectiveness of the authors' proposed approach.

Pelletier et al. [63] also used NSGA-II to optimize laminated composite materials. The algorithm was used to obtain optimal designs for two model problems having conflicting objectives. The first model's objective was the maximization and minimization of load carrying capacity and the mass of the laminates that is subjected to biaxial moments. The objective of the second model was to maximize the rigidity while minimizing the mass of the composite laminates respectively. The design variables for both optimization problems were chosen to be fiber orientations, fiber volume fractions and the thicknesses of the laminates respectively. The obtained results showed the effectiveness of the proposed methodology for the multi-objective optimization of composite materials.

Koide et al. [55] used an ACO algorithm to develop a methodology for obtaining the optimal stacking sequence of laminated composite plates. The developed methodology was evaluated on four different examples for symmetric and balanced lay-up of the laminates. Classical lamination theory was used to obtain the structural response of a rectangular plate for the first three cases. The results were compared to those obtained from the literature through GA. The fourth case was to maximize the fundamental frequencies of the rectangular plates with central holes through structural response obtained by FE analysis. The obtained results showed that the optimization technique may be successfully applied for design of laminated composites materials.

Chen et al. [51] developed a Reliability Based Design Optimization (RBDO) method for composite structures by combining PSO and FE. The methodology includes three modules: stress analysis by ANSYS, reliability calculation and optimization using MATLAB optimization toolbox. A qualified RBDO for composite materials requires an optimization technique that can efficiently find global solutions, and that is the reason PSO was selected by Chen and co-workers. Using this methodology, the authors worked out numerical examples for reliability design of a laminate and a cylindrical shell. The examples showed that the proposed method has a good good stability and is efficient in dealing with optimal design of composite structures. In addition, the design case of a composite pressure vessel was studied to further demonstrate the effectiveness of the method. The design objective here, was to minimize the total weight of the material by obtaining optimum values of the design variables (i.e. the thickness of laminates, fiber orientation angles and the wrap angle of the helical layer). It was found that the thickness of the optimum structure increases with the increase of the internal pressure. The wrap angle of the helical layer in the cylindrical region was also found to be increasing with the increase in load. From the results, it could be concluded that the method may serve as an effective tool for optimizing complex composite structures.

2.4.1 Comparison of Stochastic Multi-Objective Techniques

Table 2.1 shows a comparison of the optimization methods. Furthermore, the table shows the solution cost (the measure of the methods computational efficiency in obtaining the solution), the type of solution the method provides and the overall ranking of the method. A good optimization method is the one with the following characteristics:

- Low cost in obtaining the solution
- High overall ranking
- Obtains a global optimum solution

Table 2.1: Comparison of Optimization methods [41]

Method	**SA**	**GA**	**PSO**	**ACO**
Solution Cost	Low	Low	Less than GA in single objective only	Moderate
Optimum Solution Remark	Global	Global	Convergence difficulties	Good Performance
Overall Ranking	Moderate	High	High	Moderate

From the Table 2.1 it can be seen that both GA and SA are capable of obtaining global optimum solutions to problems, PSO is reported to have difficulties in converging to an optimum solution and the ACO generally has good performance though it does not always guarantee a global optimum (i.e. it can be trapped in a local minimum from time to time). Even though the PSO has a high overall ranking just like GA, it has tendencies of having high computational cost when solving MOO problems [41].

Numerous research works have cited GA and SA to be the most popular stochastic search optimization methods [47]. The review of the application of the methods presented in the previous section shows that the presented methods are all capable of solving various composite materials design problems. However, it has been well documented that GA are more suited for materials design problems when compared to the other methods [64]. The is because the algorithm is capable of handling complex problems with large design parameter search spaces. In addition, GAs possess the ability for adaptation given a particular computational problem. Furthermore, the algorithm can be applied to solve a variety of optimization problems in which the objective function is discontinuous, non-differentiable, stochastic and or highly non-linear [65]. Hence, in this work, GA is selected for the optimization of the mechanical properties discussed above. The validity and accuracy of the model is assessed by comparison to experimental results of mechanical properties from previous studies.

2.5 Multi-Objective Optimization (MOO) Problems

In this section, MOO is introduced and briefly described. In addition, a general MOO problem is presented. Multi-objective optimization is described as the minimization or maximization of more than one objectives subjected to a number of constraints. A general numerical optimization problem is given as follows:

$$Optimize : F(X) \tag{2.1}$$

$$Subject\ \ to : X = [x_1, x_2, ..., x_n] \tag{2.2}$$

$$X_{low} \leq X \leq X_{upp} \tag{2.3}$$

$$g_i(X) \leq 0, i = 1, 2, ..., q \tag{2.4}$$

$$h_j(X) = 0, j = 1, 2, ..., q \tag{2.5}$$

where,

$$F(X) = [f_1, f_2, ..., f_n]^T \rightarrow R^k$$

represent the objective function to be either minimized or maximized and X is a vector containing the design variables defined in the design space R^k. Subscripts k and n represent the number of objective functions and the dimension of the design space respectively. X_{low} and X_{upp} represent the lower and upper constraints of the design variables. Functions $g_i(X)$ and $h_j(X)$ are the i^{th} and the j^{th} inequality and equality constraints respectively. eqs. (2.1) to (2.5) define the feasible solution, S, in the design space.

Unlike the case of single-objective optimization, MOO problems have multiple number of solution points which are called Pareto-optimal solutions. Thus, dealing with these type of problems involves finding a set of optimal solutions for the given objectives. Hence, solving MOO problems requires finding the best trade-off solution among a pool of solutions.

From a computational point of view, this process is not as straightforward as finding a solution for a single objective optimization problem. This is because single objective optimization algorithms presuppose that the designer is able to aggregate the objectives into a single function expressing the relative importance of each design criterion. The designer is then required to specify preferences such as weighting coefficients prior to solving the optimization problem. It is worth noting that this *a priori* knowledge is usually hard to translate into quantitative information and the choice of the weighting coefficients is somewhat arbitrary [66]. The solution is thus strongly dependent on these user-defined preferences.

Pareto based algorithms which have been studied extensively during the last decade to solve for MOO problems allows the decision-maker to choose among many optimal solutions. These algorithms do not require any quantitative *a priori* information. Therefore, the decision concerning the optimal design can be made *a posteriori* [66]. A set of optimal design solutions for MOO problems are known Pareto optimal solutions [67]. Pareto based algorithms are characterized by the following:

- **Pareto Dominance**
  Pareto optimal solutions are expressed in terms of non-dominated points in the solution space. A Pareto-Optimal solution is a solution that cannot be improved with respect to any objective without worsening the other objectives [45]. Considering the above given optimization problem by eqs. (2.1) to (2.5), a solution $X_1 \in S$ dominates a solution $X_2 \in S$, if solution X_1 is not smaller than X_2 in all objectives and the solution X_1 is strictly smaller than X_2 in at least one objective (i.e solution X_1 is referred to as the non-dominated solution whereas, solution X_2 is regarded as the dominated solution, see example in Figure 2.12 for an illustration of the concept of Pareto-Dominance)

- **Pareto Optimal**
  A solution $X_1{}^* \in S$ is Pareto-Optimal if and only if it is not dominated by any other solution in S. A set or collection of all Pareto optimal solutions is called a Pareto-Optimal Set. The corresponding objective function values in the feasible region or objective space are called Pareto-Front and represents a solution of the MOO problem.

Figure 2.12 illustrates the Pareto concept of optimality for the case of a problem with two objectives. The problem has three non-dominated solution points (1, 2 and 3) belonging to a Pareto-Front. Here the optimal solution points could not be moved from 1 to 2 (or 3) or vice versa without decreasing or increasing any one of the given objectives within the solution space. Based on the above reasoning, the three points on the Pareto-Front could be defined as equally good non-dominated solution points. However, solution points 4 and 5 (dominated solutions) are not better than the points lying on the Pareto-Front. Thus, they do not form part of the Pareto Optimal Set (i.e. the solution to the given MOO problem).

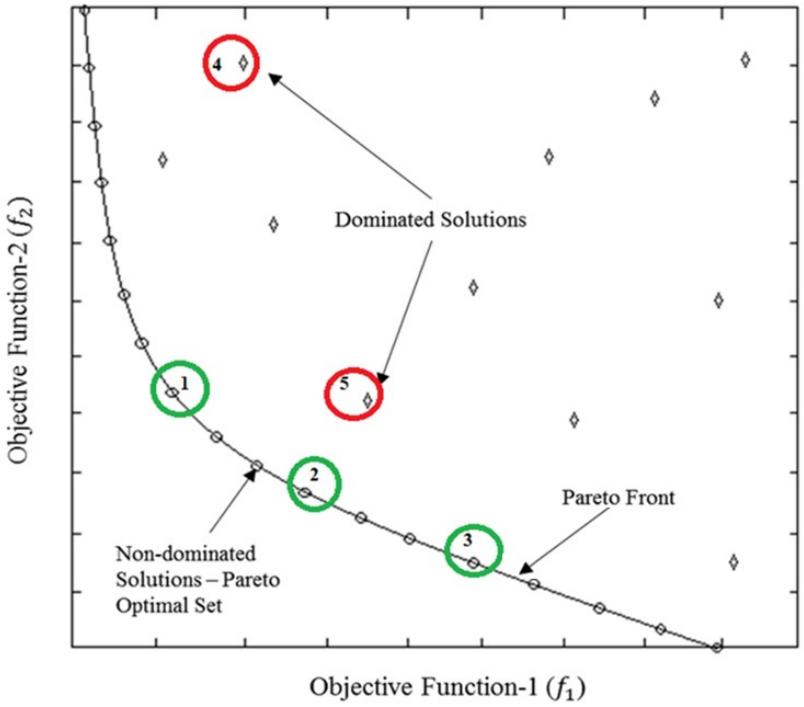

Figure 2.12: Pareto-front for two-objective optimization problem in objective space

2.5.1 Application of GA to MOO Problems

The generic GA described in section 2.3.1 addresses a case of solving a simple single optimization problem. Thus, the algorithm is modified for implementation on MOO problems. There are many variations of multi-objective GA in the literature [45]. Some of the variations that have been developed over the years include Vector Evaluated Genetic Algorithm (VEGA), Multi-Objective Genetic Algorithm (MOGA), Pareto Envelope-based Selection Algorithm (PESA) Non-dominated Sorting Genetic Algorithm (NGSA) and NSGA-II which is a variant of the NGSA. The basic approach of all GA variants for solving MOO problems is similar to that of solving simple single-objective problems. However, the algorithms differ based on their objective function selection procedure, elitism (i.e. guaranteed selection of most 'fit' individuals to the next generation) and diversification (the type of mutation the algorithm uses for mutation) when solving problems [45].

The NSGA-II is selected for the current work. This is due to the fact that the algorithm has proved itself as a very powerful tool for solving real application engineering MOO problems [68]. The original NGSA was first presented by Srinivas and Deb [69] whereas the NSGA-II was developed by Deb et al. [70]. The main advantages of NSGA-II over other variants of multi-objective GAs are given as follows [68]:

- The algorithm is relatively simple
- It provides a better convergence to a Pareto-Front solution
- It has relatively low computational cost
- It provides a wider distribution of solutions along a Pareto-Front

The NSGA-II is operated on the concept of Pareto domination rank. This means that the individuals of a particular generation during optimization are selected on the basis of their domination rank in the population [66]. By default, the algorithm assumes a minimization problem and therefore when two individuals are compared for selection, the one with the smallest rank wins. The processes of crossover and that of mutation remain unchanged. Crowd distance (i.e. the measure of local sparseness in the population) is used for the individuals with equal rank. The distance is also used for the diversification of the population. During the optimization process individuals

with the largest crowding distance are favored. As a result, individuals lying in a region where they are closer to one another are penalized to avoid premature convergence.

2.6 Modeling the Mechanical Properties

In this section, the theoretical modeling of mechanical properties (elastic modulus and tensile strength) of polymer based nanocomposite materials is introduced and discussed. Furthermore, the different types of models developed for determining these mechanical properties are compared. The best models will then be used for the formation of the objective functions to be used for the optimization of the nanocomposite design problem.

In recent decades, there has been an immense acceleration of growth in the development of reinforced polymer nanocomposites and their applications. As a result, great attention has been given to the behavior of the nano-mechanical parameters so as to have a better understanding of the structure-property relationships that exist in polymer nanocomposites. The combination of the nanofillers and polymer matrix properties ideally results in a nanocomposite material that have properties (i.e. enhanced stiffness, strength and thermal properties) distinct to those of the constituents. The factors that mainly affect the final properties of the resulting nanocomposite include nanofiller content, orientation factor, dispersion, interphase and interfacial adhesion.

From a mechanical point of view, further development and optimization of nanocomposite materials requires experimentation and application/development of theoretical models for measurement and prediction of properties, such as stiffness, strength, fracture toughness and coefficient of thermal expansion. As mentioned before, the mechanical properties of interest for the current work are the elastic modulus and the tensile strength. For this purpose, the theoretical modeling of the elastic modulus and its parameters will be discussed first and then followed by the modeling of the tensile strength. The two properties will form the first and the second objective functions for the optimization problem respectively.

2.6.1 Modeling the Elastic Modulus

The elastic modulus (or the Young's modulus) is the stiffness of a material and it defines the relationship between the stress and the strain at the elastic stage of a tensile test. The elastic modulus of nanocomposites can be improved by the addition of micro and nano fillers to a polymer matrix due to the fact that the fillers have much higher stiffness values as compared to those of the matrix.

Many analytical models and techniques have been developed over the years for the quantification of mechanical parameters and the estimation of the elastic modulus of composite materials. The development of these models has taken two approaches i.e. two-phase and three-phase models. In this section, the two approaches are discussed together with some of the commonly known micromechanical models. The models will then be compared and the best suitable model for the current study will be selected.

i). Elastic modulus prediction models for polymer nanocomposites

The two-phase models approach ignores the interphase region and the interfacial bond between the nanofiller and the matrix. These models assume a perfect bonding condition at the interphase; they assume that the bond between the matrix and the nanofiller is perfect and can be modeled using the continuity of tractions and displacements across a discrete interphase [71]. As a result, they suffer from lack of accuracy in the prediction of the properties. This is due to the fact that the interphase region properties can significantly affect the overall properties of the nanocomposite materials. It is also worth noting that the two-phase models were originally developed for the prediction of the elastic modulus properties at microscale level rather than nanoscale. Some of the most popular classical or micromechanical two-phase models for the prediction of polymer based composites are summarized below. Einstein developed an equation for the prediction of the Young's modulus of particulate composites based on the rigid filler (or particle assumption). The equation is given as follows [72]:

$$\frac{E_c}{E_m} = 1 + 2.5V_f \tag{2.6}$$

where, E_c and E_m are the Young's modulus of the composites and matrix, and V_f is the filler volume fraction.

It was found that Equation 2.6 is only valid for low concentrations of the fillers. Furthermore, the equation also assumes perfect dispersion of individual fillers and a perfect adhesion between filler and matrix [73]. In addition, the equation predicts a linear relationship between E_c and V_f. Thus, over the years, several modifications were made to the Einstein equation.

Halpin and Tsai's work found that the elastic modulus of polymer composites can be determined by using semi-empirical relationship [74]. The modified version of the model has been reported in the literature to give reliable estimates for the elastic properties of composite materials. Furthermore, the model has often been applied for comparison with experimental test results [75]. Equation 2.7 gives the modified version of the Halpin-Tsai model which was developed to incorporate the shape and the orientation of the fillers.

$$\frac{E_c}{E_m} = \frac{1 + pqV_f}{1 - qV_f} \tag{2.7}$$

$$q = \frac{(\xi E_f/E_m) - 1}{(\xi E_f/E_m) + 2p} \tag{2.8}$$

where, p and q represent the constants for a given composite. Constant p is a function of the filler shape and the Poisson's ratio, and q is related to the modulus of the filler (E_f) and the matrix (E_m). The orientation factor is given by ξ which equals unity in the original equation and 1.6 for composites with three dimensional random orientation of fillers.

Voigt and Reuss developed models for determining the Young's modulus of a two-phase composite material containing continuous fibres and matrix in parallel and series arrangements respectively. The two models provides the upper and lower bounds of elastic modulus of composite material respectively as follows [76]:

$$\frac{E_c^{upp}}{E_m} = E_f V_f + E_m(1 - V_f) \tag{2.9}$$

$$\frac{E_c^{low}}{E_m} = \frac{E_f E_m}{[E_f(1 - V_f) + E_m V_f]} \tag{2.10}$$

The given equations are commonly known as the Voigt-Reuss model and they are applicable to most micro composite materials [76]. Generally, the modulus of composites should be lower than the upper bound predicted by Equation 2.9 and higher than the lower bound predicted by Equation 2.10 [77]. However, there is a possibility for the materials to violate these bounds due to Poisson's effect whereby the filler size varies in a range of between 12 and 50 nm [78].

The other technique for approximating the elastic modulus of composite is called the modified rule of mixtures (MROM) which is an extension of the classical rule of mixtures (ROM). The modification to ROM was introduced by Fedelus et al. [79] to incorporate filler orientation and distribution. The modified model showed a good agreement between measured and predicted modulus at high filler volume fractions.

However, at very low volume fractions, dispersion of the fillers becomes challenging due to the increased interaction between the polymer matrix and the fillers. As a result, composite materials experience formation of agglomeration of the fillers which are not accounted for by the model. Hence, the model was found to be inaccurate in predicting the elastic modulus of composites at low volume fractions. The simple MROM is given by Equation 2.11. Reference [80] presents another modification of the rule of mixtures accounting for dispersion and agglomerations of nanocomposite materials.

$$E_c = \eta E_f V_f + E_m(1 - V_f) \tag{2.11}$$

where, η represent the filler orientation factor, which is also known as the Krenchel [81] factor of orientation.

Classical micromechanical techniques such as Mori–Tanaka method [82], self-consistent method, differential method and other approaches based on the concept of effective medium or effective field can be used for predicting the effective modulus of composites. These techniques however, with few exceptions, neglect the precise locations and orientations of fillers. Therefore, their applications are limited to solids that are statistically homogeneous and subjected to uniform tractions or displacements on their surfaces [76].

Independent works of [29, 83, 84] found that the elastic moduli of several polymer nanocomposites were very high such that the two-phase models are unable to predict this mechanical property. It was discovered that the two-phase models lack accuracy in prediction of the properties due to a number of issues pertaining to the assumptions when they are formulated. Takanayagi et al. [85] observed a formation of microfibrils (fine fiber like strands) with diameters ranging between 10 and 30 nm. They further noticed that the microfibrils were more influential at the boundaries of the interphase region. Their work concluded that there is a critical filler size of about 30 nm and below which composite modulus increases. This proves that the interphase region is critical and should not be neglected in the modeling of the mechanical properties of composites.

2.6.2 Modeling the Tensile Strength

The strength of a material refers to the maximum stress that the material can support under uniaxial tensile loading. For polymer based composite materials, this property is dependent on the effectiveness of the stress transfer between the fillers and the polymer matrix, again showing that the interphase region plays a critical role in the properties of nanocomposite materials. In this section, the theories and models for predicting the tensile strength of nanocomposites are briefly discussed.

i). Tensile strength prediction models for polymer nanocomposites

The tensile strength properties of nanocomposite materials depends on the weakest fracture path throughout the material. This weakest path determines the load carrying capacity (strength) throughout the structure of the nanocomposite material. Thus, the strength of nanocomposites is mainly dependent on the fracture behaviors which are associated with parameters such as the interphase adhesion, stress concentration, defects and dispersion or distribution of the matrix reinforcements.

Liang et al. [86] argued that the tensile strength models for polymeric materials filled with nanoparticles is largely dependent on the properties of the interfacial layer (region) found in between the fillers and the matrix. Their study also concluded that the degree of bonding within the interfacial region is usually categorized into poor adhesion, good adhesion and to a greater extent, the properties of the matrix materials (ductility

and brittleness) and the shape and surface modifications (or pre-treatment) of the nanoparticles.

These nanoparticles (or reinforcing fillers) affect the material's tensile strength in two ways (i.e. the weakening of the material due to the formation of stress concentration and also the reinforcing of the material through the prevention of crack propagation) [76]. For the given effects, if the weakening of the material is more predominant, the resulting nanocomposite material's strength will be lower than that of the matrix, whereas if the reinforcing effect is more prevalent, then the material will have strength higher than the matrix. This makes the prediction of the tensile strength of nanocomposites difficult as the property is not necessarily dependent on the statistical averaged values of the material.

In addition, just like the elastic modulus, the many techniques that have been developed for the prediction of the tensile strength do not take into account the effective parameters of the mechanical properties of polymer nanocomposites [87]. Hence, even though there are many published theories, there is still no universally accepted theory to date [76]. The approach of modeling these tensile strength models for composite materials is similar to that of the elastic modulus [88, 89, 76]. Some of the models that have been developed for determining the tensile strength of polymer nanocomposites are given and briefly discussed in this subsection.

The simplest form of the tensile strength model for polymer based composites was formulated and proposed by Danusso et al. [90]. The model assumes that there is poor (or no adhesion) between the matrix and the fillers. Thus, the stress cannot be transferred from the matrix to the filler and that the strength of the material can be obtained through the effective sectional area of the matrix in the absence of the fillers. The model is given as follows:

$$\sigma_c = \sigma_m \left(1 - V_f\right) \tag{2.12}$$

where, σ_c and σ_m represent the strengths of the composite and the matrix, and V_f is the filler volume fraction respectively. Equation 2.12 indicates that the strength of polymer composite materials decreases linearly with increasing filler loading. However, the results from tests conducted by Nicolais et al. [91] showed that the relationship between the composite strength and the filler volume fraction is not always linear.

Thus, the authors developed a new model by replacing the volume fraction by a power law function of the volume fraction as [91]:

$$\sigma_c = \sigma_m \left(1 - dV_f{}^e\right) \tag{2.13}$$

where, d and e are constants that depends on the filler shape and the arrangement of the fillers within the matrix. Over the years, the simple models that assumes poor adhesion have been constantly modified as to improve the accuracy of predicting the tensile strength.

For example, Bigg et al. [92] developed the tensile strength model with the consideration of some adhesion between the filler and the matrix as follows:

$$\sigma_c = \sigma_m \left(1 - dV_f{}^e + uV_f{}^v\right) \tag{2.14}$$

where, u and v are constants, and d and e represent the same constants as given in Equation 2.13 respectively. Leidner et al. [93] also developed the tensile strength model which assumes a strong filler-matrix adhesion (i.e. good adhesion), the contribution of friction between the filler and the matrix, and the residual pressure. The model further assumes that the stress within the composite is transferred through shear from the matrix to the fillers. Leidner's model for the tensile strength of polymer composites is given as follows:

$$\sigma_c = 0.83PF_rV_f + k_p\sigma_m \left(1 - V_f\right) + \sigma_i G \left(1 - V_f\right) \tag{2.15}$$

where P is pressure, F_r is friction coefficient, k_p is the relative change in strength due to the pressure of the filler, σ_i is the filler-matrix adhesion strength and G is a constant. It is worth noting that the given models were primarily developed for micro scale instead of nanoscale and thus, it has been often found that most of these models obtained inaccurate results for nanocomposite materials. Furthermore the models do not cover all the major effects affecting the tensile strength of nanocomposites. For example, Equation 2.15 considers the properties of both matrix and fillers and the interphase region, however it does not consider dispersion and orientation of fillers.

2.7 Summary of the models for mechanical properties of polymer nanocomposites

From the above discussions, the issues associated with the two phase models for determining the elastic modulus of polymer based nanocomposite materials include the following;

- The negligence of the interphase and the interfacial adhesion between the fillers and the polymer matrix
- The models assume perfect and uniform dispersion of the fillers
- The models cannot be applied successfully to composites materials with very low volume fractions
- Lastly, the models fail to accurately predict the elastic modulus at small filler sizes (i.e. at nanoscale)

As a result, over the past years, new models for the elastic modulus that addressed the given issues were developed. These models are commonly known as three-phase models, primarily due to the fact that their approach to the estimation of the properties of composites account for the three distinct phases of the material (i.e. the matrix, the interphase and the filler).

Models for the tensile strength also have shortcomings in that they do not consider all the major factors affecting the property. Even though some models consider some of the factors, it has been found that those factors (i.e. pressure due to the presence of fillers in the matrix or friction) are not significant. This therefore, results in inaccuracies of the predictions.

Hence, the focus on the current study will be placed on the models that consider all the major influences of the mechanical properties of nanocomposite materials. That is, the models that consider the three phases of the polymer nanocomposite, the dispersion of the nanofillers, the orientation of the nanofillers, nanofillers loading and the interfacial adhesion. The models used in the current work are given and discussed in the following chapter. Figure 2.13 shows the three-phases of a nanocomposite material.

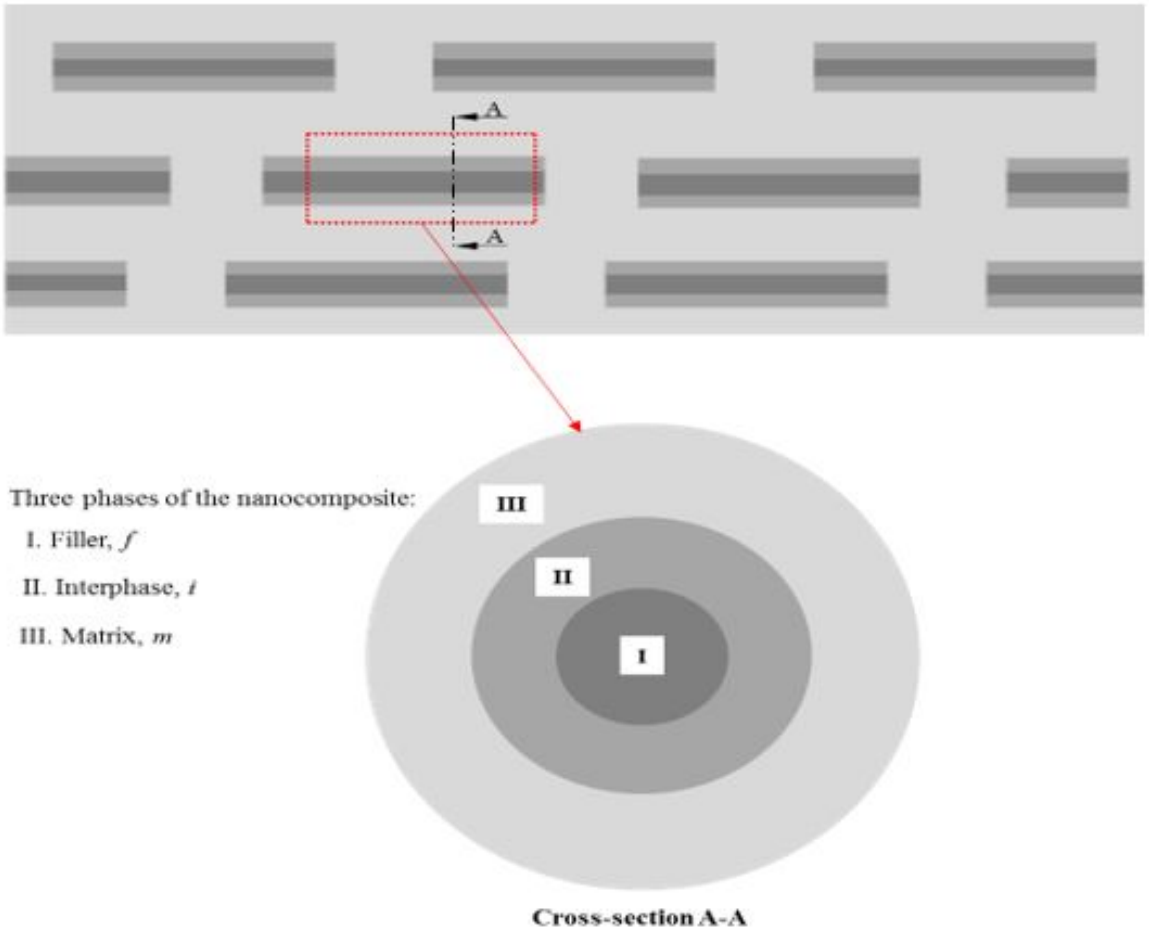

Figure 2.13: Schematic of a nanocomposite illustrating the three-phases of the material

Chapter 3 Methodology

This chapter gives a detailed procedure used for the analysis of MOO of polymer nanocomposite's elastic modulus and tensile strength. Figure 3.1 shows a flow chart of the approach used in the current study. The approach is divided into three main steps as given below:

(i) Nanocomposite design model

The first step describes the analytical modeling of the properties of polymer based nanocomposite materials and the design problem or (statement) generation. It can be seen from Figure 3.1 that this involves modeling the two objectives (i.e. elastic modulus and the tensile strength) which are to be optimized and the identification of the design parameters that are to be used for optimizing those objectives.

The formation of the objective functions and the specification of the design variables precede the conversion of the nanocomposite design statement onto a mathematical statement. As soon as the objective functions are formulated, a MATLAB m.file script (code) to be used for optimization simulation is then written. It should also be noted that this step also includes the identification of the materials properties to be used during the optimization procedure.

(ii) NSGA-II MOO problem solving procedure in MATLAB

The second step covers the main procedure for optimization of the nanocomposite material design problem within the MATLAB environment. In this step, the Fast Non-Dominated Sorted Genetic Algorithm (NSGA-II) is employed to solve the problem described in the previous step.

This step involves the usage of the m.file MATLAB code containing the objective functions of the nanocomposite design problem. Furthermore, the number of the design variables are specified in this step. The other important aspect of this step is to outline the critical parameters or the structure of the applied algorithm as it can be observed in Figure 3.1. The optimum values of the objective functions together with the design variables are obtained in this step. Thus, it can be regarded as the most important step of the current study.

(iii) Analysis and validation of optimum results

In this step, the obtained optimum results of the objective functions and the design variables are analyzed, interpreted and discussed. The accuracy of the model and the validity of the results are also tested through comparison with data from previous studies.

3.1 Nanocomposite Design Optimization Problem

An introduction of the nanocomposite design problem and a detailed discussion on the formulation of the elastic modulus and tensile strength objective functions is given in this section. The section further presents the discussion and characterization of the design parameters associated with the respective objective functions.

First, the design parameters influencing the properties of nanocomposites are identified and expressed in terms of the optimization design variables. The constraints (or boundaries) of the design variables are also outlined. Then a nanocomposite design problem for maximizing the elastic modulus and the tensile strength is converted (or transformed) into a numerical multi-objective optimization problem using the two objective functions. This is followed by a rationale for the materials selected for the current study and finally, the NSGA-II in MATLAB is used to optimize the given nanocomposite design problem. The results are processed and then validated using the available literature.

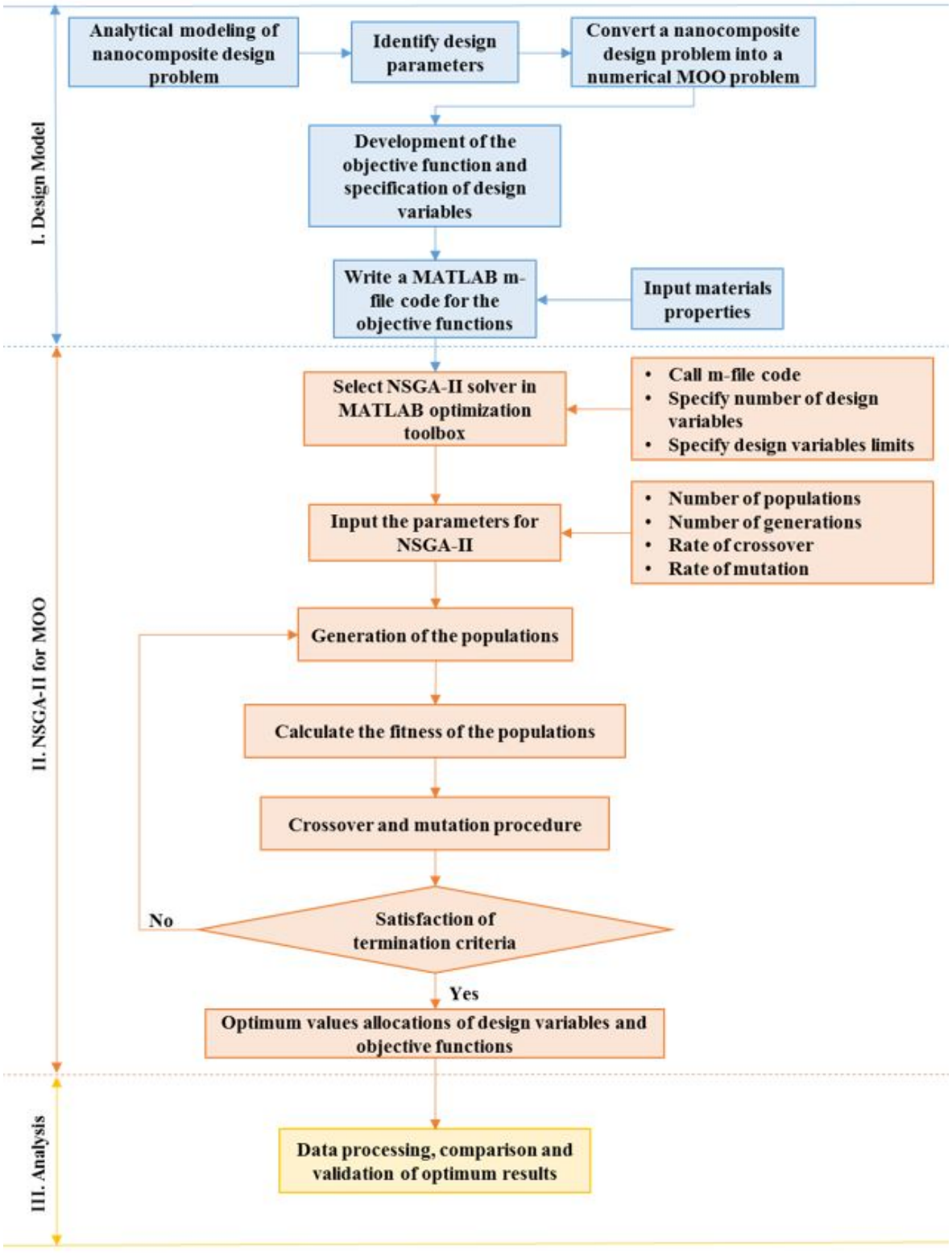

Figure 3.1: Flow chart of the optimization of mechanical properties of nanocomposites

3.1.1 First objective function (f_1)

The first objective function refers to the elastic modulus. Therefore this section covers the modeling of the elastic modulus and the design parameters that influence this mechanical property.

The formulation of the first objective function, f_1 for the MOO follows the identification of the appropriate three-phase model to be used for the prediction and determination of the elastic modulus. To the authors' knowledge, there are currently only two three-phase models for determining the elastic modulus of polymer based nanocomposites; Ji model [94] and Samandari model [95]. The current study however, will focus on Ji model. This is due to the fact that the model could be applied for a wide range of nanofillers shapes as opposed to Samandari model which could only be used for spherical nanofillers. Figure 3.2 shows a representation of the three-phase Ji model and responses to an applied load [96].

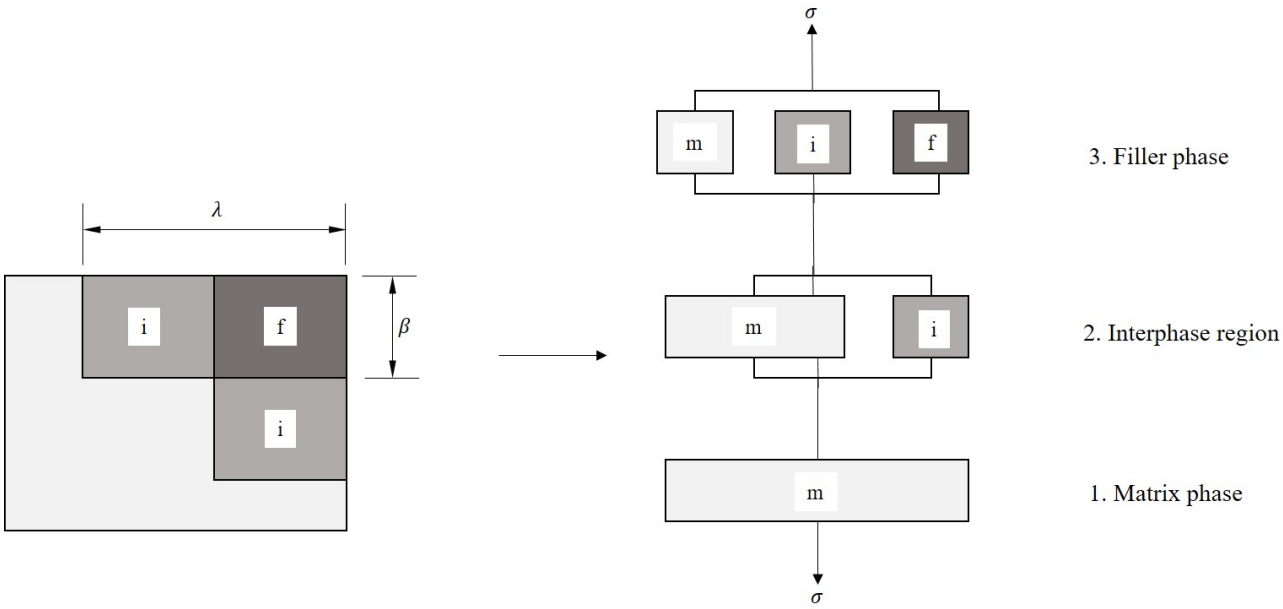

Figure 3.2: Representation of Ji model and the responses to applied load with 'm', 'f' and 'i' denoting respectively the matrix phase, filler phase and interphase regions.

Ji model was developed based on the Takayanagi's two phase model [97] and is given as follows:

$$E_R = \left[(1-\lambda) + \frac{\lambda - \beta}{(1-\lambda) + \frac{\lambda(a-1)}{ln(a)}} + \frac{\beta}{(1-\lambda) + \frac{(\lambda-\beta)(a+1)}{2} + \beta\frac{E_f}{E_m}} \right]^{-1} \tag{3.1}$$

$$E_R = \frac{E_{nc}}{E_m} \tag{3.2}$$

$$\lambda = \sqrt{\left(\frac{2t}{t_i} + 1\right)^2 \theta_f} \tag{3.3}$$

$$\beta = \sqrt{\theta_f} \tag{3.4}$$

$$a = \frac{E_i}{E_m} \tag{3.5}$$

where,

- E_f is the elastic modulus of the nanofiller
- E_i is the elastic modulus of the interphase
- E_m is the elastic modulus of the matrix
- E_{nc} is the elastic modulus of the polymer nanocomposite
- E_R is the normalized elastic modulus i.e. the ratio of the elastic modulus of the nanocomposite to that of the polymer matrix
- a is the ratio of interphase-to-polymer matrix elastic modulus which describes a linear gradient change of modulus from matrix to the surface of the nanofiller
- θ_f is the nanofiller loading
- t is the diameter of the nanofiller

- t_i is the thickness of the interphase

- β is a function of θ_f

- λ is a function of t and t_i respectively

It is worth noting that in the absence of the interphase (i.e. $t_i = 0$), Ji model reduces to the two-phase model of Takayanagi as follows:

$$E_R = \left[(1-\beta) + \frac{\beta}{(1-\beta) + \beta \dfrac{E_f}{E_m}} \right]^{-1} \tag{3.6}$$

Equation 3.1 for predicting the elastic modulus is taken to be the first objective function, for the MOO model of the current study as follows:

$$f_1 = E_R \tag{3.7}$$

i). Elastic modulus design parameters

From eqs. (3.1) to (3.5), the design parameters/variables of the first objective function can be identified as t_i, t, θ_f and E_i respectively. These are the variables that are to be optimized for obtaining the optimum value of the elastic modulus of polymer based nanocomposite materials. The limitations and constraints of the given design variables are briefly discussed in the following paragraphs.

Previous studies on nanocomposites shows that t_i can only vary between 0 - 10 nm [98, 96, 99, 94]. Zare et al. [100] reported that any value of t equal to 1 nm or less is not acceptable for the prediction of the mechanical properties of nanocomposites. Hence for the current work, both t_i and t where taken to range from 1 to 10 nm. The loading of nanofillers is not expected to exceed 10% [95].

Njuguna et al. [11] also showed that the properties of nanocomposites start to significantly deteriorate at loading levels exceeding 10% and in addition, their work concluded that the best nanofiller loading for polymer nanocomposites is approximately 2%. Zare et al. [96] obtained the highest level of polymer-fillers interfacial adhesion and nanofillers dispersion in samples containing 4% loading. Thus, the range of θ_f for the current work was taken to vary between 1 and 5%.

The design parameter a (i.e. ratio of the interphase-to-polymer matrix) is a minimum when the interphase modulus is equal to that of the modulus of the matrix and a maximum when the modulus of the interphase equals that of the nanofillers [94]. From a mathematical point of view, it can be seen that the value of a in Equation 3.1 cannot have a value of unity. Hence, the range of the interphase modulus was selected to be between 1 and E_f to avoid $ln(1)$ which could result in an unsolvable objective function.

3.1.2 Second objective function (f_2)

In the current study, Zare et al. [101] model for determining the tensile strength of polymer nanocomposites is used. The model is primarily chosen because it takes into account the material's interphase properties, nanofiller loading and the orientation of the nanofillers. The approach of the theoretical modeling of Zare model is described below.

According to Kundalwal et al. [102] the applied load to polymer nanocomposites is transferred to the nanofillers by means of shear forces at the polymer matrix-nanofiller interphase region. Furthermore, this load develops a high shear stress zone at the ends of the nanofiller. Figure 3.3 shows a schematic of the applied tensile load and the development of interfacial shear stress along the nanofiller in polymer nanocomposite.

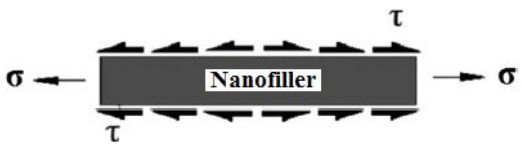

Figure 3.3: Schematic of tensile load and the development of interfacial shear stress along a nanofiller in polymer nanocomposite [101].

The breaking of the nanofillers causes its total length (L) to decrease, thus a critical length (L_c) is obtained as the maximum nanofiller length that can no longer be fractured by the stress transfer through the polymer matrix and nanofiller interphase. This means that for $L < L_c$, the shear stress transferred to nanofiller through the interphase is not large enough to reach the failure stress. However, for a case where L is greater than the L_c, the nanofiller will be pulled out of the polymer matrix before it fails. This therefore shows that the strength of the nanocomposite is significantly dependent on L_c, which is expressed as follows:

$$L_c = \frac{\sigma_f r}{\tau} = \frac{\sigma_f L}{2\tau\alpha} \tag{3.8}$$

where,

- r is the radius of the nanofillers and it is equal to $0.5t$
- α is the aspect ratio of the nanofillers which is given as the ratio of nanofiller length to that of the diameter
- σ_f is the tensile strength of the nanofiller
- τ is the interfacial shear stress

When $L < L_c$, the tensile strength of a polymer nanocomposite can be determined by a model that is based on Kelly-Tyson theory as follows [101]:

$$\sigma_R = \frac{\eta\alpha\tau\theta_f}{\sigma_m} + 1 - \theta_f \tag{3.9}$$

$$\sigma_R = \frac{\sigma_{nc}}{\sigma_m} \tag{3.10}$$

where,

- η is the nanofillers orientation factor
- σ_m is the tensile strength of the matrix
- σ_{nc} is the tensile strength of the polymer nanocomposite

- σ_R is the normalized tensile strength i.e. the ratio of the tensile strength of nanocomposite to that of the polymer matrix

When the interphase region is taken into consideration, the tensile strength of the material is obtained as follows:

$$\sigma_{nc} A_{nc} = \sigma_m A_m + \tau A_i \tag{3.11}$$

where A indicates the surface area and subscripts nc, m and i denote the nanocomposite, matrix and interphase respectively. The number of nanofillers in a nanocomposite is determined by using the following expression [104].

$$n = \frac{A_{nc}\theta_f}{\pi r^2} \tag{3.12}$$

A_m and A_i are expressed as follows:

$$A_m = A_{nc} - n\pi\left(r + t\right)^2 \tag{3.13}$$

$$A_i = 2\eta n\pi\left(r + t\right) L_p \tag{3.14}$$

L_p in this regard represent the pullout length of the nanofillers. When fracture occurs the nanofiller is pulled out of the side of the break where the length is shorter. This means that the L_p varies between the range of zero up to half the nanofiller length. Therefore, it follows that the average L_p equals quarter of the total nanofiller length i.e. $L_p = L/4$ [105]. It shows that the nanofillers do not break on the fracture of nanocomposite since they are generally much shorter than L_c and this justifies the use of suggested equation for short fibers ($L < L_c$). Replacing the eqs. (3.12) to (3.14) into Eq. 3.11, we obtain Zare's model for determining the tensile strength of polymer nanocomposites which is taken to be the second objective function as follows:

$$\sigma_R = \frac{\eta\alpha\tau}{\sigma_m}\left(1 + \frac{t_i}{r}\right)\theta_f + \left[1 - \left(1 + \frac{t_i}{r}\right)^2 \theta_f\right] \tag{3.15}$$

Thus, Equation 3.15 for predicting the tensile strength of polymer nanocomposites is taken to be the second objective function, for the MOO model of the current study as follows:

$$f_2 = \sigma_R \tag{3.16}$$

i). Tensile strength design parameters

Equation 3.15 shows that the design parameters or variables for the second objective function are t, t_i, θ_f, η and τ. The rationale for the limitations and constraints of the given design variables is given in the following paragraphs.

The orientation factor η, is also known as the Krenchel [81] factor of orientation. The factor can only assume discrete values; 1, 3/8 and 1/5 for fully aligned, randomly aligned in 2-dimensinal plane and randomly aligned in 3-dimensional plane respectively [81]. However, for the current work the factor is varied between the range of the given discrete values.

Blighe et al. [106] proposed that the strength of nanocomposites varies linearly with the orientation factor. In their work, an orientation factor of 1 was applied to the Rule of Mixtures (ROM) to calculate the theoretical elastic modulus and tensile properties of nanocomposites. The validity of the value of the orientation factor for the investigation was achieved through the use of a combination of experimental results of Raman spectroscopy and Herman's orientation factor for composite materials [107].

The interfacial shear strength, τ was computed for a range of 1 and 52 MPa based on the work done by Zare et al. [101] on the effects of the interface on the tensile properties of nanocomposites. The authors also found that the values of the thicknesses of the interphase are usually less than the thicknesses of the nanofillers of the CNTs in all reported samples.

Stojšić et al. [108] studied the tensile properties of Pa-12/Clay nanocomposites and found that the thickness of the interphase ranges between 2.36 – 4.41 nm. Wagner et al. [109] also obtained the maximum experimental values of 50 MPa for the interfacial shear strength of carbon nanotube reinforced polymers. Furthermore, Zhandarov et al. [110] reported that the interfacial shear strength determines stress transfer through the interphase and therefore significantly affects the mechanical properties of composite materials.

3.1.3 Determination of effects of dispersion

Currently, there are no known methods of directly quantifying effects of dispersion using theoretical models for determining the mechanical properties of nanocomposites [10]. Hence in this research, a combination of the optimized tensile strength equation (i.e. the second objective function) and the Pukanszky model [111] is used to determine the effects of dispersion by obtaining parameter "B" as follows [112, 113]:

$$B = \frac{1}{\theta_f} ln \left[\sigma_R \left(\frac{1 + 2.5\theta_f}{1 + \theta_f} \right) \right] \tag{3.17}$$

"B" is also dependent on the characteristics of the interphase as:

$$B = (1 + A\rho t_i)\, ln \left(\frac{\sigma_i}{\sigma_m} \right) \tag{3.18}$$

where,

- A is the specific surface area of nanofillers
- ρ is the nanofiller density
- σ_i is the tensile strength of the interphase

In Equation 3.18, A indicates the level of nanofiller dispersion whereas t_i and σ_i indicates the properties of interphase respectively [96]. This therefore, shows that the yield strength of polymer nanocomposites is mostly dependent to the interfacial adhesion between the polymer matrix and the nanofiller as well as the nanofiller dispersion [114]. As a result, parameter "B" which is determined from the results of the yield strength shows the level of interfacial interactions and the quality of dispersion in matrix [96].

The results of Zare et al.'s [96] investigation on the interphase properties of polymer nanocomposites showed that the optimum mechanical properties of polymer based nanocomposites can be obtained at nanofiller loadings of 0.04 and parameter "B" of 3.37. The tensile strength of the interphase (σ_i) can also be calculated by B parameter.

The specific area of the nanofillers at the interphase (A) can be given by [101]:

$$A = \frac{A_i}{m} = \frac{2\pi rL}{\rho V} = \frac{2\pi rL}{\rho\pi r^2 L} = \frac{2}{\rho r} \tag{3.19}$$

where,

- A_i is the interphase area
- L is the critical length of the nanofillers
- m and V represent mass and total volume of the nanofillers

By substituting A in Eq. 3.18, we get:

$$B = \left(1 + \frac{2t_i}{r}\right) \ln\left(\frac{\sigma_i}{\sigma_m}\right) \tag{3.20}$$

And, σ_i can be determined by rearranging of Eq. 3.20 as:

$$\sigma_i = \sigma_m exp\left(\frac{B}{1 + \frac{2t_i}{r}}\right) \tag{3.21}$$

Equations 2.28 to 2.32 are used to characterize effects of dispersion on the tensile properties of polymer nanocomposite materials. It should be noted that the equations can also be used to determine the interphase strength of the materials.

3.1.4 The numerical optimization problem

The modeled objective functions and their respective design variables given in the previous sections are used to formulate a multi-objective optimization problem of the current study. Table 3.1 shows the design variables of each objective function and their constraints. As discussed in the previous section, the constraints are there to ensure that the search region (space) for the optimization algorithm is within the feasible region (or the acceptable range). The constraints also improve the efficiency of the algorithm as it is quick to eliminate those values of the design variables that fall in the unfeasible region.

Table 3.1 also shows the parameters or design variables that are found in each objective function that is to be optimized. From the table it can be seen that the common parameters in both objectives are; thickness of the interphase x_1, thickness of the nanofiller x_2 and the nanofiller loading respectively x_3. Figure 3.4 shows the relationship between the objective functions and the design variables.

Table 3.1: Optimization design variables and constraints

Design Parameter	Variable (X)	Constraints	Objective functions	
			Ji model (f_1)	Zare model (f_2)
t_i (interphase thickness)	x_1	$10^{-9} \leq x_1 \leq 10^{-8}$	✓	✓
t (nanofiller diameter)	x_2	$10^{-9} \leq x_2 \leq 10^{-8}$	✓	✓
θ_f (nanofiller loading)	x_3	$0.01 \leq x_3 \leq 0.05$	✓	✓
E_i (interphase modulus)	x_4	$1 \leq x_4 \leq E_f$	✓	×
τ (interfacial shear strength)	x_5	$1 \leq x_5 \leq 52$	×	✓
η (orientation factor-alignment)	x_6	$0.2 \leq x_6 \leq 1$	×	✓

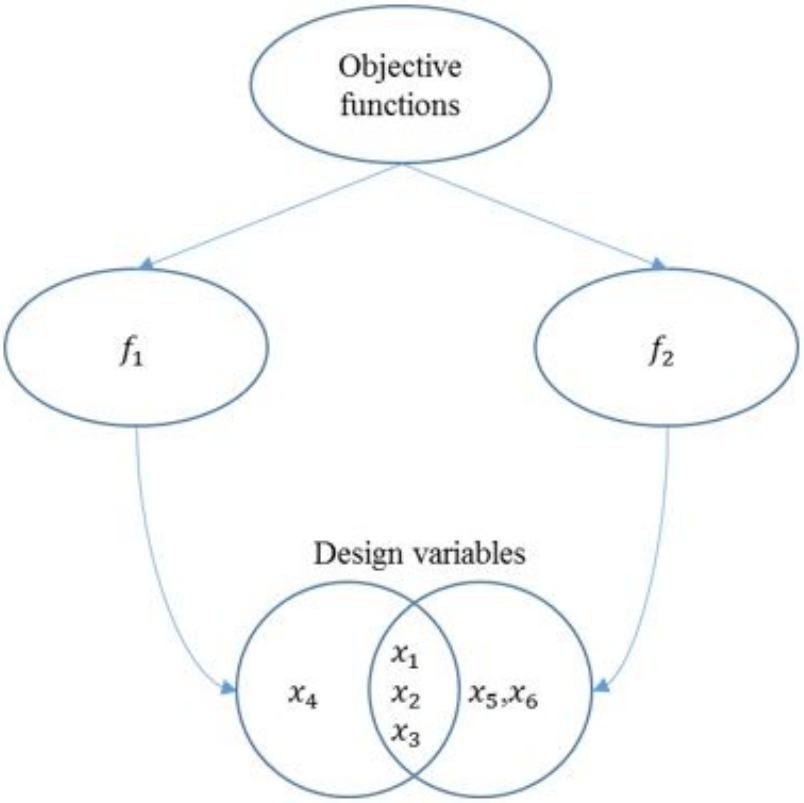

Figure 3.4: Relationship between the objective functions and the design variables

Using the design variables, the optimization design problem is then expressed as a numerical multi-objective optimization problem as given below:

$$\begin{aligned} Maximize: & f_1 = E_R \\ & f_2 = \sigma_R \end{aligned} \tag{3.22}$$

$$Subject\ \ to: X = [x_1, x_2, ..., x_6] \tag{3.23}$$

$$X_{low} \leq X \leq X_{upp} \tag{3.24}$$

The representation of the nanocomposite design problem into a numerical optimization problem is followed by writing an m-file script of the two objective or fitness functions in MATLAB. This is a callable script used in the MATLAB optimization tool for solving the multi-objective optimization problems. The script contains the input variables such as the elastic modulus of both the polymer and the nanofiller and the tensile strength of the polymer matrix.

Figure A.1 in the Appendix shows the m-file script of the objective functions. Various materials from literature have been selected for the current study and the properties of the matrix and the nanofillers are given in Table 3.2.

Table 3.2: Materials used for numerical optimization

Polymer + Nanofillers	Polymer Properties		Filler Properties
	E_m [GPa]	σ_m [MPa]	E_f [GPa]
Nylon-6 + Montmorillonite (MMT)	3.2	46.1	20.36
Styrene Butadiene Rubber (SBR) + MWCNTs	2	20	900
Polyamide (Pa) + Calcium Carbonate (CaCO3)	0.509	65	37
Isotactic Polypropylene (iPP) + MWCNTs	1.6	40	900

3.2 NSGA-II for MOO in MATLAB

The NSGA-II algorithm setup in MATLAB is described in this section. Figure A.2 in the Appendix shows the nanocomposite design problem setup in the optimization toolbox and Figures A.3 and A.4 shows the 'options' windows within the optimization toolbox environment.

Once the objective functions and the input variables have been written and completed, the *gamultiobj*-function which is based on the NSGA-II in global optimization toolbox for MATLAB is then used to solve for the maximization of the elastic modulus and the tensile strength of polymer nanocomposite materials (Step II in flow chart: Figure 3.1). The step is regarded as the main part of the proposed approach for optimizing the mechanical properties of polymer nanocomposites. The NSGA-II framework's procedure is shown in Figure 3.5 and is briefly explained below:

- Stages - 1→2: The procedure starts by executing Eq. 3.25 which randomly selects a set of parameters X as initial population,

$$X = gamultobj\left(f_{objective}, n_{vars}, Z, b, Z_{eq}, b_{eq}, X_{low}, X_{upp}, options\right) \tag{3.25}$$

where, $f_{objective}$ represent the objective function of the algorithm, n_{vars} is the number of independent variables for the objective function and *options* refers to the structure containing the options for GA.

The constraints (i.e.both equality and inequality) of the design variables satisfy the following equations:

$$ZX \leq b \tag{3.26}$$

$$Z_{eq}X = b_{eq} \tag{3.27}$$

$$X_{low} \leq X \leq X_{upp} \tag{3.28}$$

For the current study, only Eq. 3.28 is used and Z, b, Z_{eq}, b_{eq} are set to be empty matrices. This is because the design variables are only constrained by the lower and upper limits respectively. For every iteration, the *gamultiobj* calls the objective function represented as follows:

$$OF = f_{objective}\,(X) \tag{3.29}$$

The objective function is the MATLAB m-file script containing the model equations that describes the relationship between the design variables and objective functions 1 and 2 (i.e. elastic modulus and the tensile strength) respectively.

- Stages - 2 $\rightarrow$ 3: The objective values are stored and evaluated in $f_{objective}$
- Stages - 3 $\rightarrow$ 4: The resulting objective values of each individual (solution points) are returned as output variables of $f_{objective}$ to *gamultiobj*.
- Stages - 4 $\rightarrow$ 5: The NSGA-II then processes the objectives and the diversity of the individuals and selects the best (elite) and most diverse individuals as the parent individuals of the next generation (iteration). Refer to Figure 3.5.
- Stages - 5 $\rightarrow$ 6: Random recombination (crossover) and mutation of individuals occurs to generate new individuals.
- Stages - 6 $\rightarrow$ 7, 2: A set of new design variables X is generated and the iteration re-starts until the termination criteria is met.

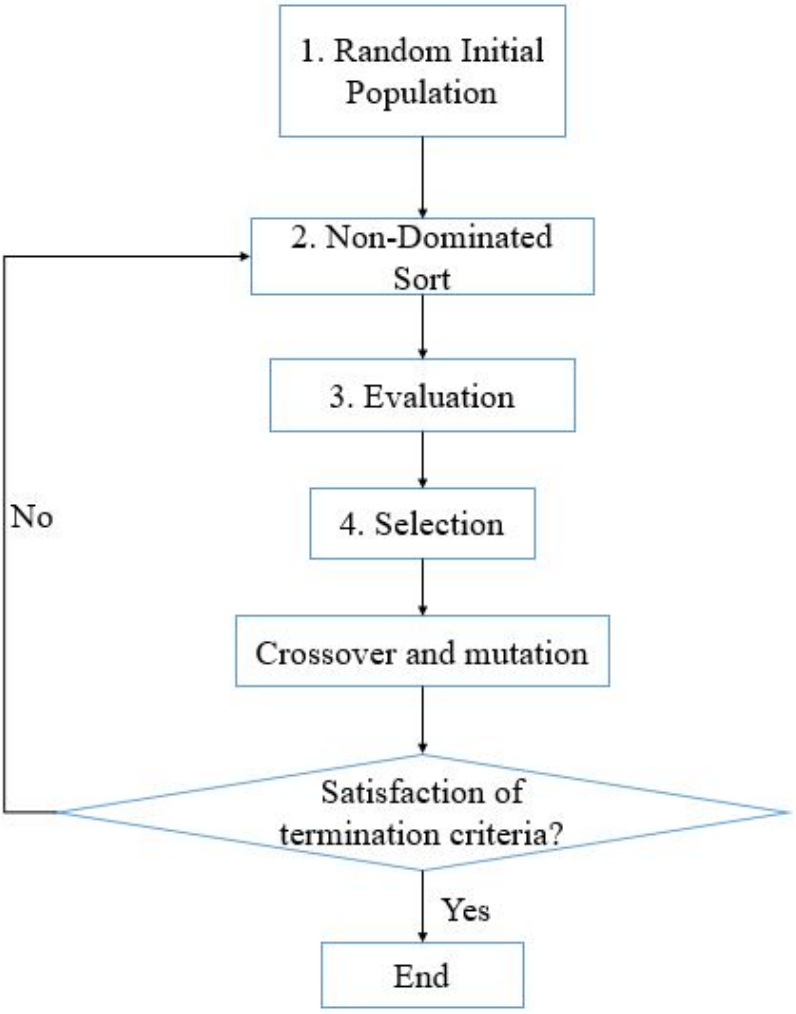

Figure 3.5: MATLAB's NSGA-II optimization procedure for maximizing mechanical properties of nanocomposites

The above algorithm procedure was followed for the selected nanocomposite pairs (Polymer Matrix and Nanofillers) as given in Table 3.2. All optimization experiments were performed with Intel Core i5 processor running at 3.20GHz Windows 10 operating system. The NSGA-II in MATLAB's optimization toolbox was used to optimize the objective functions f_1 and f_2. Due to the stochastic nature of the MOO algorithm, the solutions from the optimization model show scattered or clustered phenomenon. Hence, it was deemed necessary to run multiple computations to ensure reliability and convergence of the optimization solutions.

A total of six computations were run for the optimization of each nanocomposite materials pair. The obtained optimum results for the individual pairs were recorded for further analysis. Descriptive statistics analysis and interpretation method were used for the characterization of MOO optimization results.

Before starting the optimization procedure, a number of important parameters were assigned to obtain reliable optimized solutions. This area called the 'options' or the structural set up of the algorithm as it contributes to the effectiveness of solving the given problem. Hence, appropriate population type and size, number of generations, cross-over rate and mutation rate must be defined. For all the experiments, the population type was set to be a default double vector with the size of 200. The crossover rate, mutation rate and number of generations were set to be 0.55, 0.05 and 3500 respectively (see Figures A.2 to A.4 in the Appendix). This was done to ensure that the optimization run was always exhaustive with regard to the search space.

Furthermore, as shown in Figure 3.5, the elastic modulus (f_1) is dependent on interphase thickness (x_1) and interphase elastic modulus (x_4), nanofiller thickness (x_2) and nanofiller loading (x_3). The tensile strength (f_2) on the other hand is dependent on interphase thickness (x_1) and interfacial shear stress (x_5) nanofiller thickness (x_2) and nanofiller loading (x_3) and nanofillers orientation factor(x_6). Hence for every optimization run, a set of optimized design variables X along with the optimum values of the objective functions f_1 and f_2 will be returned when the termination criteria is satisfied. This means that the algorithm returns with each optimized value of the design variable, $X = [x_1, x_2, \ldots, x_6]$, that gives the maximum elastic modulus and the tensile strength of the optimized nanocomposite pair.

Chapter 4 Results and Discussion

The overall results of design variables obtained by the proposed MOO model are characterized and discussed in this chapter. In addition, the effects of the design variables and their influences on the mechanical properties of polymer nanocomposite materials will also be discussed. This chapter is divided into two main sections, namely; overall results of the MOO model (section 4.1) and the effects of the design variables on the mechanical properties of nanocomposites (section 4.2). Section 4.2 is further divided into subsections i.e. effects of nanofiller loading (subsection 4.2.1), effects of interphase properties (subsection 4.2.2) and lastly, effects of dispersion (subsection 4.2.3).

The results of the optimization model were analyzed by using two different methods (i.e. the mean and the median). A detailed description of the two methods of analyzing the obtained optimization results is given in Appendix A. These methods are known as descriptive statistical analysis of data methods and they include the use of graphs, charts and tables, and the calculation of measures of central tendencies of data (i.e. averages, mode, median, ranges and percentiles).

The measures of variation for determining how the results vary from the expected central values were also used for analysis. These measures of variation include, the standard deviation (SD) which measures the variation of data from the mean and the quartiles on box and whisker plots which measures the variation of data from the median. The measures of variation are also presented and explained in Appendix A. Each of the results sections of the chapter mentioned in the paragraph above are divided into the two methods of analysis. The overall results are then compared to each other and further compared to the experimental results from previous studies for validation.

It should be noted that the design variables are optimized to maximize the normalized elastic modulus (E_R) and the normalized tensile strength (σ_R). The design variables of the mechanical properties of the current study are given below. The variables are given as both their notation in the analytical models for determining the elastic modulus and tensile strength as well as the notation used in the mathematical problem for optimization as follows:

- Thickness of the interphase, t_i (x_1)
- Diameter of nanofillers, t (x_2)
- Nanofiller loading, θ_f (x_3)
- Interphase modulus, E_i (x_4)
- Interfacial shear stress, τ (x_5)
- Orientation factor, η (x_6)

It is expected that the final overall results of the mechanical properties of the MOO model for both mean and median analyses will be higher or (better) than the physical experimentation results from literature. This is due to the fact that the main purpose of the current work is to obtain the optimum values for the given design variables to maximize the mechanical properties of nanocomposites using numerical multi-objective optimization methods, in particular, the Fast Non-dominated Sorted Genetic Algorithms (NSGA-II) in MATLAB. In addition, numerical optimization generally deals with finding and locating 'best' solutions to problems. Thus, it follows that the solutions obtained through this technique would always be better compared to the physical experimental results.

4.1 Overall results of MOO model

The overall results of the NSGA-II optimization model for the different pairs of the nanocomposites are presented in Table 4.1 and Table 4.2 for both the mean and median analysis respectively. The experimental results obtained from literature used for the comparison purposes are given in Table 4.3 and Table 4.4 for the normalized elastic modulus and tensile strength respectively.

It should be noted that the overall results given in Table 4.1 refers to the averaged results for the individual nanocomposite pairs whereas those in Table 4.2 are the median results obtained from the box and whisker analysis respectively. As it could be seen from both results the optimized mechanical properties are comparable with the experimental data.

For example, consider the Nylon-MMT nanocomposite pair, the optimization mean results of the normalized elastic modulus and tensile strength for the 2.95 wt.% MMT loading are 1.81 and 0.92 respectively. The optimization results obtained through the median analysis on the other hand were determined to be 1.54 and 0.93 for the elastic modulus and the tensile strength respectively with the MMT loading of 3.21 wt.%. For the same material combination, the experimental results of the normalized elastic modulus for the MMT loading of 3 wt.% is 1.48 [94] and that of the tensile strength is 0.935 for 5 wt.% MMT loading [115].

Furthermore, the mean normalized elastic modulus and tensile strength of 4 wt.% of $CaCO_3$ are 2.01 and 0.96, 4.2 wt.% of MWCNTs with SBR are 1.82 and 0.97 and 3.47 wt.% of MWCNTs with iPP are 1.70 and 0.97 respectively. The median normalized elastic modulus and tensile strength of 4.52 wt.% of $CaCO_3$ are 1.75 and 0.97, 4.69 wt.% of MWCNTs with SBR are 1.85 and 0.97 and lastly, 4.53 wt.% of MWCNTs with iPP are 1.84 and 0.97 respectively. From tables 4.1 to 4.4 it can be seen that the experimental results from literature are matching well with the optimized nanocomposite material properties.

It is worth noting that some of the nanocomposite materials pairs from the experimental results used for the comparison of the tensile strength results of the optimization model do not exactly match the nanocomposite materials pairs used in the current study (i.e. Polyethylene (PE)-MWCNT pair) is used for the comparison of SBR-MWCNT. The rationale here is that the most important material in nanocomposites is the nanofiller, this is due to the fact that they are the regarded as the material that reinforces or improves the properties. In addition, some of the exact nanofillers-matrix pairs that were used in the current study could not be found in the literature.

Table 4.1: Optimized mean design variables and the corresponding normalized mechanical properties.

Nanocomposite Material	t_i (nm)	t (nm)	θ_f (wt.%)	E_i (GPa)	τ (MPa)	η	E_R	σ_R
Nylon-MMT	4.07	5.65	2.95	19.72	50.69	1.00	1.81	0.92
Pa- $CaCO_3$	2.78	6.36	4	31.28	51.16	1.00	2.01	0.96
SBR-MWCNT	2.17	6.50	4.29	600.88	50.12	1.00	1.82	0.97
iPP-MWCNT	2.32	7.07	3.47	512.47	51.32	1.00	1.70	0.97

Table 4.2: Optimized median design variables and the corresponding normalized mechanical properties.

Nanocomposite Material	t_i (nm)	t (nm)	θ_f (wt.%)	E_i (GPa)	τ (MPa)	η	E_R	σ_R
Nylon-MMT	2.96	5.41	3.21	19.87	51.92	1.00	1.54	0.93
Pa-$CaCO_3$	2.24	6.42	4.52	31.31	51.97	1.00	1.75	0.97
SBR-MWCNT	2.12	6.18	4.69	551.04	50.36	1.00	1.85	0.97
iPP-MWCNT	2.31	7.01	4.53	539.39	51.92	1.00	1.84	0.97

Table 4.3: Experimental results of the normalized elastic modulus (E_R).

Nylon/MMT [94]		Pa/$CaCO_3$ [116]		SBR/MWCNT [117]		iPP/MWCNT [117]	
θ_f (x_3) (wt.%)	E_R	θ_f (x_3) (wt.%)	E_R	θ_f (x_3) (wt.%)	E_R	θ_f (x_3) (wt.%)	E_R
0	1	0	0	1	1.1	1	1.1
1	1.25	1	1.1	3	1.2	2	1.12
2	1.4	2.1	1.2	5	1.3	3	1.2
3	1.48	4.6	1.6	-	-	5	1.35

Figure 4.1 shows the comparison the normalized elastic moduli of the optimization model obtained through the mean and median analysis against the normalized elastic modulus from the experimental data. Figure 4.2 shows the percentage increase in E_R of the optimization model compared to the experimental data.

Table 4.4: Experimental results of the tensile strength (σ_R).

Nylon6/MMT [115]		Pa/$CaCO_3$ [118]		PE/MWCNT [119]		iPP/MWCNT [120]	
θ_f (wt.%)	σ_R	θ_f (wt.%)	σ_R	θ_f (wt.%)	σ_R	θ_f (wt.%)	σ_R
0	0.89	0	0.71	0	0.78	0	0.7
1	0.91	1	0.76	0.5	0.86	1	0.78
3	0.92	2.1	0.83	1	0.91	2	0.875
5	0.935	3	0.94	2	0.94	2.4	0.81
-	-	-	-	3	0.95	4.2	0.75

From Figure 4.2 it could be seen that the median analysis shows the lowest percentage increase for Nylon-MMT and Pa-$CaCO_3$ (i.e. about 4% and 9% for the two materials compared to 22% and 26% for mean analysis respectively). The percentage increase for median analysis of SBR-MWCNTs and iPP-MWCNTs on the other hand is the highest (i.e. 42% and 36%) compared to the mean analysis (i.e. 40% and 26%) for the two materials respectively. The increase is due to the fact that numerical optimization model was able to determine and obtain the best combinations of the design parameters which could not be easily obtained through physical experimental methods. Thus, it is plausible from the results that, the optimization model could provide a comprehensive list of design variables for obtaining better mechanical properties.

The optimization model has also provided additional advantages over the experimental analysis. The optimization results have given the specific range of values of other design parameters such as alignment and interphase properties. From the results (tables 4.1 and 4.2), it could be noted that the aligned nanofillers with the orientation factor, η =1 have shown improved nanocomposite properties including to the interphase properties such as the interphase modulus E_i and the interfacial shear strength τ. Experimentally, the predicted interphase properties could be achieved by functionalization of nanofillers.

Similar trends could also be seen for other composite pairs. This proves that the proposed optimization model could be used for obtaining the combination of design variables that could tailor the nanocomposites' properties for the required applications. The optimized results were also used to understand the effect of the individual design variables on the normalized elastic and tensile strength of the selected nanocomposites pairs. The effects of the design variables are presented and described in section 4.2 respectively.

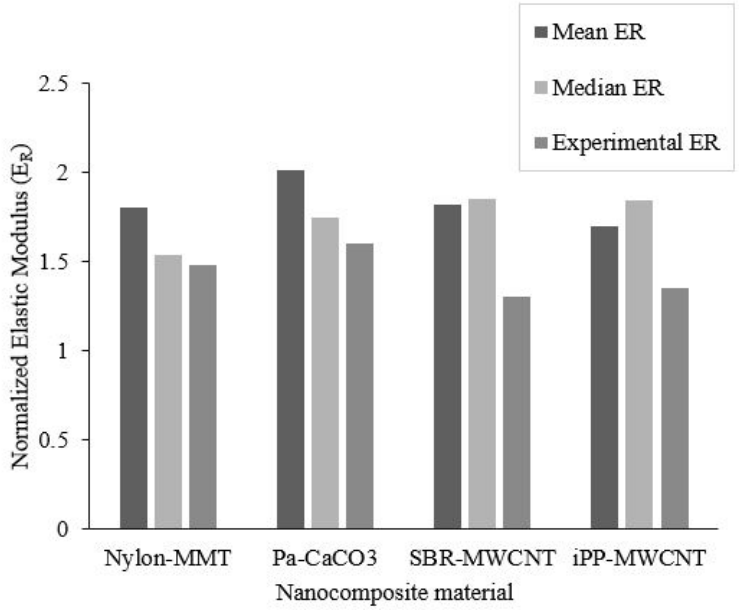

Figure 4.1: Optimum normalized elastic modulus of MOO model vs. normalized elastic modulus (E_R) of the experimental data.

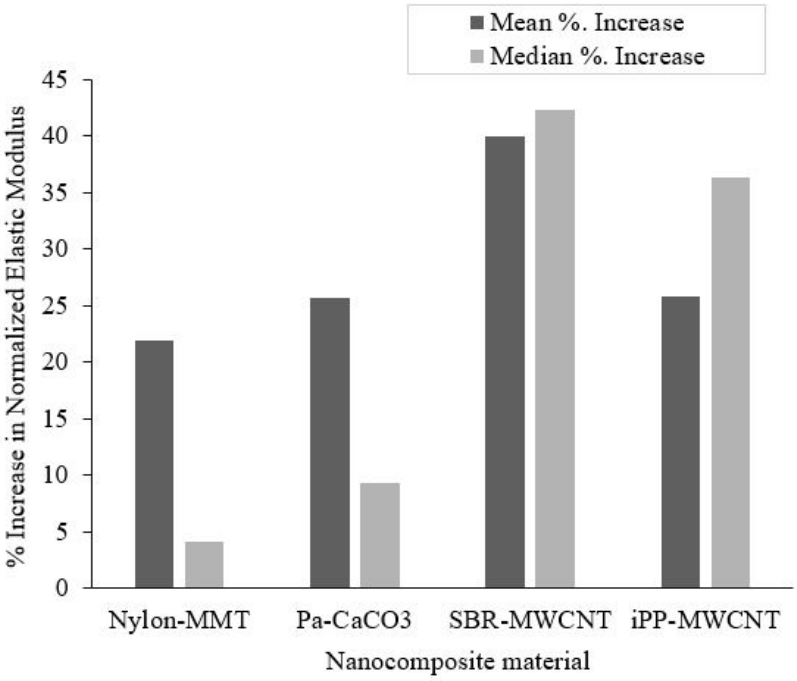

Figure 4.2: Percentage increase in normalized elastic modulus for both mean and median analysis.

4.1.1 Variation of Overall Optimization Results

This section briefly discusses the variation of the overall results for both mean and median statistical analyses of data approaches (i.e. the degree of scattering of the data from the expected point of measure). The measure of variation of the mean is given by the standard deviation whereas that on the median is given by the box and whiskers plot (see the Appendix A for the definitions and brief description of the two measures of variation).

The section only shows the standard deviations of the objectives (i.e. the normalized elastic modulus and the tensile strength). The standard deviations of the design variables are given in Table A.1 in Appendix A. Table 4.5 shows the standard deviations of the normalized elastic modulus and tensile strength. From the table it can be seen that the standard deviations of Nylon-MMT and Pa-$CaCO_3$ are high for both mechanical properties. This means that the data for the two materials have a higher variation from the mean as compared to that of SBR-MWCNT and iPP-MWCNT respectively.

Table 4.5: Standard deviations of the normalized elastic modulus and the tensile strength.

Nanocomposite	E_R	σ_R
Nylon-MMT	0.69	0.07
Pa-$CaCO_3$	0.58	0.03
SBR-MWCNT	0.30	0.02
iPP-MWCNT	0.38	0.02

Figures 4.3 and 4.4 show the box and whiskers diagram for the normalized elastic modulus and the tensile strength of the sampled nanocomposite materials. From Figure 4.3, Nylon-MMT and Pa-$CaCO_3$, the box and whiskers plots show that there is more variation (or scattering) of data as compared to that of SBR-MWCNT and iPP-MWCNT. These are indicated by the wide boxes and long whiskers of Nylon-MMT and Pa-$CaCO_3$ in comparison to those of the other nanocomposites. The plots also show that the median values of SBR-MWCNT and iPP-MWCNT are similar and higher than those of Nylon-MMT and Pa-$CaCO_3$.

Furthermore, Nylon-MMT and Pa-$CaCO_3$ plots of the elastic modulus also exhibit skewness to right. This means that the values are clustering below the median and the scattering of the data is observed above the median. SBR-MWCNT and iPP-MWCNT on the other hand show skewness to the left. It should also be noted from the plots that SBR-MWCNT and iPP-MWCNT have the same median.

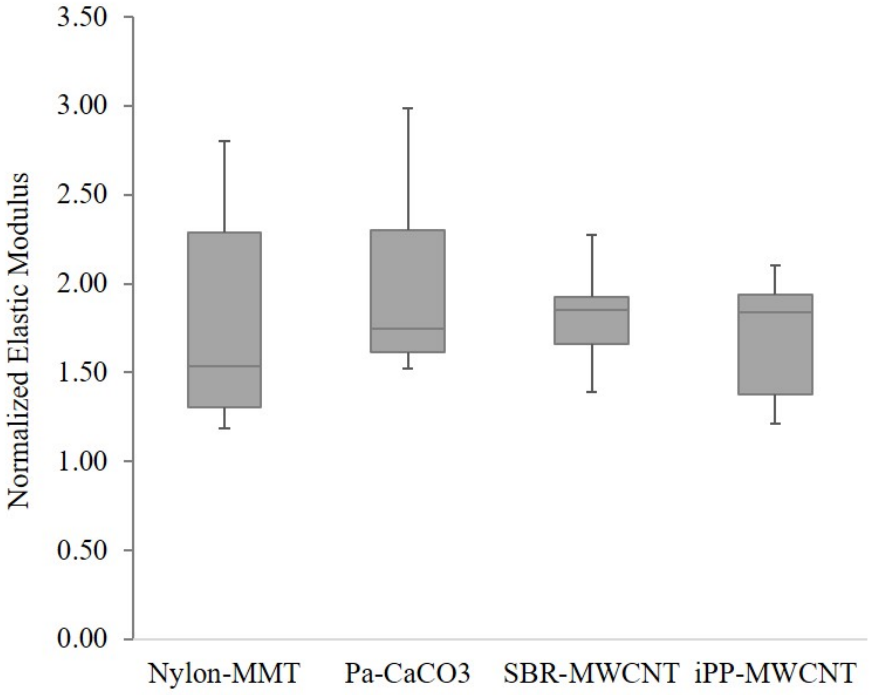

Figure 4.3: Box and whisker plot for the normalized elastic modulus

Figure 4.4 shows the variation of the overall normalized tensile strength for sampled nanocomposites. The figure shows that the variation of the results for the normalized tensile strength follows those of the elastic modulus. From the figure, it can also be seen that the median values of Pa-$CaCO_3$, SBR-MWCNT and iPP-MWCNT are the same (see also Table 4.2). Nylon-MMT on the other hand had a slightly lower median value of the normalized tensile strength.

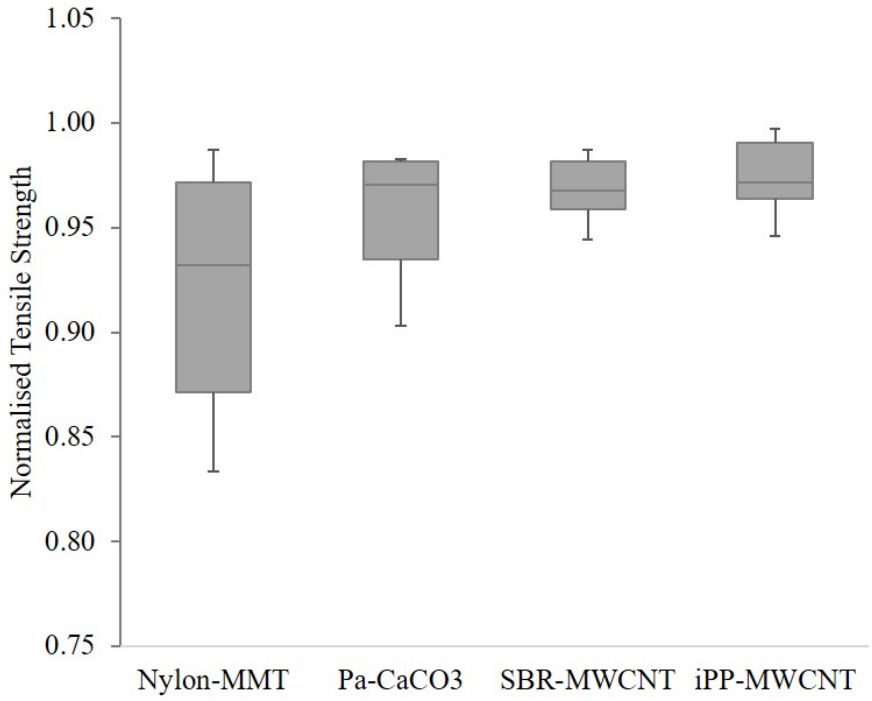

Figure 4.4: Box and whisker plot for the normalized tensile strength

The measures of variation for both the mean and median analyses shows that the overall data has similar variation trends. Thus, the data for Nylon-MMT and that of Pa-$CaCO_3$ shows a higher degree of sparsity as compared to that of SBR-MWCNT and iPP-MWCNT. It is worth noting that the modulus of MWCNTs is very high compared to that of MMT and $CaCO_3$ and this might be the reason the optimization results of both SBR-MWCNT and iPP-MWCNT clusters around the mean and the median. However, more research is still required to prove this to be the case or not.

4.2 Effects of the design variables on the mechanical properties

In this section, the effects of the design variables on the elastic modulus and the tensile strength are investigated and discussed. It is worth noting that due to the nature of numerical optimization techniques, the MOO model also simultaneously optimizes the given objectives. Thus, all the optimum values of the design variables are computed simultaneously during the process of optimization whereby the 'desired' (or maximum) mechanical properties are obtained.

The investigation of the individual effects of the design variables is done to compare the obtained optimum values with some of the values from previous studies. Furthermore, the investigation is also done to establish and characterize the behavior of the mechanical properties with respect to the given design variables.

4.2.1 Effects of nanofiller loading on the mechanical properties

i). Nanofiller loading on the elastic modulus

Figures 4.5 to 4.8 show the normalized elastic modulus (E_R) to the nanofiller loading (θ_f) of the four combinations of polymer nanocomposites. The mean normalized elastic modulus, (Mean E_R) is also indicated in the figures. It could be seen from the figures that the normalized elastic modulus of the optimization model is within range of the experimental data and thus proving that the optimization model is sufficiently accurate in predicting the optimized mechanical properties of polymer nanocomposites. The experimental data shows that the elastic modulus linearly increases with increasing nanofiller loading. However, the optimization results on the other hand, show a clustered or scattered behavior as mentioned before, but are still within the experimental data range.

Figure 4.5 shows the normalized elastic modulus to the nanofiller loading of Nylon-MMT nanocomposite. From the figure it can be seen that about 66.7% of the optimization data is lower than the experimental data. However, the Mean E_R is still higher than the highest experimental normalized elastic modulus. Figure 4.9 shows the box and whisker plot (i.e. median analysis) for the nanofillers loading. From the figure it can be observed that Nylon-MMT has a wide box but short whiskers. This means that the nanofillers loading have more variation from the median (i.e. 3.21 wt.%). The short whiskers however, indicate that the data does not have many outliers. In addition, the figure shows that the results of MMT loading are skewed to the left i.e. the loadings above the median exhibit some level of clustering.

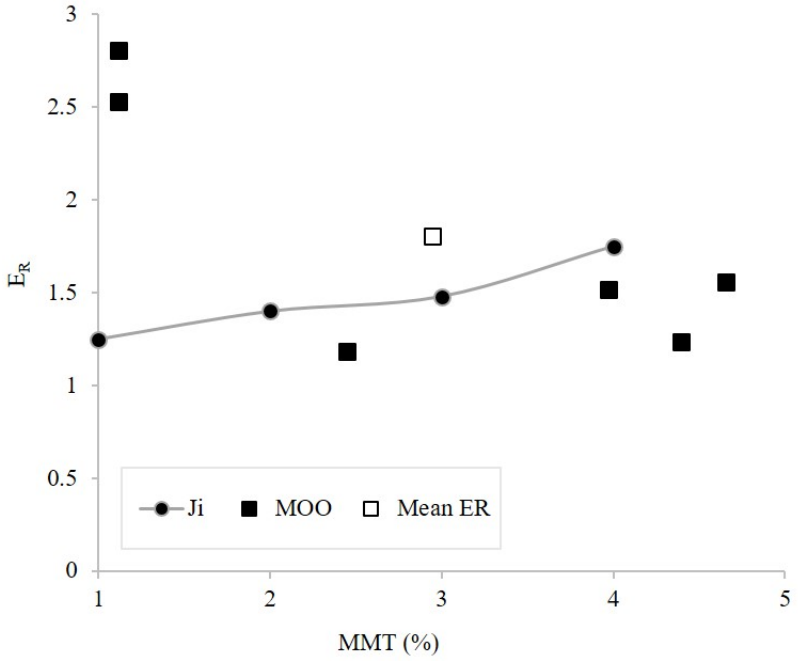

Figure 4.5: Normalized elastic modulus (E_R) vs. nanofiller loading (θ_f) for Nylon-MMT.

Figure 4.6 shows the normalized elastic modulus to the nanofiller loading of Pa-$CaCO_3$. The figure shows that about 83.3% of the optimization data is higher than the experimental data. The figure also shows that the Mean E_R is higher than all the experimental data. In addition, from Figure 4.9, it can be seen that the results of $CaCO_3$ loading has a very short box with long whiskers. Thus, the results are clustering around the median (i.e. 4.52 wt.%). The long whiskers on the plot suggest that the results have some outliers which can be ignored when analyzing the data. In this instance the outlier is at $CaCO_3$ loading of 1.1 wt.% with the normalized elastic modulus of about 3 respectively (see Figure 4.6).

Figure 4.7 shows the normalized elastic modulus to the nanofiller loading of SBR-MWCNT nanocomposite. The figure shows that the optimization data at any given MWCNTs loading is higher than those of the experimental data. The median analysis of the MWCNTs loading within SBR shown in Figure 4.9 shows that the optimization data clusters around the median (i.e. at 4.69 wt.%). This is indicated by the short box of the nanocomposite data. The presence of the long whiskers on the box however, indicates that the data has outliers. From Figure 4.7 it can be observed that the outlier point is at about 2.45 wt.% MWCNTs loading and 1.4 normalized elastic modulus.

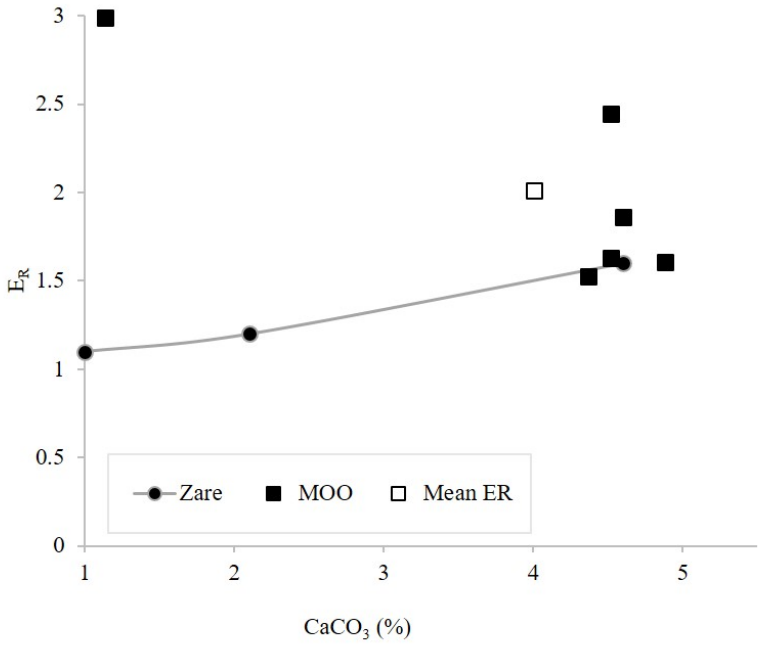

Figure 4.6: Normalized elastic modulus (E_R) vs. nanofiller loading (θ_f) for Pa-$CaCO_3$.

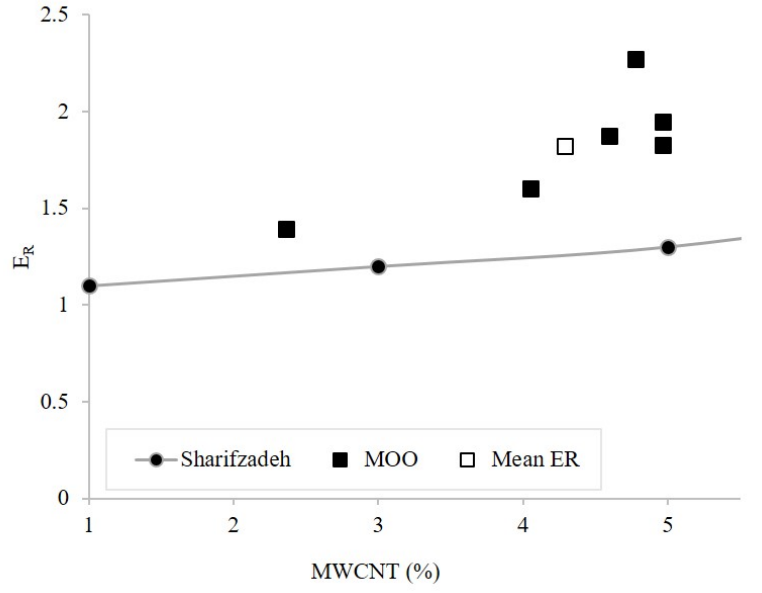

Figure 4.7: Normalized elastic modulus (E_R) vs. nanofiller loading (θ_f) for SBR-MWCNTs.

Figure 4.8 shows the normalized elastic modulus to the nanofiller loading of iPP-MWCNTs. Just like that of SBR-MWCNTs, the figure shows that the optimization data at any given MWCNTs loading is higher than the experimental data. The median analysis of iPP-MWCNTs data given in the Figure 4.9 shows that the optimization data has a relatively high level of variation below the median (4.53 wt%). Furthermore, the data shows skewness to the left and the box is very wide with relatively long lower whisker. Thus, suggesting that there are outliers in the data. From Figure 4.8 it can be seen that the data outliers lie at MWCNTs loading of 1 wt.% and the normalized elastic modulus of about 1.1 respectively.

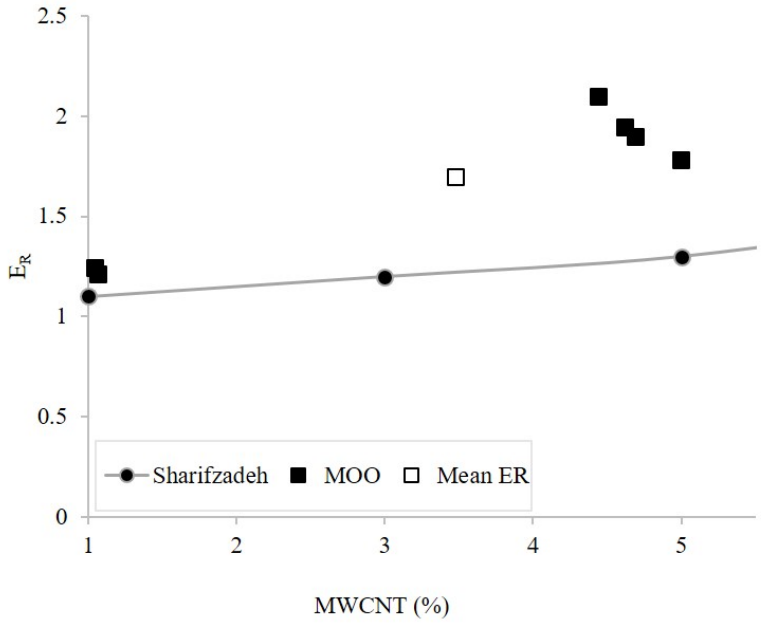

Figure 4.8: Normalized elastic modulus (E_R) vs. nanofiller loading (θ_f) for iPP-MWCNTs.

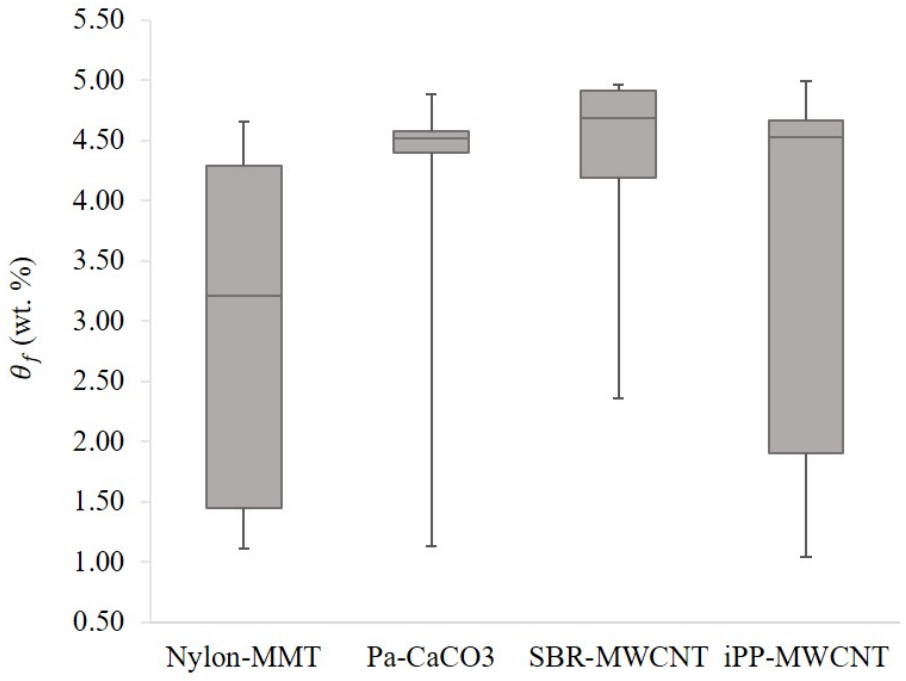

Figure 4.9: Box and whisker plot for nanofillers loading

ii). Nanofiller loading on tensile strength

Figures 4.10 to 4.13 show the relationship between normalized tensile strength (σ_R) with the nanofiller loading (θ_f) of both the optimization model and the experimental results. The mean normalized tensile strength is also indicated in the figures. It could be observed from the figures that the normalized tensile strength results from the optimization model generally out-perform the experimental results from literature. From the figures, it can be seen that the normalized tensile strength, σ_R is in the range of 0.8 to 0.95 for Nylon-MMT, whereas for Pa-$CaCO_3$, SBR-MWCNT and iPP-MWCNT are between 0.9 and 0.99.

Figure 4.10 shows the normalized tensile strength to the nanofiller loading of Nylon-MMT. The figure shows that the optimization results have some outliers with a lot of variation. However, about 67% of the optimization data is higher than the experimental data used for comparison. The highest value of the experimental data is 0.935 at MMT loading of 5 wt.%.

The optimization model results yielded the normalized mean and median tensile strengths of 0.92 and 0.93 at the MMT loadings of 2.95 wt.% and 3.21 wt.% respectively. The normalized mean tensile strength (Mean σ_R) is only 1.6% less than the highest point on the experimental data whereas the median was determined to be about 0.5% less. Even though the optimization model for the tensile strength yielded lower results than the experimental results, it should be noted that the percentage difference is small and thus both the results from the physical experiment and the optimization model can be regarded to be very similar. In addition and as mentioned before, the mean analysis is known to be more affected by outliers than the median. Therefore, a truer representation of the optimization results would be that of the median analysis.

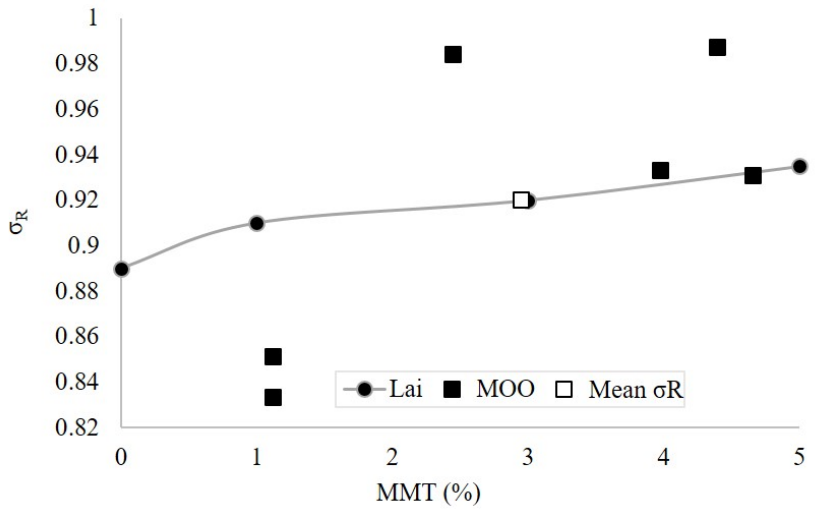

Figure 4.10: Normalized tensile strength (σ_R) vs. nanofiller loading (θ_f) for Nylon-MMT.

Figure 4.11 shows the normalized tensile strength to the nanofiller of Pa-$CaCO_3$ nanocomposite. From the Figure it can be seen that about 67% of the optimization results are higher than the experimental results obtained from literature. However, unlike the optimization results of Nylon-MMT, the results exhibit clustering. The value of the normalized mean tensile strength together with the median are higher than the highest value of the experimental results. The highest value for the normalized tensile strength of the experimental results is 0.94 at $CaCO_3$ loading of 3 wt.%. The normalized mean and median tensile strengths from the optimization model results were determined to be 0.96 and 0.97 at the $CaCO_3$ loadings of 4 wt.% and 4.52 wt.% respectively.

Figure 4.12 shows the normalized tensile strength to the nanofiller of SBR-MWCNTs nanocomposite. The figure illustrates that about 83% of the obtained optimization data is higher than the experimental results. Both the normalized mean and median tensile strengths are higher than the experimental results. The highest value for the normalized tensile strength of the experimental results is 0.95 at MWCNT loading of 3 wt.%. The optimization model had the normalized mean and median tensile strengths of 0.97 at MWCNTs loadings of 4.29 wt.% and 4.69 wt.% respectively.

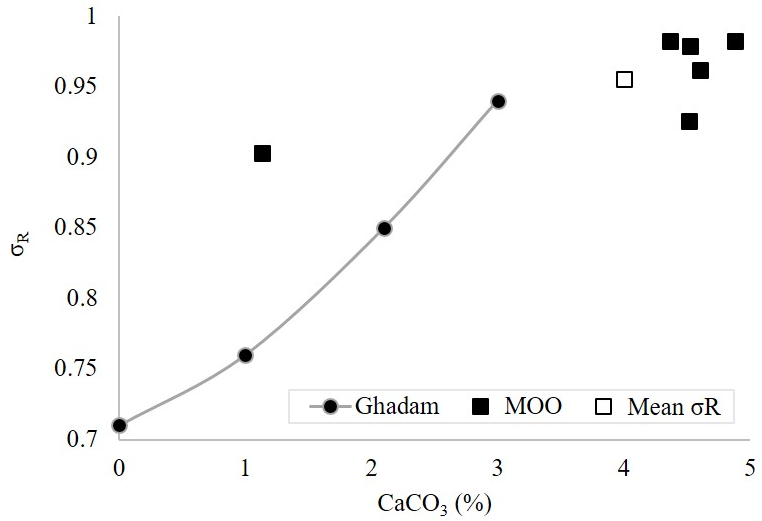

Figure 4.11: Normalized tensile strength (σ_R) vs. nanofiller loading (θ_f) for Pa-$CaCO_3$.

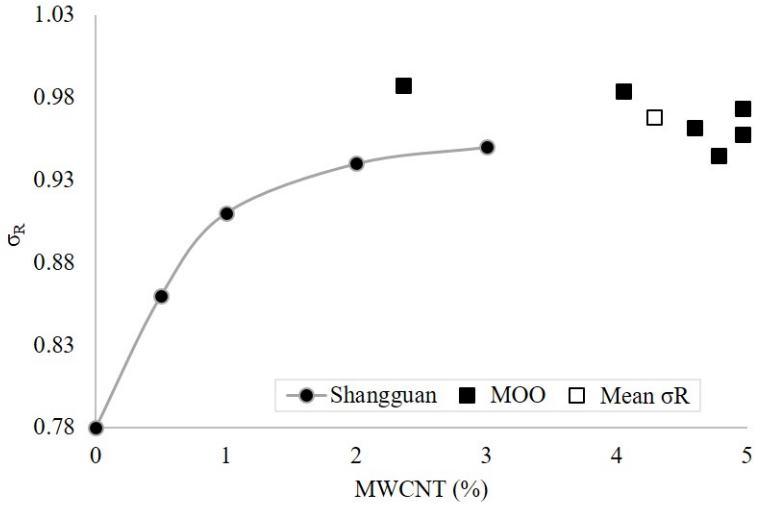

Figure 4.12: Normalized tensile strength (σ_R) vs. nanofiller loading (θ_f) for SBR-MWCNTs.

Figure 4.13 shows the normalized tensile strength to the nanofiller of iPP-MWCNTs nanocomposite. From the figure, it can be seen that 100% of the optimization data is higher than the experimental results from literature. The highest value for the normalized tensile strength of the experimental results is about 0.88 at 2.1 wt.% MWCNT loading. The normalized mean tensile strength is 0.97 at 3.47 wt.% MWCNT loading, whereas that of the median analysis is also 0.97 at the MWCNT loading of 4.53 wt.% respectively.

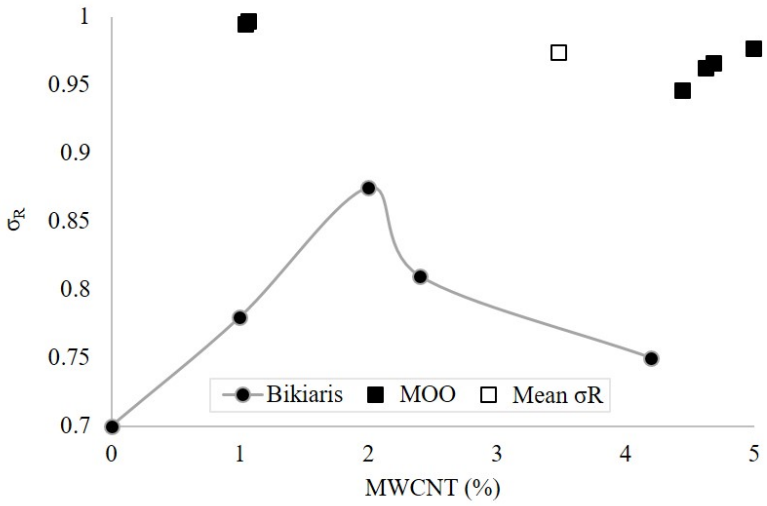

Figure 4.13: Normalized tensile strength (σ_R) vs. nanofiller loading (θ_f) for iPP-MWCNTs.

Zare et al. [98] found that the normalized tensile strength does not exceed 1 for polymer nanocomposites with nanofiller loadings of 5 wt.% and below. In addition, their investigation also concluded that the optimum values of the nanofiller loading and the thickness of nanofillers for obtaining the maximum tensile strength of polymer nanocomposites are 4 wt.% and 10 nm respectively. From Figures 4.10 to 4.13 it could be established that the optimization results analysis (thus either the mean and the median) for the tensile strength sampled nanocomposites are within the range of 0.92 and 0.97. The range of the highest values of the experimental results is 0.88 and 0.95. This shows an improvement of the tensile strength property of nanocomposites and therefore proving that the optimization model could be essential in the design of nanocomposite materials.

4.2.2 Effects of interphase properties

This section presents and discusses the effects of the interphase properties (i.e. interphase elastic modulus (E_i), interphase thickness (t_i) and interfacial shear strength (τ) on both the elastic modulus and the tensile strength of polymer nanocomposites). It is worth noting that the interphase thickness is the only design variable that is common in the two objectives of the current study. The interphase elastic modulus can only influence the elastic modulus of the nanocomposite whereas, the interfacial shear strength can only influence the tensile strength (see Figure 3.4). Thus, this section will be subdivided into; (i) the effects of the thickness of the interphase on both elastic modulus and tensile strength, (ii) effects of interphase elastic modulus on the nanocomposite elastic modulus and (iii) lastly, effects of the interfacial shear strength on the tensile strength of nanocomposites.

i). Effects of interphase thickness on elastic modulus and tensile strength

Figures 4.14 to 4.17 show the effect of interphase thickness on the normalized elastic modulus and Figures 4.18 to 4.21 show the effect of the interphase thickness on the normalized tensile strength. Figure 4.22 shows the box and whisker plot for the thickness of the interphase. From the figures it can be observed that the optimum mean interphase thickness that could produce improved properties for Nylon-MMT is 4.07 nm, for Pa-$CaCO_3$ is 2.78 nm and for SBR-MWCNTs and iPP-MWCNTs is 2.17 nm and 2.32 nm respectively. From the median analysis, it can be seen from Figure 4.22 that the optimum interphase thickness that could produce improved mechanical properties for the sampled nanocomposites are 2.96 nm for Nylon-MMT, 2.24 nm for Pa-$CaCO_3$, 2.12 nm for SBR-MWCNTs and 2.31 nm for iPP-MWCNTs respectively.

Figure 4.22 also illustrates that the interphase thickness data of Nylon-MMT has a lot of variation and possible outliers. The values of the interphase thicknesses are skewed to the right (i.e. the variation of the data is above the median). From the same figure, it can be observed that the optimization values of the thickness of interphase for Pa-$CaCO_3$ shows some level of clustering. The plot has a long whisker on the upper side of the box and thus indicating the presence of outliers. Just like Nylon-MMT data distribution, the distribution of Pa-$CaCO_3$ also exhibit skewness to the right.

The interphase thickness data of SBR-MWCNTs and iPP-MWCNTs shows a high level of clustering and absence of outliers. Furthermore, the plot also shows that there is symmetrical distribution of data around the median values. From the analysis of the obtained optimum values of the interphase thickness, it follows that the nanocomposites that are reinforced with carbon nanotubes shows clustering of results as desired and those reinforced with other materials have a relatively high level of variation. Thus, further research should be done to verify this to be the case or not.

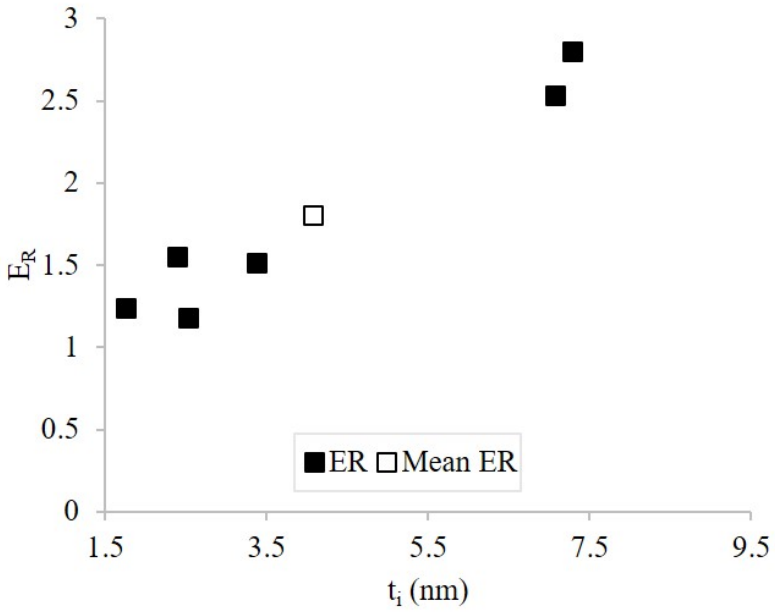

Figure 4.14: Effect of interphase thickness on the normalized elastic modulus for Nylon-MMT.

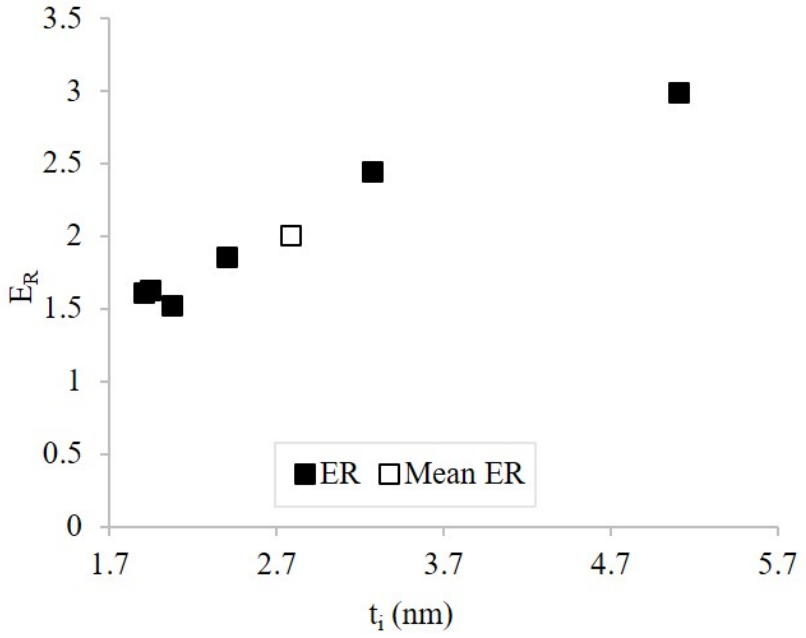

Figure 4.15: Effect of interphase thickness on the normalized elastic modulus for Pa-$CaCO_3$.

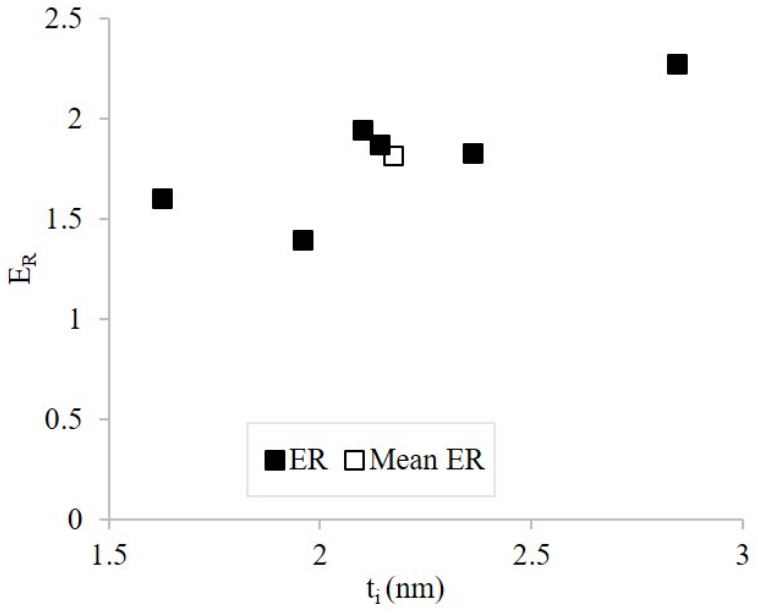

Figure 4.16: Effect of interphase thickness on the normalized elastic modulus for SBR-MWCNTs.

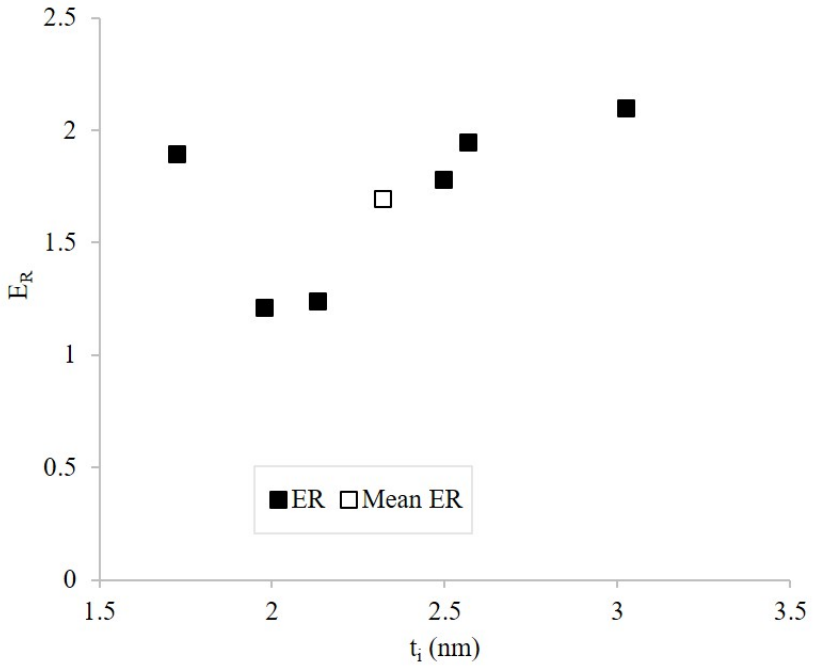

Figure 4.17: Effect of interphase thickness on the normalized elastic modulus for iPP-MWCNTs.

The comparison of the effects of thickness of interphase on the elastic modulus against that of the tensile strength shows that the design variable has inverse effects on the two properties. (i.e Figures 4.14 to 4.17, the elastic modulus is generally increasing with an increasing interphase thickness whereas the inverse effect is seen on Figures 4.18 to 4.21 for the tensile strength). For example, the normalized elastic modulus of Pa-$CaCO_3$ is about 1.5 with the corresponding interphase thickness of about 1.7 nm and 2.5 with the interphase thickness of about 5.2 nm respectively. For the same material and the same interphase thicknesses, the normalized tensile strength was computed to be 0.98 and 0.9 respectively.

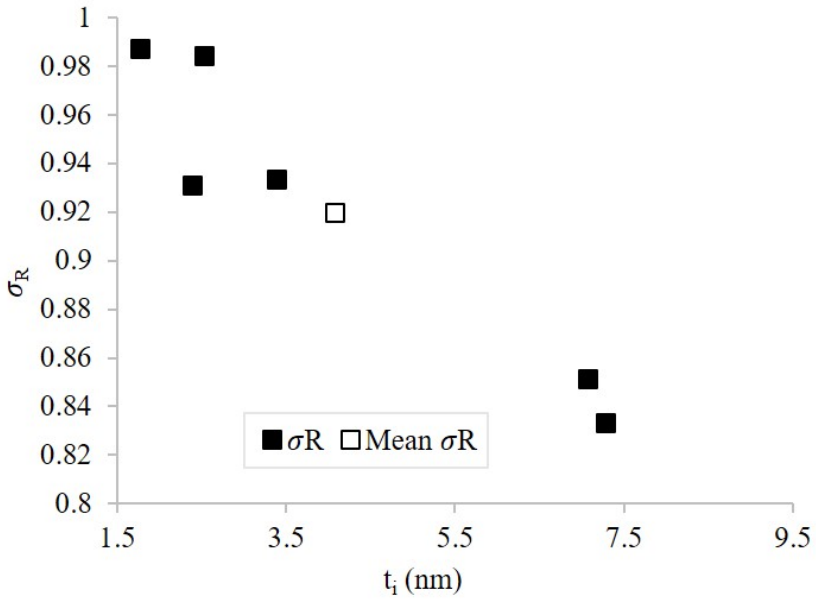

Figure 4.18: Effect of interphase thickness on the normalized tensile strength for Nylon-MMT.

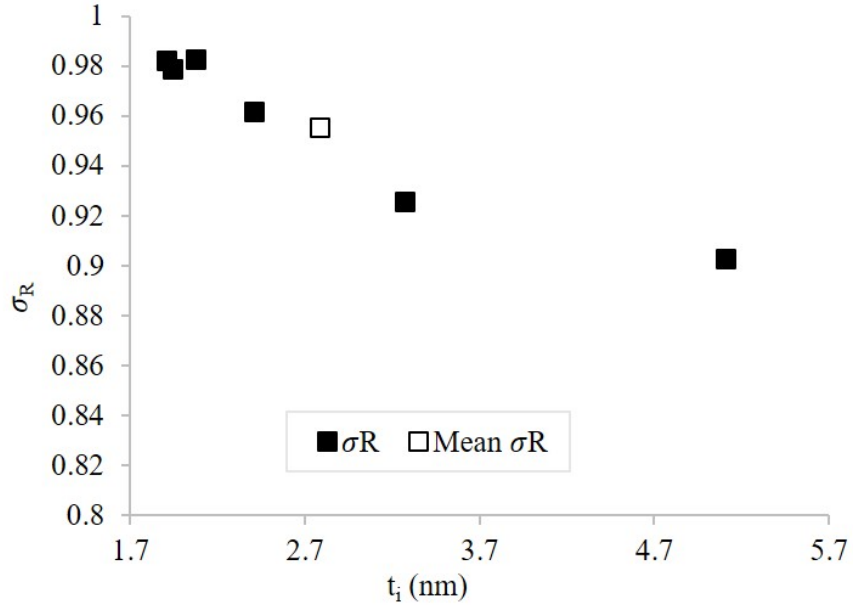

Figure 4.19: Effect of interphase thickness on the normalized tensile strength for Pa-$CaCO_3$.

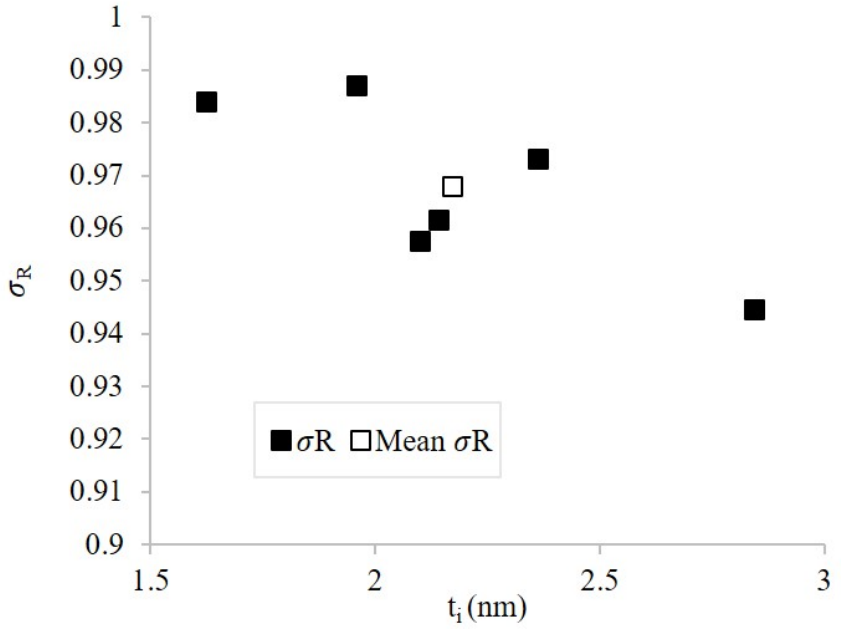

Figure 4.20: Effect of interphase thickness on the normalized tensile strength for SBR-MWCNTs.

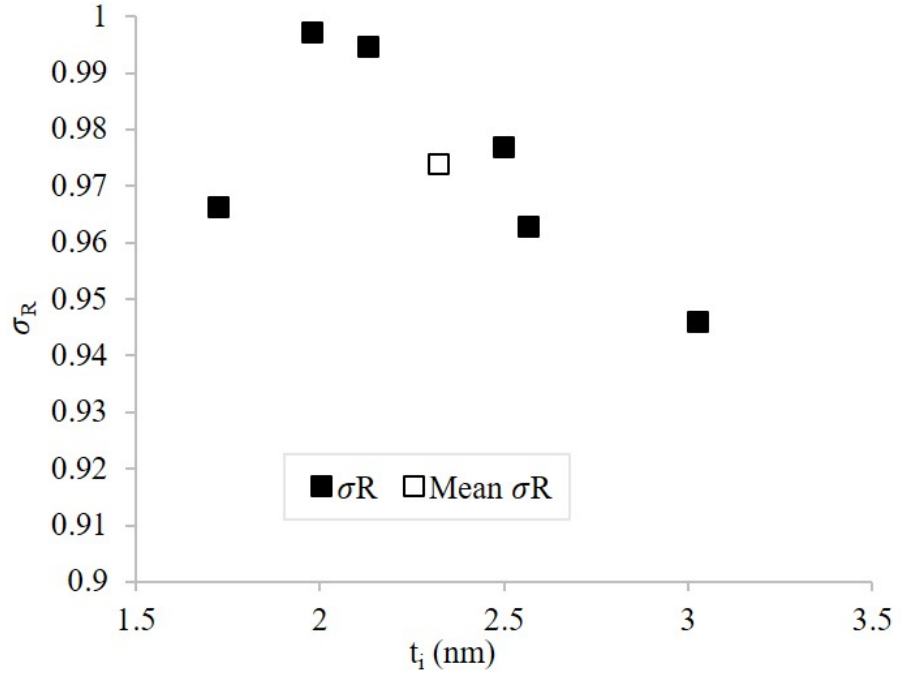

Figure 4.21: Effect of interphase thickness on the normalized tensile strength for iPP-MWCNTs.

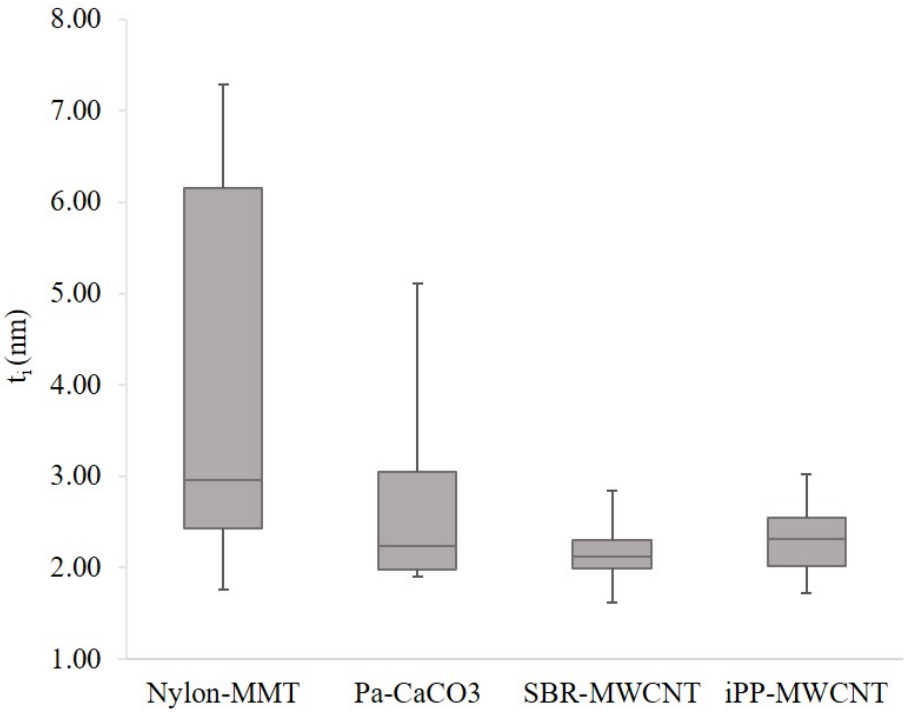

Figure 4.22: Box and whisker plot for thickness of the interphase

Zare et al. [101] on their investigation of the effects of interphase on the tensile strength of polymer nanocomposites have shown that the values of interphase thickness (t_i) were in the range of 2.38 to 13.6 nm for their sampled nanocomposites. In another study, Zare et al. [100] investigated the interphase elastic modulus and the tensile strength of polymer nanocomposites and found that the values of the interphase thickness were between 5.7 and 12.5 nm.

For the current optimization model, the smallest and highest interphase thickness were found to be 1.5 and 7.5 nm respectively. The ranges of the optimum interphase thickness from both mean and median analysis were determined to be 4.07 - 2.78 nm and 2.96 - 2.31 nm respectively. This shows the predictions of optimized model are still within the accepted region. It is worth noting that the interphase thickness from Zare et al. [101] were obtained through fitting experimental tensile strength data. The optimization model on the other hand directly determined the values of the design variables. This therefore further shows another advantage that the model possess with regard to the design and development of nanocomposites in general.

ii). Effects of interphase elastic modulus on the nanocomposite elastic modulus

This subsection discusses the effects of the interphase elastic modulus on the elastic modulus. Figures 4.23 to 4.26 show the effect of the interphase modulus on the normalized elastic modulus of the selected nanocomposite pairs. Figure 4.27 shows the box and whisker plot for the interphase modulus. The mean interphase modulus for obtaining an optimum tensile strength of the selected nanocomposite pairs are 19.72 GPa for Nylon-MMT, 31.28 GPa for Pa-$CaCO_3$, 600.88 GPa for SBR-MWCNTs and 512.47 GPa for iPP-MWCNTs respectively. The median analysis on the other hand yielded optimum values of 19.87 GPa for Nylon-MMT, 31.31 GPa for Pa-$CaCO_3$, 551.04 GPa for SBR-MWCNTs and 539.39 GPa for iPP-MWCNTs. The median analysis gave higher values of the interphase modulus compared to those of the mean analysis for all sampled nanocomposites except for SBR-MWCNTs.

From Figure 4.27 it can be seen that the optimum values of the interphase modulus for Nylon-MMT cluster around the median. For the other nanocomposites, the box plots are wider therefore suggesting that the optimum values have more variation from the median. The Figure also shows that interphase modulus values of Nylon-MMT and Pa-$CaCO_3$ exhibit a symmetrical distribution of data whereas that of SBR-MWCNT and iPP-MWCNT shows distributions skewed to the right and skewed to the left respectively. In addition, the plots of SBR-MWCNTs and iPP-MWCNTs nanocomposites have relatively long whiskers compared to those of Pa-$CaCO_3$ and Nylon-MMT. This therefore shows that the optimum interphase modulus values for those materials have outliers. It could also be seen from the plots that the median values of the nanocomposites reinforced with MWCNTs are similar.

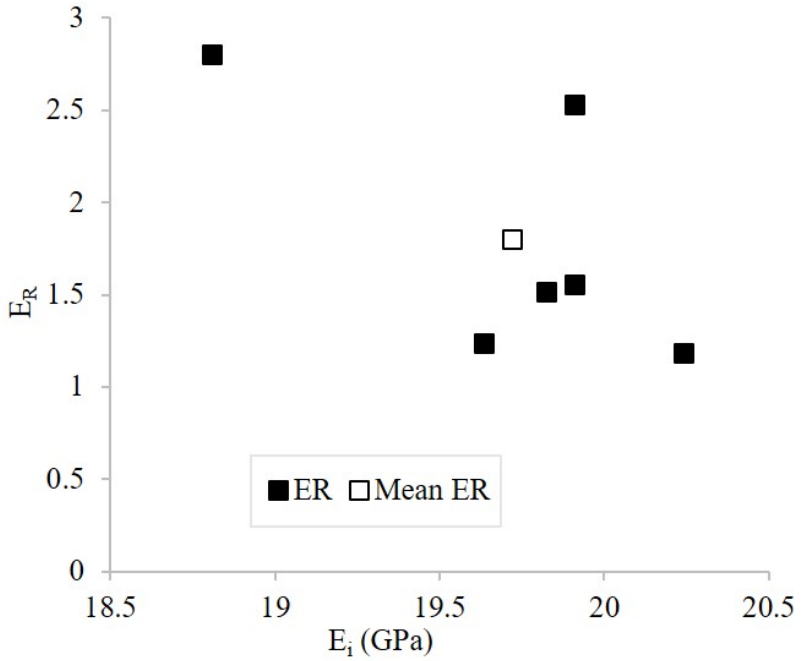

Figure 4.23: Effect of interphase modulus on the normalized elastic modulus for Nylon-MMT.

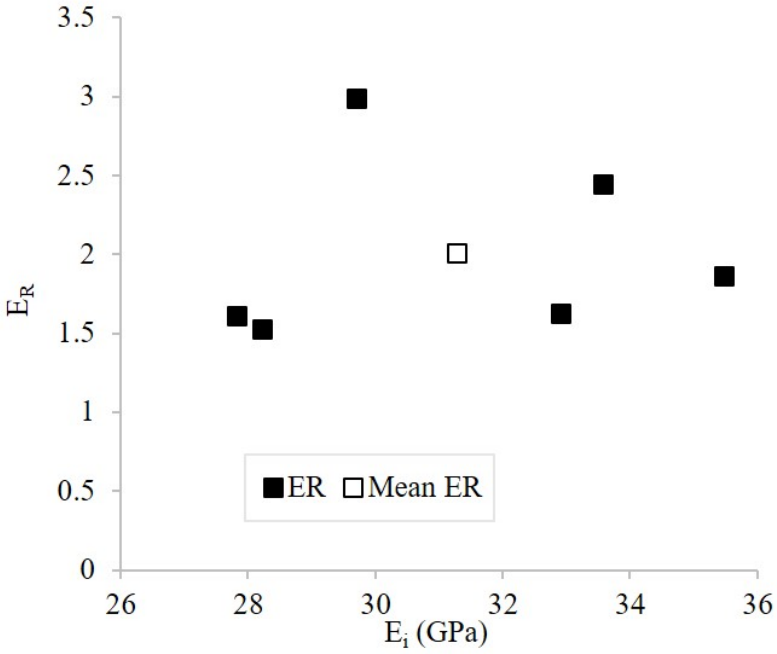

Figure 4.24: Effect of interphase modulus on the normalized elastic modulus for Pa-$CaCO_3$.

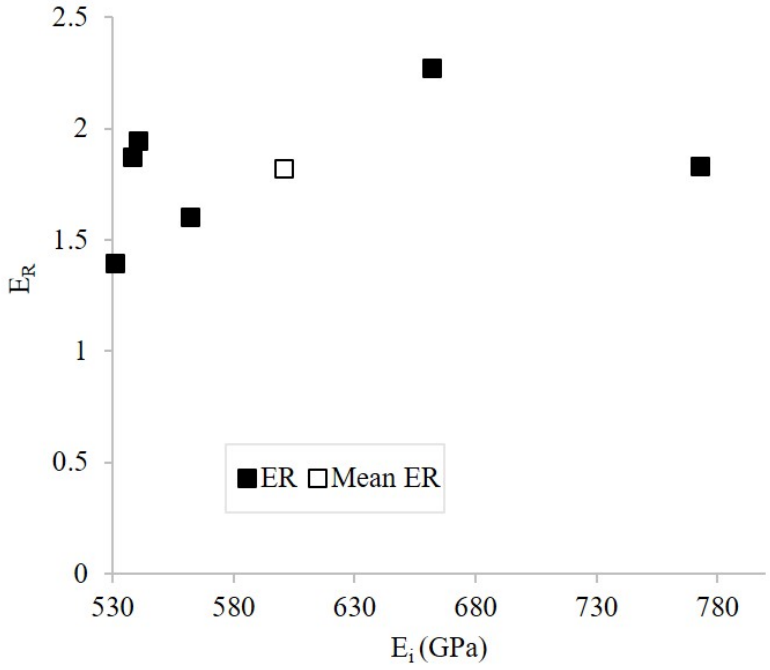

Figure 4.25: Effect of interphase modulus on the normalized elastic modulus for SBR-MWCNTs.

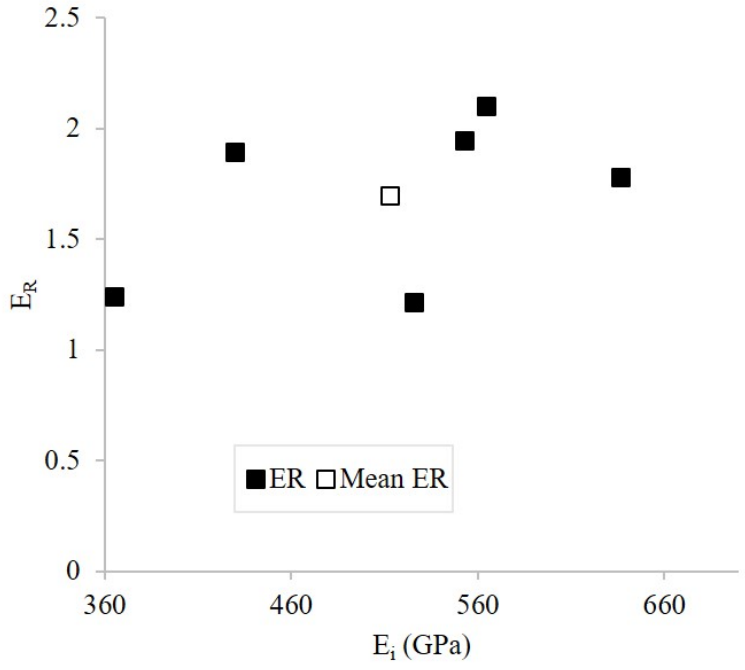

Figure 4.26: Effect of interphase modulus on the normalized elastic modulus for iPP-MWCNTs.

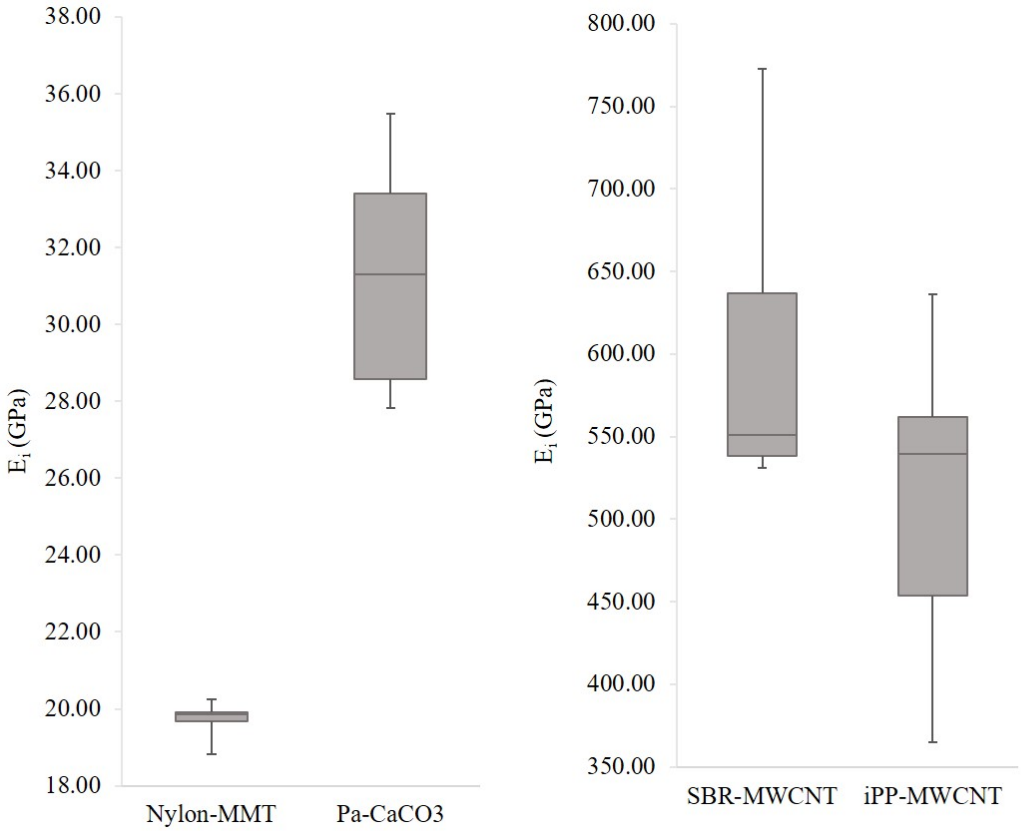

Figure 4.27: Box and whisker plot for the elastic modulus of the interphase

From the mean analysis the interphase modulus was determined to be at least 6 times the modulus of the matrix for Nylon-MMT, 60 times for Pa-$CaCO_3$, 300 times for SBR-MWCNT and 320 times for iPP-MWCNT. From the median analysis, the interphase modulus was found to be about 6 times that of Nylon for Nylon-MMT nanocomposite, for Pa-$CaCO_3$ the interphase modulus was calculated to be 61 times that of Polyamide, and for SBR-MWCNT and iPP-MWCNT, the interphase modulus was determined to be about 275 and 337 times that of the respective matrices. Zare et al. [100] found that the smallest interphase modulus for their sampled nanocomposites were at least 10 times that of the matrix. Therefore, this clearly shows that, the numerical optimization model of the current study was able to improve the properties of the sampled nanocomposite materials.

It could further be seen that the MWCNTs composites have higher interphase modulus and thus provide improved properties. This therefore indicates the important role of the reinforcing agents on the overall properties of the nanocomposites. In addition, it also showed the reason MWCNTs are mainly preferred in nanocomposites design as reinforcements for many structural applications.

It is also worth mentioning that the this ratio of the modulus of the interphase to the matrix is implicitly given within Ji model that was used as the first objective function (see Equation 3.5). The ratio describes a linear change of the modulus from the matrix to the surface of the nanofiller reinforcement. In previous investigations where Ji model was applied, the given ratio was usually determined through curve fitting [96, 100, 94]. Thus, until now a model that computes and determine the interphase modulus through Ji model was not in existence. This further cements the advantages that the optimization model brings in the design of polymer based nanocomposite materials.

Figures 4.28 and 4.29 shows the comparison of the elastic moduli (GPa) of the different constituents of the sampled polymer nanocomposites for both mean and median analysis. This was done so as to compare and contrast the values of the elastic modulus of the sampled nanocomposite materials. From both figures it can be seen that modulus of the interphase is much closer to the modulus of the nanofiller (reinforcement) than that of the matrix.

Figure 4.30 illustrates the percentage difference between the elastic modulus of the nanofillers and that of the interphase. It is worth noting from Figure 4.30 that the difference in percentage between the interphase modulus and the nanofiller is less for nanocomposites with lower elastic modulus of the reinforcing material (i.e. MMT and $CaCO_3$) whereas those reinforced with nanofillers that have high elastic modulus (MWCNTs) have a higher percentage difference. Even though that is the case, the overall interphase modulus properties for the materials with MWCNTs as reinforcements are higher compared to the other sampled materials.

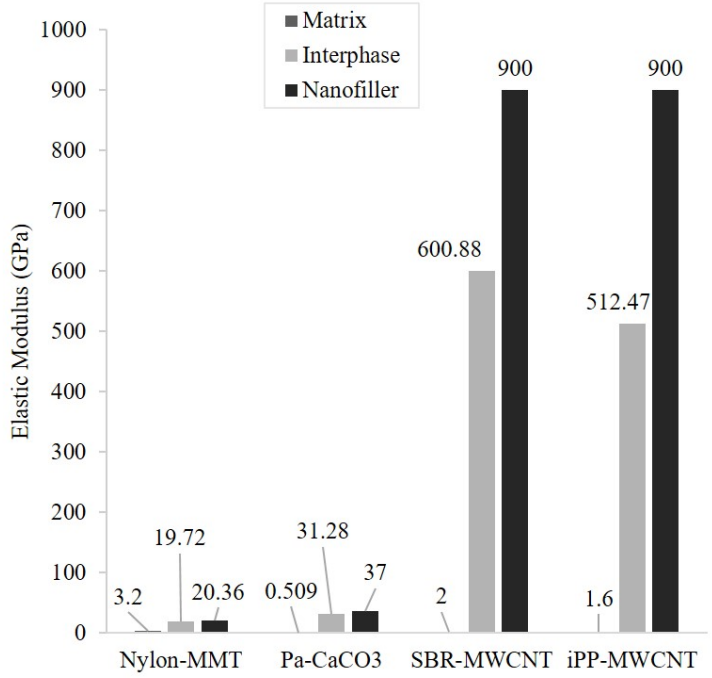

Figure 4.28: Comparison of elastic modulus of nanocomposites constituent for mean analysis.

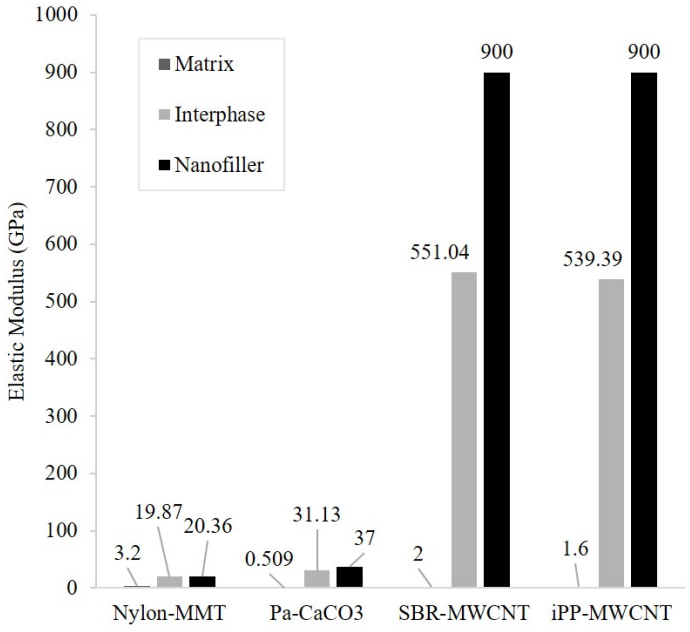

Figure 4.29: Comparison of elastic modulus of nanocomposites constituent for median analysis.

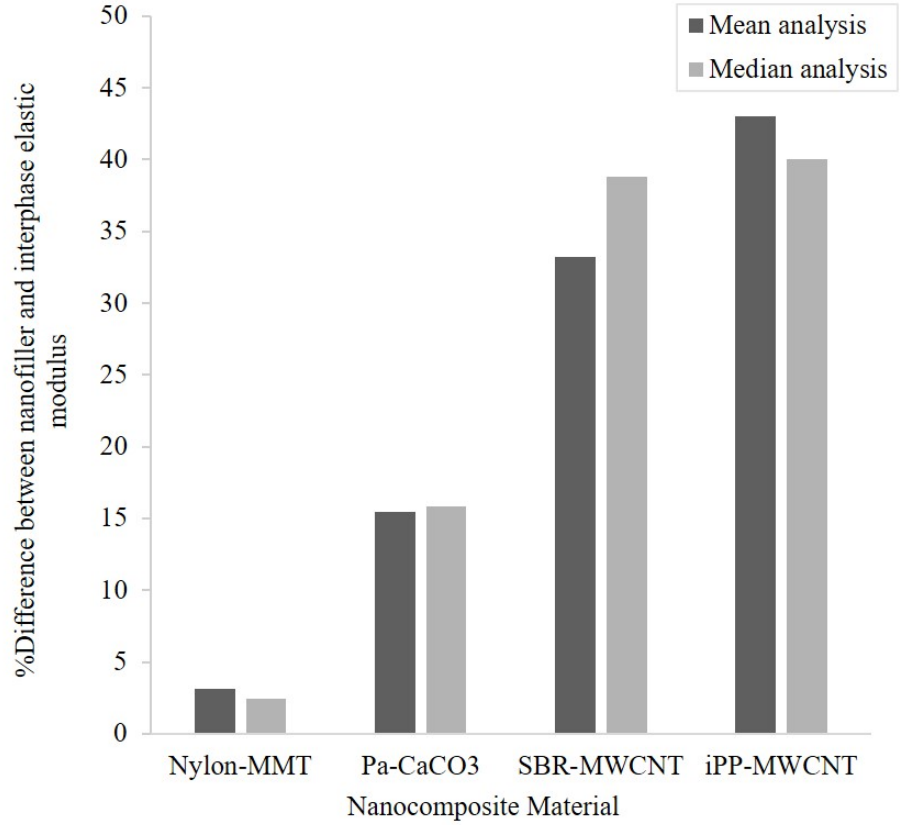

Figure 4.30: Percentage difference between the elastic modulus of the nanofiller and the interphase

iii). Effects of the interfacial shear strength on the tensile strength

Figures 4.31 to 4.34 show the effect of interfacial shear strength (τ) on the normalized tensile strength (σ_R). Figure 4.35 shows the box and whiskers plot for the interfacial shear stress. The optimum mean τ of the sampled nanocomposites were determined to be 50.69 MPa for Nylon-MMT, 51.16 MPa for Pa-$CaCO_3$, 50.12 MPa for SBR-MWCNTs and 51.32 MPa for iPP-MWCNTs. The median optimum values of the interfacial shear stress were computed to be 51.92 MPa for Nylon-MMT, 51.97 MPa for Pa-$CaCO_3$, 50.36 MPa for SBR-MWCNTs and 51.92 MPa for iPP-MWCNTs respectively. The comparison of the optimum interfacial shear stress values shows that the results obtained through median analysis are relatively higher compared to those that were obtained from the mean analysis.

From Figure 4.35, it can be observed that SBR-MWCNT has the wide box plot, followed by that of Nylon-MMT and Pa-$CaCO_3$. iPP-MWCNT on the other hand has the smallest box plot compared to the all the other sampled nanocomposites. This means that the optimum interfacial shear stress values of iPP-MWCNTs clusters around the median as compared to the other nanocomposites. It should be noted that the median of iPP-MWCNT plot coincides with the upper quartile and thus the data is more clustered above the median. The optimum values of SBR-MWCNT have more variation compared to those of Nylon-MMT and Pa-$CaCO_3$ respectively. The median values of Nylon-MMT and Pa-$CaCO_3$ also coincides with the upper quartile just like that of iPP-MWCNTs. In addition, the plots of Nylon-MMT, Pa-$CaCO_3$ and iPP-MWCNTs exhibit skewness to the right whereas that of SBR-MWCNTs is symmetrical. All the plots have relatively long whiskers below the median values therefore indicating the presence of outliers in the data.

It could be seen from Figures 4.31 to 4.34 that the interfacial shear strength was optimized to within approximately 95% of the upper limit constraint (i.e. 52 MPa) imposed on the optimization model for all sampled nanocomposites. Equation 3.15 (the second objective function equation), shows that τ together with the polymer matrix strength plays a significant role in determining the overall tensile strength of polymer nanocomposites. Thus, it could be concluded that the large values of τ suggests strong interphase regions and therefore can prevent nanocomposites from failing through debonding during loading. Consequently, this also implies that smaller values of the interfacial shear strength would mean that the interactions between the nanofillers and the polymer matrix are weak.

The overall analysis of the interfacial shear strength analysis suggests that the optimization model could be influenced by constraints that are imposed on the different design variables. It follows therefore, that, it is very important for nanocomposite materials designers to have a clear understanding of the impacts that the different design variables may have on the entire model. This can be done through sensitivity analysis of those variables on the objective functions of the optimization model (i.e. the extent to which each of the design variable affect the objective function).

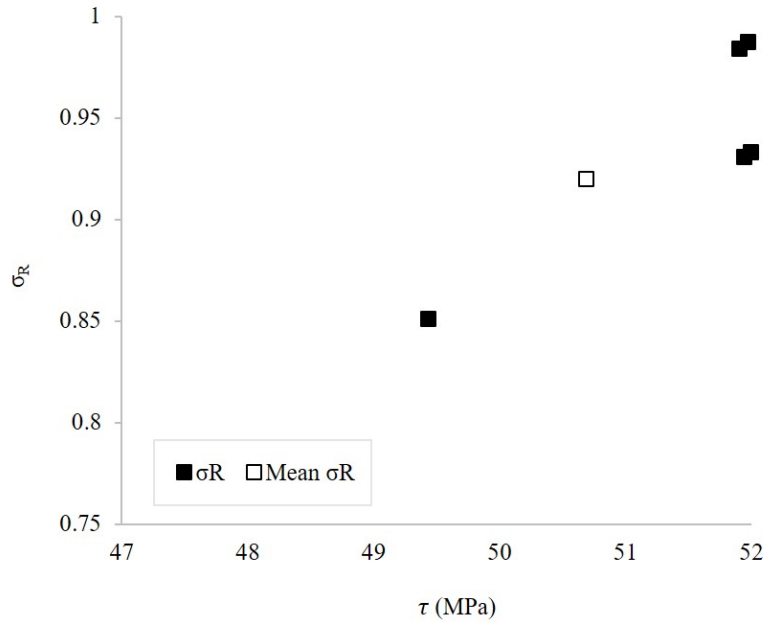

Figure 4.31: Effect of interfacial shear strength on the normalized tensile strength for Nylon-MMT.

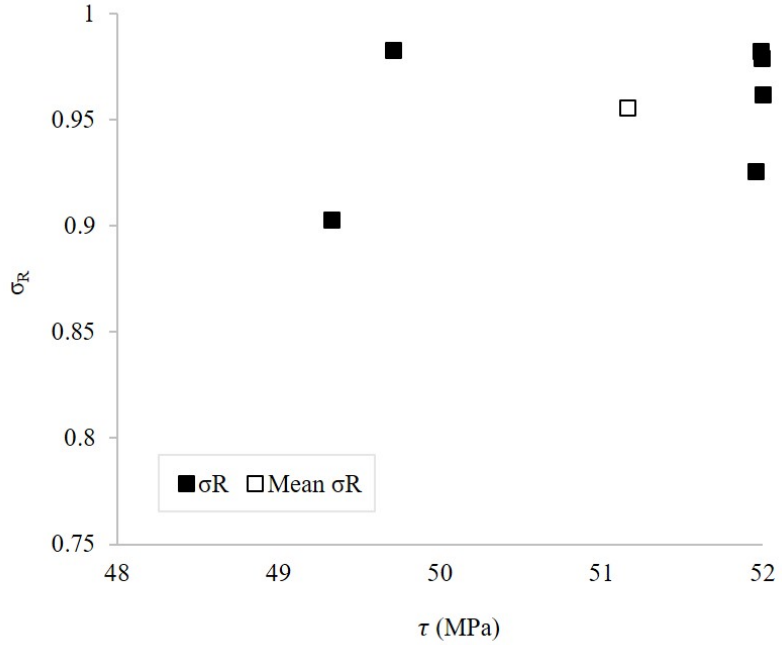

Figure 4.32: Effect of interfacial shear strength on the normalized tensile strength for Pa-$CaCO_3$.

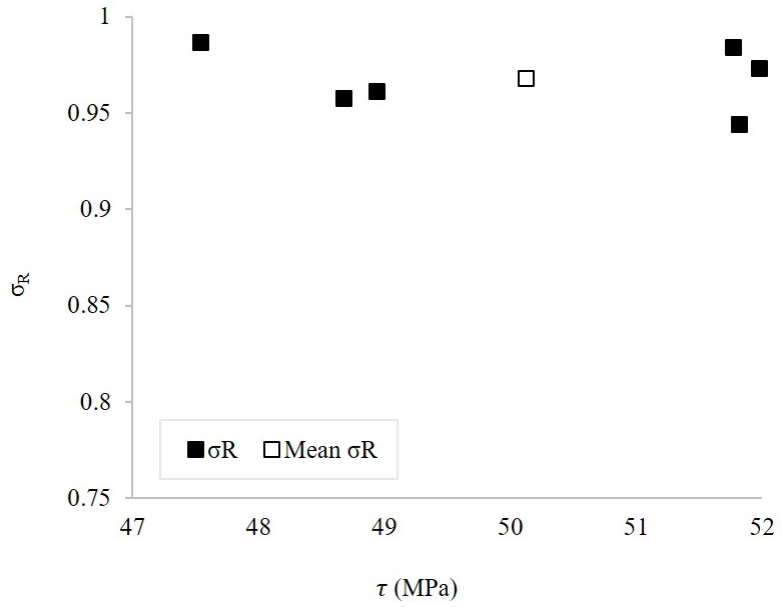

Figure 4.33: Effect of interfacial shear strength on the normalized tensile strength for SBR-MWCNTs.

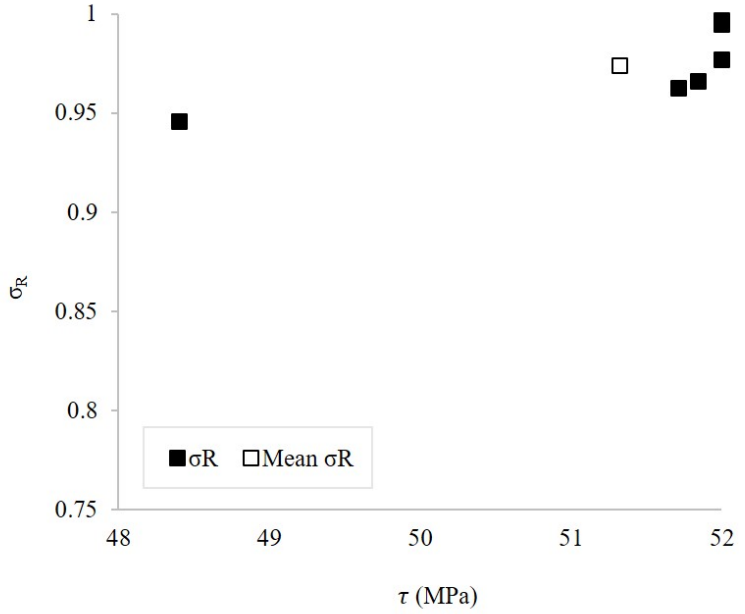

Figure 4.34: Effect of interfacial shear strength on the normalized tensile strength for iPP-MWCNTs.

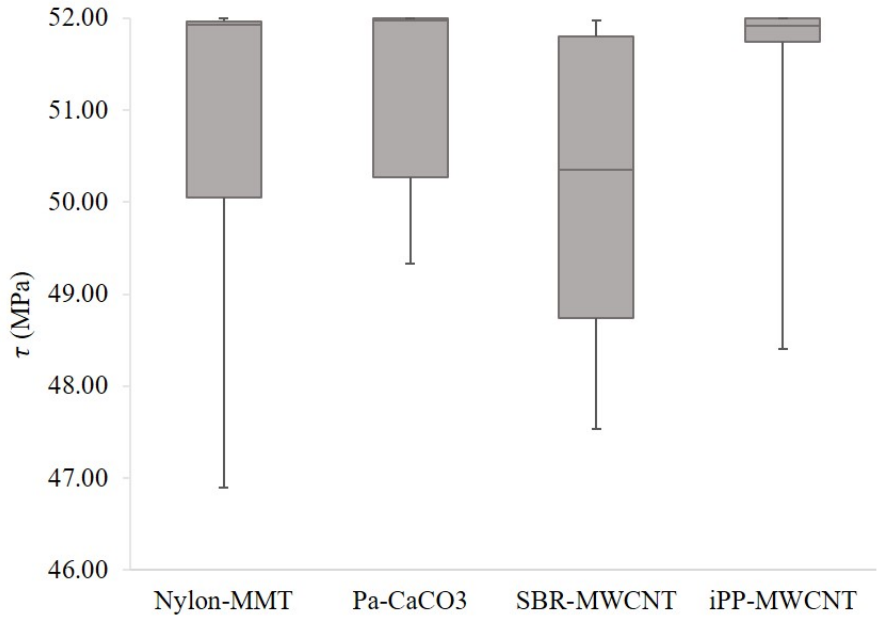

Figure 4.35: Box and whisker plot for interfacial shear stress

4.2.3 Effects of dispersion on the tensile strength

To the author's knowledge, there is currently no known direct theoretical models that could be used to quantify and understand the effects of dispersion on the mechanical properties of nanocomposite materials. Hence, for the current analysis, parameter B which was obtained by combining the normalized tensile strength, σ_R or the second objective function, f_2 (see Equation 3.15) and the Pukanszky model (Zare et al. [101]) was used for such purpose.

Figures 4.36 to 4.39 show the effects of dispersion on the normalized tensile strength. Figure 4.40 shows the box and whisker plot for parameter B. From Figures 4.36 to 4.39 it can be observed that the range of optimum parameter B values for the sampled nanocomposites are 2.8 - 2.85 for Pa-$CaCO_3$, 3.1 - 3.2 for Nylon-MMT, 4.4 - 4.6 for SBR-MWCNTs and 3.25 - 3.35 for iPP-MWCNTs respectively. The mean B values are 3.14 for Nylon-MMT, 2.83 for Pa-$CaCO_3$, 4.5 for SBR-MWCNTs and 3.33 for iPP-MWCNTs respectively. The median B values were determined to be 3.16 for Nylon-MMT, 2.84 for Pa-$CaCO_3$, 4.55 for SBR-MWCNTs and 3.34 for iPP-MWCNTs (see Table A.16 in the Appendix). Figure 4.40 shows that the optimum values of B clusters around the median (i.e. the boxes are very short and indicate symmetrical

distributions). In addition, it can be observed that both analysis yield results which are almost the same.

Zare et al. [96] reported that the optimum value for parameter B (i.e. good dispersion of nanofillers within the matrix) is about 3.37. In a different study, Zare [116] found that the values of B less than 2.4 yields undesirable interphase properties. Thus, it is necessary for the values of parameter B to be greater than 2.4 in order to obtain optimum overall tensile properties of polymer nanocomposites. Another investigation by Lazzeri and Phuong [121] also reported that parameter B has a minimum critical value of about 3. Conclusively, the optimum values of the parameter B are comparable with those in the literature and therefore, this again shows that the proposed optimization model is accurate enough in predicting and optimizing the mechanical properties of nanocomposites.

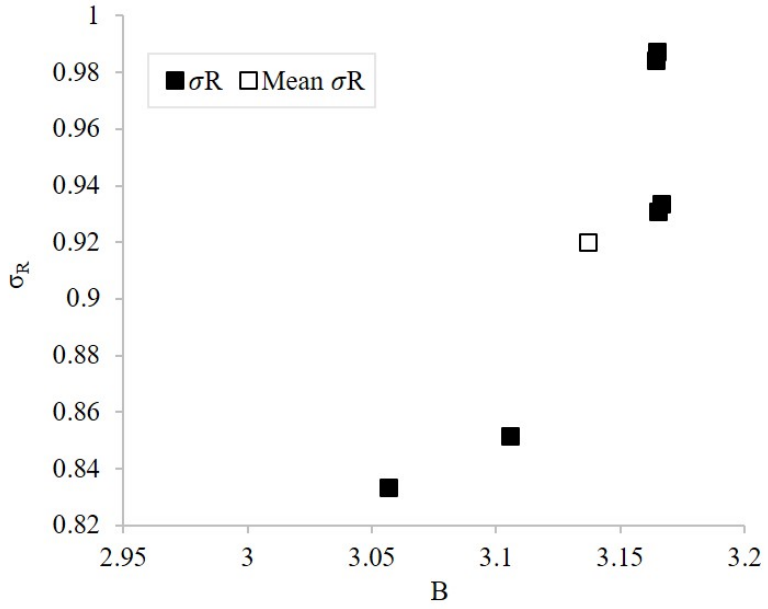

Figure 4.36: Effect of interfacial shear strength on the normalized tensile strength for Nylon-MMT.

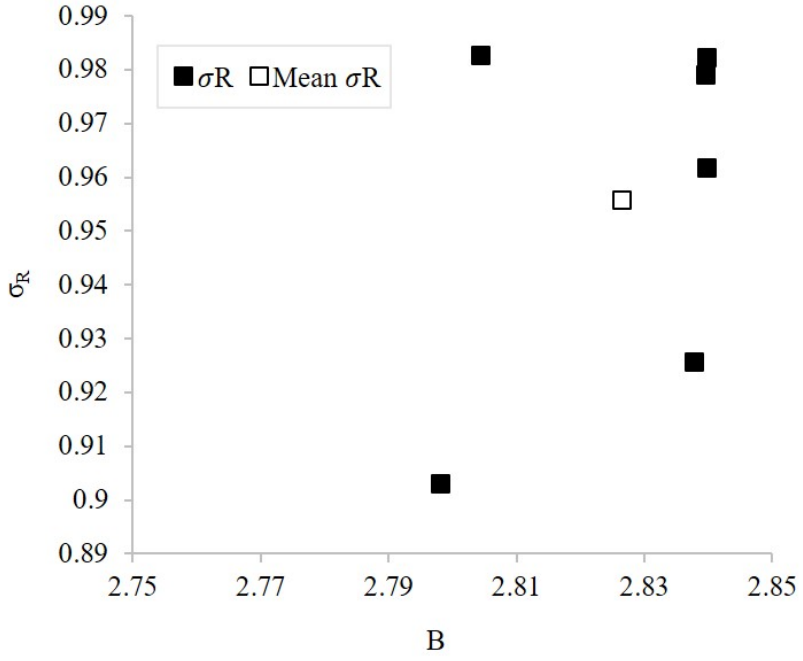

Figure 4.37: Effect of interfacial shear strength on the normalized tensile strength for Pa-$CaCO_3$.

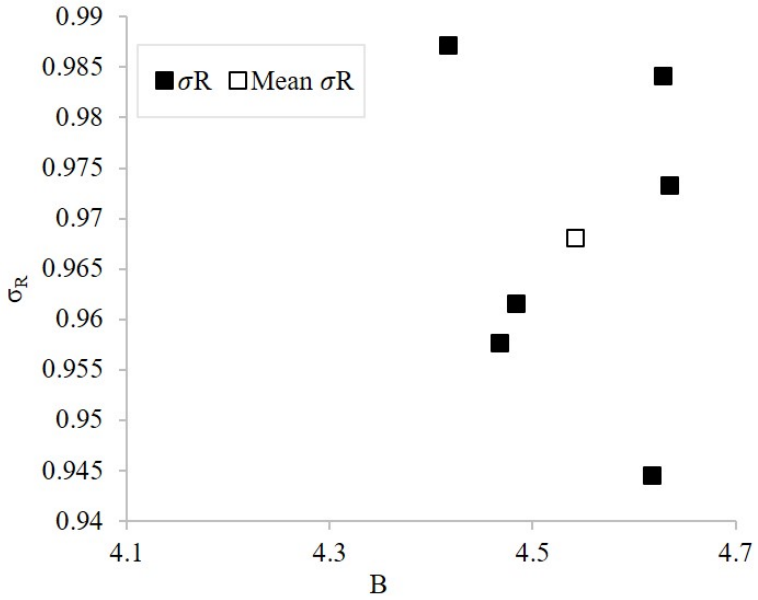

Figure 4.38: Effect of interfacial shear strength on the normalized tensile strength for SBR-MWCNTs.

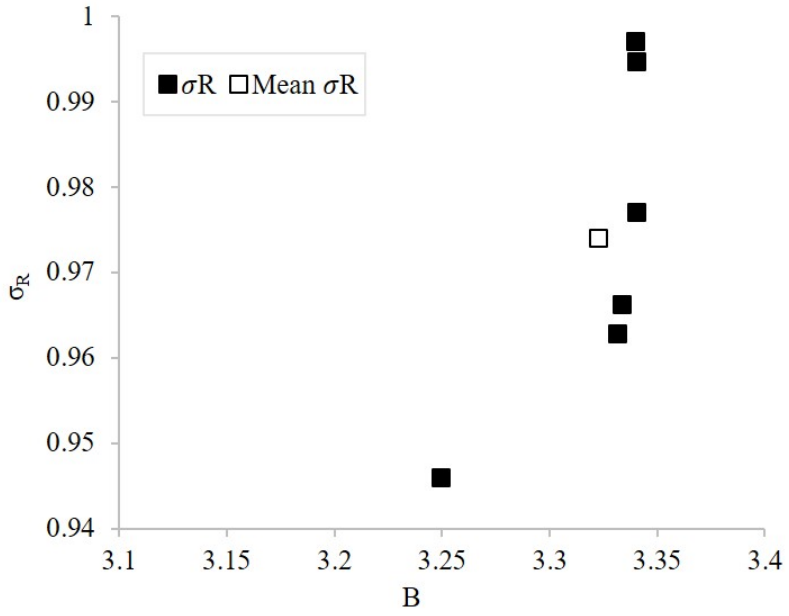

Figure 4.39: Effect of interfacial shear strength on the normalized tensile strength for iPP-MWCNTs.

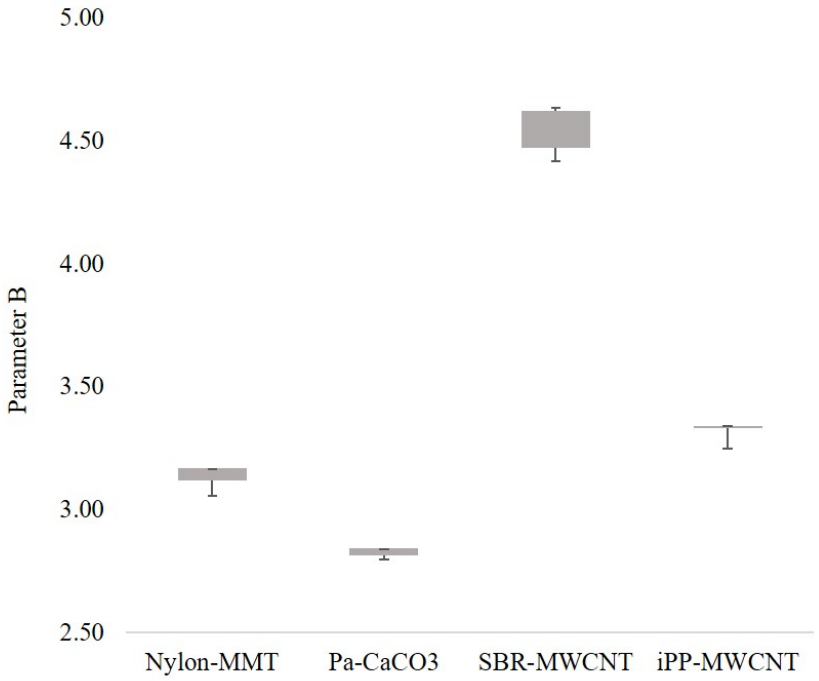

Figure 4.40: Box and whisker plot for the parameter B

It is worth noting that the dispersion parameter in the current study has no relations to the elastic modulus as the property is not included in the formulation of the Pukanszky model. However, even though that is the case, it is deemed necessary for nanocomposite materials designers to find alternative ways and develop models that can determine the effect of dispersion on the mechanical properties. This is of significant importance due to the fact that dispersion is regarded as one of the most important design parameters in nanocomposite materials.

Chapter 5 Conclusions and Recommendations

5.1 Conclusions

In the present study, a multi-objective optimization (MOO) model was developed to simultaneously maximize the elastic modulus and the tensile strength of polymer nanocomposites. For this purpose, four major factors (i.e. interphase and interfacial adhesion, nanofillers loading, dispersion and alignment) that influence the mechanical properties of nanocomposites were studied. Using these factors, a nanocomposite design problem was established and then converted into a mathematical problem for optimization.

The objective functions of the optimization model were based on Ji model and Zare model for determining the elastic modulus and the tensile strength of polymer based nanocomposites respectively. The design parameters for optimizing the mechanical properties of polymer nanocomposites were identified as (i) thickness of the nanofillers, (ii) thickness of the interphase, (iii) nanofillers loading, (iv) modulus of the interphase, (v) interfacial shear stress and (vi) nanofillers orientation factor. The Fast Non-dominated Sorting Genetic Algorithm (NSGA-II) was then implemented in MATLAB to solve for the given nanocomposite material design problem.

The proposed optimization model was able to successfully find the optimum solutions of the design parameters. The results were analyzed by using the mean and median descriptive statistical analysis of data. The difference in results from the two methods of analysis were not significantly large and therefore, it can be concluded that both approaches yield approximately the same results. However, it should be noted that unlike the mean approach, the median analysis is said to be unaffected by the outliers. Hence, it is deemed to be more reliable in comparison with regard to descriptive statistical analysis of data. Given the fact that some of the results from the optimization model contained outliers, the results obtained through the median analysis are thus taken to be a truer reflection of the model solutions.

The overall optimization results from both approaches were found to be in good agreement with the experimental results from literature. The optimized results for the normalized elastic modulus were found to be higher than the experimental results. The optimum values of the normalized tensile strength were also found to be high compared to the experimental results. Furthermore, the optimum results of the normalized elastic modulus and the normalized tensile strength were found to be in the ranges between 1.54 - 1.85 and 0.9 - 1 for the two mechanical properties of the sampled polymer nanocomposites respectively.

It was expected that the optimization model would perform better than the experimental results since the maximization of the design parameters means obtaining the 'best' solutions and combinations that will yield better mechanical properties. Overall, the developed optimization model was found to be significantly accurate in finding the mechanical properties of nanocomposites. From the optimization model the optimum values of the design parameters for obtaining the best mechanical properties of the selected nanocomposites are proposed to be as follows:

(i) Nanofillers loading should be between 2.95 and 4.69 wt.%.

(ii) The thickness of the interphase ranges between 2.12 and 2.96 nm.

(iii) Nanofillers dimeter should be between 5.41 and 7.01 nm.

(iv) The orientation factor for fully aligned nanofillers is 1.

It was further discovered that the elastic modulus of the interphase is directly proportional to that of the nanofillers. Thus, nanofillers with high modulus of elasticity yielded nanocomposites with a relatively high elastic interphase modulus. This further outlined the reason nanofillers such as carbon nanotubes (CNTs) are usually preferred as reinforcements in many structural applications of composite materials. The tensile strength on polymer nanocomposites was found to be highly influenced by the interfacial shear strength.

It should be noted that this design parameter was optimized to within at least 95 % of the imposed optimization constraint. This suggests that great care must be given to the interfacial shear strength when modeling the tensile properties of polymer nanocomposites. In addition, the optimum tensile strength results were used to determine the dispersion parameter of nanofillers within the polymer matrix. The optimum values of the dispersion parameter were found to be within the acceptable range when compared to literature. The optimum values of dispersion parameter were determined to be between the ranges 3 and 4.6.

The current study has shown that numerical multi-objective optimization methods could be used to design and improve the mechanical properties of polymer based nanocomposite materials for broad structural applications. With this model, the best combinations of solutions for the major factors that affect the mechanical properties of nanocomposites can be obtained with relative ease. Thus, the optimization model has shown that it could be advantageous during the preliminary design stages in terms of time saving compared to conducting of physical experiments which are very time consuming in their nature.

5.2 Recommendations

In order to ensure that the proposed approach is robustly developed as a tool for preliminary design of nanocomposite materials, the following additional work is recommended:

(i) Research into ways of directly quantifying dispersion of nanofillers within polymer matrix. This will enable one to be able to identify optimum parameters that will ensure uniform dispersion as it was found to be one of the major factors affecting the mechanical properties.

(ii) Perform physical experiments using the suggested values of the design parameters to further verify and validate the optimization model.

(iii) Use other numerical optimization approaches and compare the findings with the results obtained from the current study.

(iv) Perform sensitivity analysis to determine the design parameters that have a higher influence on the optimization model.

In addition, it is worth noting that while the work here represents progress towards the design of nanocomposites materials, more research is still required to further understand the fundamental principles on mechanical reinforcement in polymer based nanocomposites.

Bibliography

[1] M. M. Abolhasani et al. 'Poly (vinylidene fluoride)–acrylic rubber partially miscible blends: phase behavior and its effects on the mechanical properties'. In: *Journal of applied polymer science* 130.2 (2013), pp. 1247–1258.

[2] N. Subramanian, A. Rai and A. Chattopadhyay. 'Atomistically informed stochastic multiscale model to predict the behavior of carbon nanotube-enhanced nanocomposites'. In: *Carbon* 94 (2015), pp. 661–672.

[3] S. M. Razavi et al. 'Thermal, mechanical, and corrosion resistance properties of vinyl ester/clay nanocomposites for the matrix of carbon fiber-reinforced composites exposed to electron beam'. In: *Journal of Applied Polymer Science* 132.33 (2015).

[4] M. Bhattacharya. 'Polymer nanocomposites - A comparison between carbon nanotubes, graphene, and clay as nanofillers'. In: *Materials* 9.4 (2016), p. 262.

[5] H. U. Zaman et al. 'Polypropylene/clay nanocomposites: effect of compatibilizers on the morphology, mechanical properties and crystallization behaviors'. In: *Journal of Thermoplastic Composite Materials* 27.3 (2014), pp. 338–349.

[6] M. S. Islam, R. Masoodi and H. Rostami. 'The effect of nanoparticles percentage on mechanical behavior of silica-epoxy nanocomposites'. In: *Journal of Nanoscience* 2013 (2013).

[7] I. Y. Stein et al. 'Processing and mechanical property characterization of aligned carbon nanotube carbon matrix nanocomposites'. In: *54th AIAA Structures, Structural Dynamics, and Materials (SDM) Conference, Boston, MA*. 2013.

[8] Y. Hua et al. 'Role of Interphase in the Mechanical Behavior of Silica/Epoxy Resin Nanocomposites'. In: *Materials* 8.6 (2015), pp. 3519–3531.

[9] Y. Zare. 'Assumption of interphase properties in classical Christensen–Lo model for Young's modulus of polymer nanocomposites reinforced with spherical nanoparticles'. In: *RSC Advances* 5.116 (2015), pp. 95532–95538.

[10] H. S. Khare and D. L. Burris. 'A quantitative method for measuring nanocomposite dispersion'. In: *Polymer* 2.3 (2010), pp. 719–729.

[11] J. Njuguna and K. Pielichowski. 'Polymer nanocomposites for aerospace applications: fabrication'. In: *Advanced Engineering Materials* 6.4 (2004), pp. 193–203.

[12] E. T. Thostenson, C. Li and T.-W. Chou. 'Nanocomposites in context'. In: *Composites Science and Technology* 65.3 (2005), pp. 491–516.

[13] W. Gacitua, A. Ballerini and J. Zhang. 'Polymer nanocomposites: synthetic and natural fillers a review'. In: *Maderas. Ciencia y tecnologia* 7.3 (2005), pp. 159–178.

[14] H. Ghasemi et al. 'Optimal fiber content and distribution in fiber-reinforced solids using a reliability and NURBS based sequential optimization approach'. In: *Structural and Multidisciplinary Optimization* 51.1 (2015), pp. 99–112.

[15] K. R. Shankar. 'Preparation and characterization of magnetically aligned carbon nanotube buckypaper and composite'. In: (2003).

[16] B. L. Wardle et al. 'Fabrication and characterization of ultrahigh-volume-fraction aligned carbon nanotube–polymer composites'. In: *Advanced Materials* 20.14 (2008), pp. 2707–2714.

[17] Q. Cheng et al. 'High mechanical performance composite conductor: multi-walled carbon nanotube sheet/bismaleimide nanocomposites'. In: *Advanced Functional Materials* 19.20 (2009), pp. 3219–3225.

[18] M. K. Shin et al. 'Elastomeric conductive composites based on carbon nanotube forests'. In: *Advanced materials* 22.24 (2010), pp. 2663–2667.

[19] I. Guz et al. 'Developing the mechanical models for nanomaterials'. In: *COMPOSITES Part A: applied science and manufacturing* 38.4 (2007), pp. 1234–1250.

[20] M. Bruyneel. 'Optimization of laminated composite structures: problems, solution procedures and applications'. In: *Composite Materials Research Progress* (2008).

[21] R. Khandan et al. 'Optimum design of fibre orientation in composite laminate plates for out-plane stresses'. In: *Advances in Materials Science and Engineering* 2012 (2012).

[22] A. H. Ertas. 'Optimization of fiber-reinforced laminates for a maximum fatigue life by using the particle swarm optimization. Part II'. In: *Mechanics of Composite Materials* 49.1 (2013), pp. 107–116.

[23] A. H. Ertas and F. O. Sonmez. 'Design optimization of fiber-reinforced laminates for maximum fatigue life'. In: *Journal of Composite Materials* 48.20 (2014), pp. 2493–2503.

[24] E. L. Camponeschi. 'Dispersion and alignment of carbon nanotube polymer based composites'. PhD thesis. Georgia Institute of Technology, 2007.

[25] B. Zhang. 'Manufacturing, characterization, and modeling of graphene-based nanocomposites for aircraft structural and lightning strike applications'. PhD thesis. Wichita State University, 2012.

[26] Q. Zeng, A. Yu and G. Lu. 'Multiscale modeling and simulation of polymer nanocomposites'. In: *Progress in Polymer Science* 33.2 (2008), pp. 191–269.

[27] M. Greenwald. 'Beyond benchmarking—how experiments and simulations can work together in plasma physics'. In: *Computer physics communications* 164.1 (2004), pp. 1–8.

[28] L. W. Carter, J. G. Hendricks and D. S. Bolley. *Elastomer reinforced with a modified clay.* US Patent 2,531,396. 1950.

[29] Y. Kojima et al. 'Mechanical properties of nylon 6-clay hybrid'. In: *Journal of Materials Research* 8.5 (1993), pp. 1185–1189.

[30] S. Chatterjee. 'Structural and Physical Effects of Carbon Nanofillers in Thermoplastic and Thermosetting Polymer Systems'. PhD thesis. Acta Universitatis Upsaliensis, 2012.

[31] D. A. Jesson and J. F. Watts. 'The interface and interphase in polymer matrix composites: Effect on mechanical properties and methods for identification'. In: *Polymer Reviews* 52.3 (2012), pp. 321–354.

[32] S. Pfeifer and P. Bandaru. 'A methodology for quantitatively characterizing the dispersion of nanostructures in polymers and composites'. In: *Materials Research Letters* 2.3 (2014), pp. 166–175.

[33] A. Poorsolhjouy and M. Hassan Naei. 'Effects of carbon nanotubes' dispersion on effective mechanical properties of nanocomposites: A finite element study'. In: *Journal of Reinforced Plastics and Composites* 34.16 (2015), pp. 1315–1328.

[34] F. Deng et al. 'Elucidation of the reinforcing mechanism in carbon nanotube/rubber nanocomposites'. In: *ACS nano* 5.5 (2011), pp. 3858–3866.

[35] V. Mirjalili and P. Hubert. 'Modelling of the carbon nanotube bridging effect on the toughening of polymers and experimental verification'. In: *Composites Science and Technology* 70.10 (2010), pp. 1537–1543.

[36] P. Joshi and S. Upadhyay. 'Analysis of alignment effect on carbon nanotube layer in nanocomposites'. In: *Physica E: Low-dimensional Systems and Nanostructures* 66 (2015), pp. 221–227.

[37] A. Z. Zakaria and K. Shelesh-Nezhad. 'The effects of interphase and interface characteristics on the tensile behaviour of POM/CaCO3 nanocomposites'. In: *Nanomaterials and Nanotechnology* 4 (2014), p. 17.

[38] R. Wongpajan et al. 'Interfacial shear strength of glass fiber reinforced polymer composites by the modified rule of mixture and Kelly-Tyson model'. In: *Energy Procedia* 89 (2016), pp. 328–334.

[39] Y. Zare. 'Development of simplified Tandon-Weng solutions of Mori-Tanaka theory for Young's modulus of polymer nanocomposites considering the interphase'. In: *Journal of Applied Polymer Science* 133.33 (2016).

[40] S. Bandyopadhyay and S. Saha. 'Some single-and multiobjective optimization techniques'. In: *Unsupervised Classification*. Springer, 2013, pp. 17–58.

[41] A. Axinte et al. 'Modern Approaches on the Optimization of Composite Structures'. In: *Buletinul Institutului Politehnic din lasi. Sectia Constructii, Arhitectura* 59.6 (2013), p. 43.

[42] J. H. Holland. *Adaptation in natural and artificial systems: an introductory analysis with applications to biology, control, and artificial intelligence*. MIT press, 1992.

[43] E. K. Chong and S. H. Zak. *An introduction to optimization*. Vol. 76. John Wiley & Sons, 2013.

[44] M. Mahdavi Jafari, S. Soroushian and G. R. Khayati. 'Hardness Optimization for Al6061-MWCNT Nanocomposite Prepared by Mechanical Alloying Using Artificial Neural Networks and Genetic Algorithm'. In: *Journal of Ultrafine Grained and Nanostructured Materials* 50.1 (2017), pp. 23–32.

[45] A. Konak, D. W. Coit and A. E. Smith. 'Multi-objective optimization using genetic algorithms: A tutorial'. In: *Reliability Engineering & System Safety* 91.9 (2006), pp. 992–1007.

[46] M. Moghri et al. 'The effect of different parameters on mechanical properties of PA-6/clay nanocomposite through genetic algorithm and response surface methods'. In: *International Nano Letters* 5.3 (2015), pp. 133–140.

[47] O. Erdal and F. O. Sonmez. 'Optimum design of composite laminates for maximum buckling load capacity using simulated annealing'. In: *Composite Structures* 71.1 (2005), pp. 45–52.

[48] S. Kirkpatrick, C. D. Gelatt, M. P. Vecchi et al. 'Optimization by simulated annealing'. In: *science* 220.4598 (1983), pp. 671–680.

[49] S. Xavier-de-Souza et al. 'Coupled simulated annealing'. In: *IEEE Transactions on Systems, Man, and Cybernetics, Part B (Cybernetics)* 40.2 (2010), pp. 320–335.

[50] S. Ledesma, J. Ruiz and G. Garcia. 'Simulated annealing evolution'. In: *Simulated Annealing-Advances, Applications and Hybridizations*. InTech, 2012.

[51] J. Chen et al. 'Reliability design optimization of composite structures based on PSO together with FEA'. In: *Chinese journal of aeronautics* 26.2 (2013), pp. 343–349.

[52] K. E. Parsopoulos and M. N. Vrahatis. 'Particle swarm optimization method in multiobjective problems'. In: *Proceedings of the 2002 ACM symposium on Applied computing*. ACM. 2002, pp. 603–607.

[53] S. Suresh, P. Sujit and A. Rao. 'Particle swarm optimization approach for multi-objective composite box-beam design'. In: *Composite Structures* 81.4 (2007), pp. 598–605.

[54] S. J. Nanda. 'Artificial immune systems: principle, algorithms and applications'. PhD thesis. 2009.

[55] R. M. Koide, G. v. Z. d. França and M. A. Luersen. 'An ant colony algorithm applied to lay-up optimization of laminated composite plates'. In: *Latin American Journal of Solids and Structures* 10.3 (2013), pp. 491–504.

[56] M. Yousefikhoshbakht, F. Didehvar and F. Rahmati. 'Modification of the ant colony optimization for solving the multiple traveling salesman problem'. In: *Romanian Journal of Information Science and Technology* 16.1 (2013), pp. 65–80.

[57] M. Dorigo and K. Socha. *An introduction to ant colony optimization*. 2006.

[58] T. Kumazawa et al. 'Ant Colony Optimization Based Model Checking Extended by Smell-like Pheromone'. In: *proceedings of the 9th EAI International Conference on Bio-inspired Information and Communications Technologies (formerly BIONETICS) on 9th EAI International Conference on Bio-inspired Information and Communications Technologies (formerly BIONETICS)*. ICST (Institute for Computer Sciences, Social-Informatics and Telecommunications Engineering). 2016, pp. 214–220.

[59] Z. Fawaz and F. Ellyin. 'Fatigue failure model for fibre-reinforced materials under general loading conditions'. In: *Journal of composite materials* 28.15 (1994), pp. 1432–1451.

[60] Z. Awad et al. 'Multi-objective design optimization of an innovative fibre composite sandwich panel for civil engineering applications'. In: *Proceedings of the 21st Australasian Conference on the Mechanics of Structures and Materials (ACMSM 21)*. Taylor & Francis (CRC Press)/Balkema. 2011, pp. 801–806.

[61] Y. Rostamiyan and A. Fereidoon. 'Preparation, modeling, and optimization of mechanical properties of epoxy/HIPS/silica hybrid nanocomposite using combination of central composite design and genetic algorithm. Part 1. Study of damping and tensile strengths'. In: *Strength of Materials* 45.5 (2013), pp. 619–634.

[62] T. Vo-Duy et al. 'Multi-objective optimization of laminated composite beam structures using NSGA-II algorithm'. In: *Composite Structures* 168 (2017), pp. 498–509.

[63] J. L. Pelletier and S. S. Vel. 'Multi-objective optimization of fiber reinforced composite laminates for strength, stiffness and minimal mass'. In: *Computers & Structures* 84.29 (2006), pp. 2065–2080.

[64] M. W. Bloomfield, J. E. Herencia and P. M. Weaver. 'Analysis and benchmarking of meta-heuristic techniques for lay-up optimization'. In: *Computers & structures* 88.5 (2010), pp. 272–282.

[65] H. Ghiasi et al. 'Optimum stacking sequence design of composite materials Part I: Constant stiffness design'. In: *Composite Structures* 90.1 (2009), pp. 1–11.

[66] F. Ratle et al. 'Multi-objective optimization of a composite material spring design using an evolutionary algorithm'. In: *Parallel Problem Solving from Nature-PPSN VIII*. Springer. 2004, pp. 803–811.

[67] M. Ehrgott. 'Vilfredo Pareto and multi-objective optimization'. In: *Doc. Math* (2012), pp. 447–453.

[68] S. Y. Ivanov and A. K. Ray. 'Multiobjective optimization of industrial petroleum processing units using Genetic algorithms'. In: *Procedia Chemistry* 10 (2014), pp. 7–14.

[69] N. Srinivas and K. Deb. 'Muiltiobjective optimization using nondominated sorting in genetic algorithms'. In: *Evolutionary computation* 2.3 (1994), pp. 221–248.

[70] K. Deb et al. 'A fast elitist non-dominated sorting genetic algorithm for multi-objective optimization: NSGA-II'. In: *International Conference on Parallel Problem Solving From Nature*. Springer. 2000, pp. 849–858.

[71] S. Nie and C. Basaran. 'A micromechanical model for effective elastic properties of particulate composites with imperfect interfacial bonds'. In: *International Journal of Solids and Structures* 42.14 (2005), pp. 4179–4191.

[72] A. Einstein. *Investigations on the Theory of the Brownian Movement*. Courier Corporation, 1956.

[73] I. Tavman. 'Thermal and mechanical properties of aluminum powder-filled high-density polyethylene composites'. In: *Journal of Applied Polymer Science* 62.12 (1996), pp. 2161–2167.

[74] J. Halpin. 'Stiffness and expansion estimates for oriented short fiber composites'. In: *Journal of Composite Materials* 3.4 (1969), pp. 732–734.

[75] T. Thorvaldsen et al. 'Investigation of theoretical models for the elastic stiffness of nanoparticle-modified polymer composites'. In: *Journal of Nanomaterials* 2015 (2015), p. 1.

[76] S.-Y. Fu et al. 'Effects of particle size, particle/matrix interface adhesion and particle loading on mechanical properties of particulate–polymer composites'. In: *Composites Part B: Engineering* 39.6 (2008), pp. 933–961.

[77] M. Lin et al. 'Elastic and plastic analyses of functionally graded elements'. In: *Materials Science Forum*. Vol. 423. Trans Tech Publ. 2003, pp. 731–736.

[78] E. Reynaud et al. 'Nanofillers in polymeric matrix: a study on silica reinforced PA6'. In: *Polymer* 42.21 (2001), pp. 8759–8768.

[79] J. Fidelus et al. 'Thermo-mechanical properties of randomly oriented carbon/epoxy nanocomposites'. In: *Composites Part A: Applied Science and Manufacturing* 36.11 (2005), pp. 1555–1561.

[80] T. Thorvaldsen et al. 'A three-phase rule of mixtures model for the effective elastic properties of the combination of dispersed and agglomerated multi-wall carbon nanotubes in a polymer matrix'. In: *Proceedings of the" 15th European Conference on Composite Materials*. 2012.

[81] H. Krenchel. *Fibre reinforcement*. Alademisk forlag, 1964.

[82] T. Mori and K. Tanaka. 'Average stress in matrix and average elastic energy of materials with misfitting inclusions'. In: *Acta metallurgica* 21.5 (1973), pp. 571–574.

[83] K. Yano et al. 'Synthesis and properties of polyimide–clay hybrid'. In: *Journal of Polymer Science Part A: Polymer Chemistry* 31.10 (1993), pp. 2493–2498.

[84] F. Xiqiao. 'Effective elastic moduli of polymer-layered silicate nanocomposites'. In: *Chinese Science Bulletin* 46.13 (2001), pp. 1130–1133.

[85] M. Takayanagi et al. 'Polymer composites of rigid and flexible molecules: system of wholly aromatic and aliphatic polyamides'. In: *Journal of Macromolecular Science, Part B: Physics* 17.4 (1980), pp. 591–615.

[86] J. Liang and R. Li. 'Prediction of tensile yield strength of rigid inorganic particulate filled thermoplastic composites'. In: *Journal of Materials Processing Technology* 83.1-3 (1998), pp. 127–130.

[87] Y. Zare and H. Garmabi. 'Analysis of tensile modulus of PP/nanoclay/CaCO3 ternary nanocomposite using composite theories'. In: *Journal of Applied Polymer Science* 123.4 (2012), pp. 2309–2319.

[88] C. Albano et al. 'Prediction of mechanical properties of composites of HDPE/HA/EAA'. In: *Journal of the mechanical behavior of biomedical materials* 4.3 (2011), pp. 467–475.

[89] A. Montazeri et al. 'Mechanical properties of multi-walled carbon nanotube/epoxy composites'. In: *Materials & Design* 31.9 (2010), pp. 4202–4208.

[90] F. Danusso and G. Tieghi. 'Strength versus composition of rigid matrix particulate composites'. In: *Polymer* 27.9 (1986), pp. 1385–1390.

[91] L. Nicolais and L. Nicodemo. 'The effect of particles shape on tensile properties of glassy thermoplastic composites'. In: *International Journal of Polymeric Materials* 3.3 (1974), pp. 229–243.

[92] D. Bigg. 'Mechanical properties of particulate filled polymers'. In: *Polymer Composites* 8.2 (1987), pp. 115–122.

[93] J. Leidner and R. Woodhams. 'The strength of polymeric composites containing spherical fillers'. In: *Journal of Applied Polymer Science* 18.6 (1974), pp. 1639–1654.

[94] X. L. Ji et al. 'Tensile modulus of polymer nanocomposites'. In: *Polymer Engineering & Science* 42.5 (2002), pp. 983–993.

[95] S. Saber-Samandari and A. Afaghi Khatibi. 'The effect of interphase on the elastic modulus of polymer based nanocomposites'. In: *Key Engineering Materials*. Vol. 312. Trans Tech Publ. 2006, pp. 199–204.

[96] Y. Zare and H. Garmabi. 'A developed model to assume the interphase properties in a ternary polymer nanocomposite reinforced with two nanofillers'. In: *Composites Part B: Engineering* 75 (2015), pp. 29–35.

[97] M. Takayanagi, S. Uemura and S. Minami. 'Application of equivalent model method to dynamic rheo-optical properties of crystalline polymer'. In: *Journal of Polymer Science: Polymer Symposia*. Vol. 5. 1. Wiley Online Library. 1964, pp. 113–122.

[98] Y. Zare, K. Y. Rhee and S.-J. Park. 'Modeling of tensile strength in polymer particulate nanocomposites based on material and interphase properties'. In: *Journal of Applied Polymer Science* 134.21 (2017).

[99] J.-J. Luo and I. M. Daniel. 'Characterization and modeling of mechanical behavior of polymer/clay nanocomposites'. In: *Composites science and technology* 63.11 (2003), pp. 1607–1616.

[100] Y. Zare and H. Garmabi. 'Thickness, modulus and strength of interphase in clay/polymer nanocomposites'. In: *Applied Clay Science* 105 (2015), pp. 66–70.

[101] Y. Zare. 'Effects of interphase on tensile strength of polymer/CNT nanocomposites by Kelly–Tyson theory'. In: *Mechanics of Materials* 85 (2015), pp. 1–6.

[102] S. Kundalwal, M. Ray and S. Meguid. 'Shear lag model for regularly staggered short fuzzy fiber reinforced composite'. In: *Journal of Applied Mechanics* 81.9 (2014), p. 091001.

[103] D. Vlasveld et al. 'Fibre-matrix adhesion in glass-fibre reinforced polyamide-6 silicate nanocomposites'. In: *Composite Part A: Applied Science Manufacturing* 36.1 (2005), pp. 1–11.

[104] A. Kelly and G. J. Davies. 'THE PRINCIPLES OF THE FIBRE REINFORCEMENT OF METALS'. In: *Metallurgical Reviews* 10.1 (1965), pp. 1–77.

[105] J. N. Coleman et al. 'High performance nanotube-reinforced plastics: Understanding the mechanism of strength increase'. In: *Advanced Functional Materials* 14.8 (2004), pp. 791–798.

[106] F. M. Blighe et al. 'The effect of nanotube content and orientation on the mechanical properties of polymer–nanotube composite fibers: separating intrinsic reinforcement from orientational effects'. In: *Advanced Functional Materials* 21.2 (2011), pp. 364–371.

[107] J. Hermans et al. 'Quantitative evaluation of orientation in cellulose fibres from the X-ray fibre diagram'. In: *Recueil des Travaux Chimiques des Pays-Bas* 65.6 (1946), pp. 427–447.

[108] J. Stojšić, P. Raos and A. Kalendová. 'A study of structure and tensile properties of polyamide 12/clay nanocomposites'. In: *Polymer Composites* 37.3 (2016), pp. 684–691.

[109] H. D. Wagner and R. A. Vaia. 'Nanocomposites: issues at the interface'. In: *Materials Today* 7.11 (2004), pp. 38–42.

[110] S. Zhandarov and E. Pisanova. 'Two interfacial shear strength calculations based on the single fiber composite test'. In: *Mechanics of composite materials* 31.4 (1996), pp. 325–336.

[111] B. Pukanszky. 'Influence of interface interaction on the ultimate tensile properties of polymer composites'. In: *Composites* 21.3 (1990), pp. 255–262.

[112] Y. Zare et al. 'An analysis of interfacial adhesion in nanocomposites from recycled polymers'. In: *Computational Materials Science* 81 (2014), pp. 612–616.

[113] Y. Zare. 'Determination of polymer–nanoparticles interfacial adhesion and its role in shape memory behavior of shape memory polymer nanocomposites'. In: *International Journal of Adhesion and Adhesives* 54 (2014), pp. 67–71.

[114] Y. Zare, H. Garmabi and F. Sharif. 'Optimization of mechanical properties of PP/Nanoclay/CaCO3 ternary nanocomposite using response surface methodology'. In: *Journal of applied polymer science* 122.5 (2011), pp. 3188–3200.

[115] D. Lai, D. Li and J. Yang. 'Improved Mechanical Properties of Montmorillonite/Nylon 6 Nanocomposites by the Modification of Novolac'. In: *Journal of Macromolecular Science, Part A* 52.12 (2015), pp. 1009–1016.

[116] Y. Zare. 'Estimation of material and interfacial/interphase properties in clay/polymer nanocomposites by yield strength data'. In: *Applied clay science* 115 (2015), pp. 61–66.

[117] E. Sharifzadeh et al. 'A new approach in modeling of mechanical properties of nanocomposites: effect of interface region and random orientation'. In: *Iranian Polymer Journal* 23.11 (2014), pp. 835–845.

[118] A. Ghadami Jadval Ghadam. 'Investigation of Mechanical Properties Prediction of Synthesized Nylon-66/Nano-Calcium Carbonate Composites'. In: *Journal of Particle Science & Technology* 1.4 (2015), pp. 241–251.

[119] F. HUANG and L.-j. SHANGGUAN. 'Morphology and Mechanical Properties of Low Density Polyethylene/Multi-walled Carbon Nanotubes Nanocomposites'. In: *Materials Science* 23.2 (2017), pp. 129–132.

[120] D. Bikiaris. 'Microstructure and properties of polypropylene/carbon nanotube nanocomposites'. In: *Materials* 3.4 (2010), pp. 2884–2946.

[121] A. Lazzeri and V. T. Phuong. 'Dependence of the Pukánszky's interaction parameter B on the interface shear strength (IFSS) of nanofiller-and short fiber-reinforced polymer composites'. In: *Composites Science and Technology* 93 (2014), pp. 106–113.

[122] J. Isotalo. 'Basics of statistics'. In: *Finland: University of Tampere* (2001).

[123] A. Alan and F. Barbara. *Statistical methods for the social sciences*. 2009.

[124] PurpleMath. *Box and Whiskers Plots*. http://www.flinders.edu.au/slc_files/Documents/ [Online; accessed 07-January-2018]. 2017.

Appendix A Nanocomposite Design Optimization

A.1 MATLAB Setup

A.1.1 Objective Function

Figure A.1 shows the m-file script of the two objective functions of the MOO problem.

Figure A.1: MATLAB m-file script for the objective function

A.1.2 Optimization Toolbox

Figure A.2 shows the problem setup in the optimization toolbox.

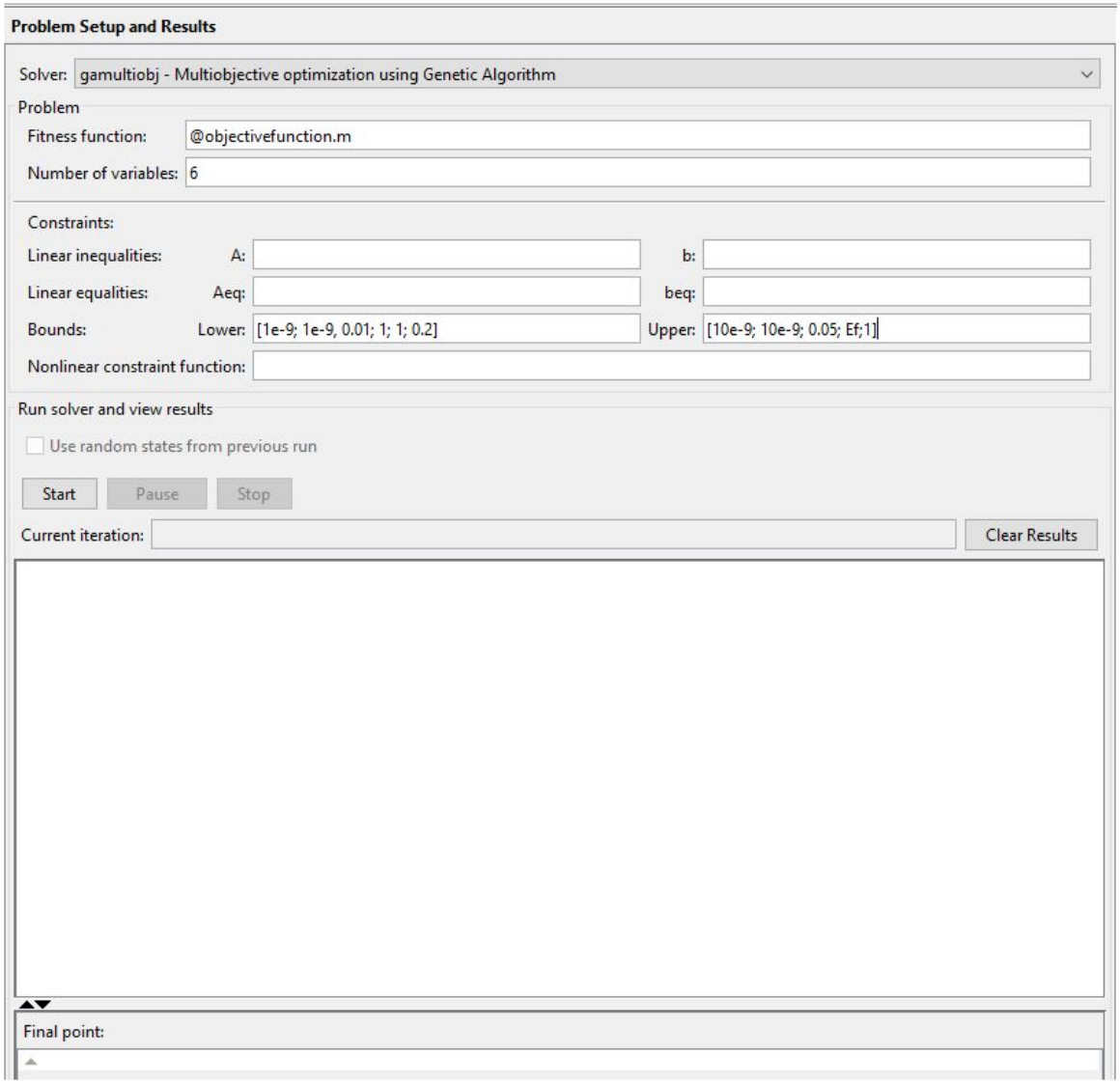

Figure A.2: Problem setup

Figure A.3 shows part 1 of the 'options' window in the optimization toolbox.

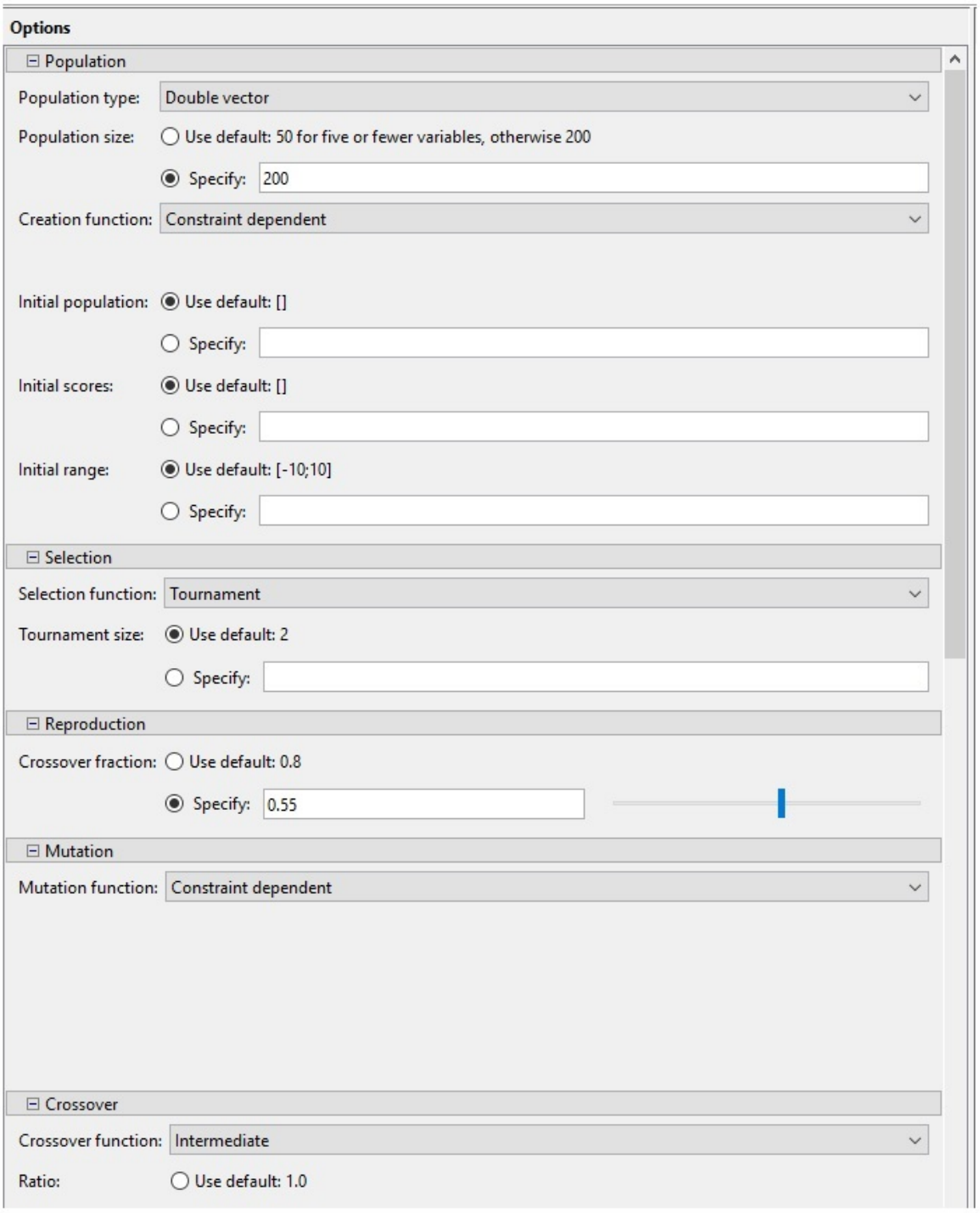

Figure A.3: 'Options' part 1

Figure A.4 shows part 2 of the 'options' window in the optimization toolbox.

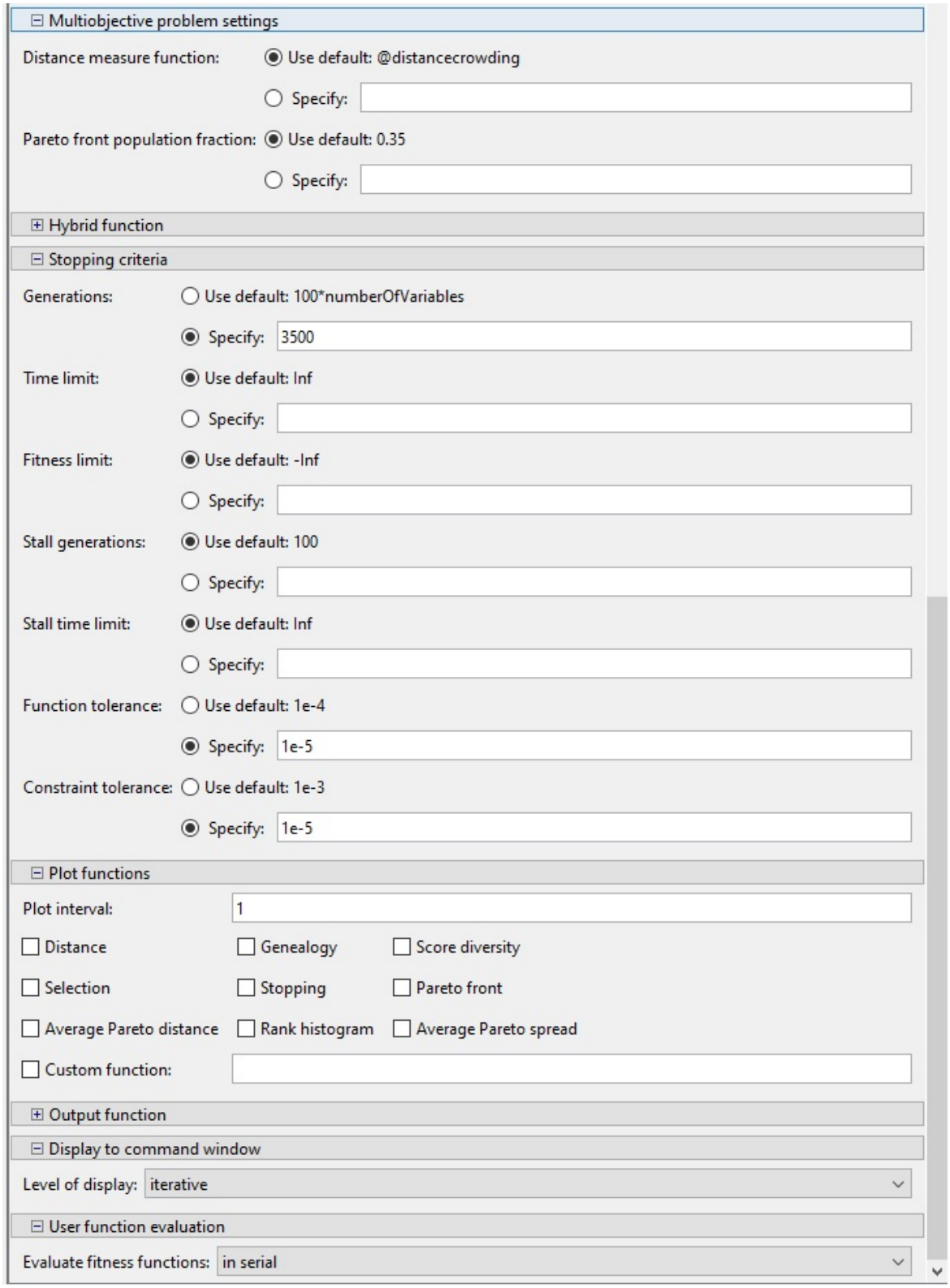

Figure A.4: 'Options' part 2

A.2 Descriptive Statistical Analysis of Data

Descriptive statistics includes the use of graphs, charts, and tables, and the calculation of measures of central tendency which include averages (mean), median, mode and measures of variation (i.e. range, percentiles, quartiles, deviations and etc.). The aim of statistical analysis is to gain and understanding from data. Figure A.5 shows the steps followed for any statistics analysis of data [122]. For data that is distributed symmetrically, the mean, median and mode can be used almost interchangeably. However, in statistics, it follows that the mean is basically the center of gravity of the distribution, the median divides the area of data distribution into two equal parts and the mode on the other hand represent the highest point of the distribution.

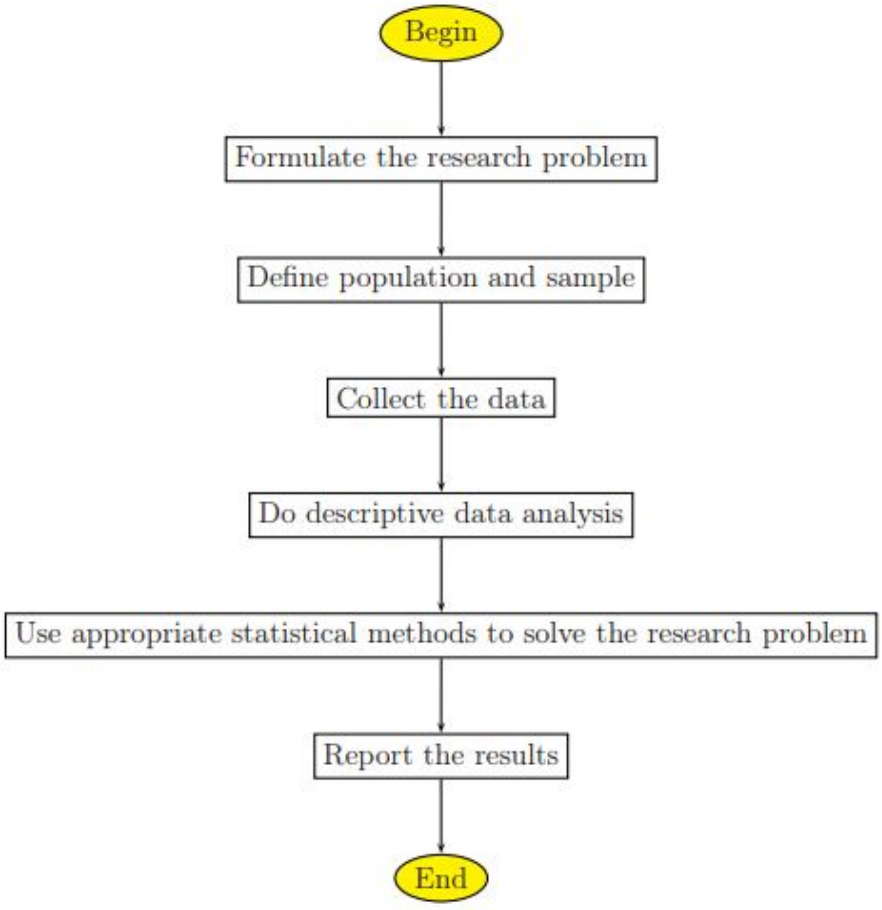

Figure A.5: Steps for statistics analysis of data

The two most commonly used measures of center for quantitative variable are the sample mean and median. The mean is defined as the sum of the all the data under observations divided by the number of the data (also called as sample size). The sample size is usually symbolized by n and for a variable that is denoted by z, its observations are denoted by $z_1, z_2, z_3..., z_n$. The sample mean is then denoted by $\bar{z}$. The expression for the sample mean is given as follows:

$$\bar{z} = \frac{\sum z_i}{n} \tag{A.1}$$

where, $\sum z_i$ represents $z_1 + z_2 + z_3 + ... + z_n$. The symbol stands for the sum of z-values and the subscript i, represents a typical value in the range 1 to n. It is worth noting that the mean is highly influenced by outliers (i.e. data observations that fall far from the rest of the data, either well above or well below the bulk of the data).

The median is often described as simple measure of central tendency in descriptive statistical analysis of data and it is known to be the most important statistical measure of data [123]. This is because the median has some advantages as compared to the mean (i.e. the median unlike the mean is that it is less affected by outliers and skewed data). Hence, it is usually the preferred measure of tendency when the distribution of data is not symmetrical.

A.2.1 Measures of variation of data

Sometimes the mean and the median may not be able to reflect the true picture of the data under observation due to variations and scattering. The measures of variation are given and described as follows:

- **Range** - The range is the simplest measure of variation and it is obtained by taking the difference between two extreme values of the given data.
- **Standard deviation** (SD) - The standard deviation is defined as a quantity that expresses how the individual data points differ or vary from the mean value.

The standard deviation is given as follows:

$$SD = \sqrt{\frac{\sum_{i=1}^{n}(z_i - \bar{z}^2)}{n-1}} \tag{A.2}$$

where $\bar{z}$ is the sample mean, z_i is the i^{th} observation, n represents the sample size and the notation $\sum_{i=1}^{n}$ represents the addition of all the squared deviations from the sample mean from the $(i = 1)$ to the last (n^{th}) observation respectively. The SD can only be ≥ 0. $SD = 0$ only when all the the observations have the same values. A value of SD that is high shows that the data has more variation whereas a low value of SD means that the data is centered around the mean.

- **Quartiles** - Quartiles are the most commonly used values of position which divides the data into four groups containing an approximately equal number of observations whereby 25% are $\leq Q_1$, 50% of the observations are $\leq Q_2$ and lastly 75% of the observations are $\leq Q_3$ respectively. Q_1, Q_2 and Q_3 are called as lower, middle and upper quartiles respectively. The quartiles are used to determine the variation of data for median analysis. This is done through 'box and whisker' plot.

  Box and whisker plot is based on the five-number summary and can be used to provide a graphical display of the center and variation of the observed values of variable in a data set [122]. The five-number summary of variables is composed of the minimum (Min), maximum (Max) and quartiles $(Q_1, Q_2, Q_3$). Figure A.6 shows a generic box and whisker plot. Q_2 i.e. the median is the middle value in the distribution of data when the data is arranged in ascending or descending order. Each side of the median represent 50% of the data.

A.2.1.1 Interpretation of box and whisker plot

In the plot, the box basically contains the middle portion of the data (i.e. the center) and the whiskers show how large the spread or the variation of the data is. The box plot can illustrate whether the data under observation is symmetric or skewed. A symmetric data set shows the median roughly in the middle of the box. Skewed data on the other hand shows a lopsided box plot, whereby the median cuts the box into two unequal parts. The box also gives the Interquartile Range (IQR).

Interquartile range (IQR) - The IQR tells how spread-out the middle values are and it can also be used to determine when some of the values are too far from the central value (i.e. when the values are outliers). Equation A.3 shows the IQR measure of variation. An outlier is any value that lies more than 1.5 times IQR from either end (i.e. this means that any data that is $Q_1 - 1.5(IQR)$ or above $Q_3 + 1.5(IQR)$ is regarded as an outlier) [124].

$$IQR = Q_3 - Q_1 \tag{A.3}$$

As mentioned before, statistics usually assumes that the data values are around some central value.

In addition, the box and whisker plot is interpreted as follows:

- A wide box and long whiskers means that the data doesn't cluster as one would have hoped (or at least assumed)
- A small box and long whiskers means that the data clusters, however it has some outliers that should be investigated further
- If the longer part of the box is to the right (or above) the median, the data is said to be skewed right
- If the longer part of the box is to the left (or below) the median, the data is skewed left

It should be noted that if a side of the box is longer than the other, it does not mean that side contains more data. Thus one cannot tell the sample size by looking at the box plot since it is based on the percentages of the sample size itself. Each section of the box plot (i.e. from the min to Q_1, Q_1 to the median, median to Q_3 and Q_3 to the max) represent 25% of the data.

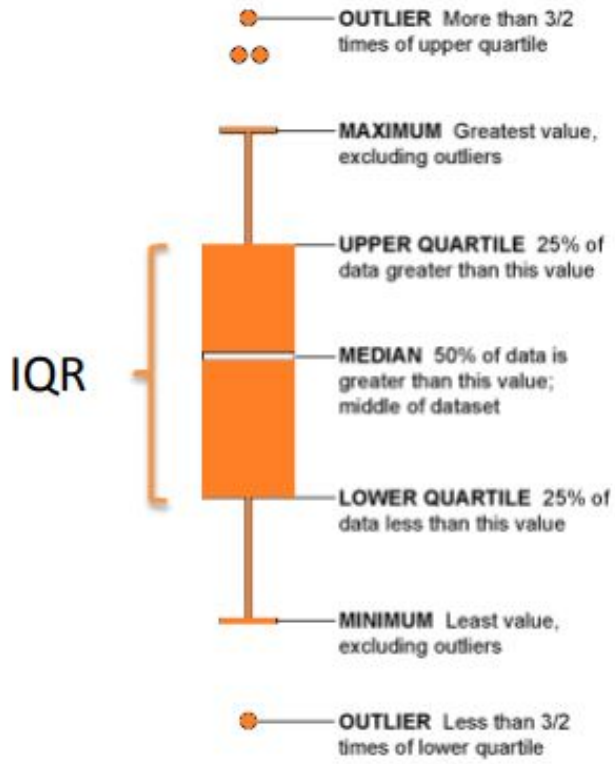

Figure A.6: Generic box and whisker plot

A.3 Analysis of MOO Results

This section gives the additional analysis of the optimization results.

A.3.1 Mean Analysis of Optimization model results

Table A.1 shows the standard deviations (SD) of the overall optimization results.

A.3.2 Median Analysis of Optimization model results

This subsection gives additional data and information on the median analysis of the optimization results. This additional information includes the data used for the box and whiskers plots for the objective functions together with the design variables. It

Table A.1: Standard deviations of the overall optimization results.

Nanocomposite Material	t_i (nm)	t (nm)	θ_f (wt.%)	E_i (GPa)	τ (MPa)	η	E_R	σ_R
Nylon-MMT	2.46	1.48	1.61	0.49	2.12	0.00	0.69	0.07
Pa-CaCO3	1.25	1.43	1.42	3.14	1.28	0.00	0.58	0.03
SBR-MWCNT	0.41	0.71	1.00	97.24	1.96	0.00	0.30	0.02
iPP-MWCNT	0.47	1.30	1.88	98.35	1.44	0.00	0.38	0.02

should be noted that the orientation factor was not selected due to the fact that its value was always equal to one for all the optimization computations.

A.3.2.1 Objective functions

A.3.2.1.1 Elastic modulus

Table A.2 shows the five-number summary variables for the normalized elastic modulus. Table A.3 gives the comparison of the mean and median results of the normalized elastic modulus. The table also provides the IQR and SD (which shows the variation of data) of the two analyses respectively. The values of IQR are relatively higher compared to those of SD, and thus indicating that the median analysis is showing a higher degree of variation as compared to the mean analysis.

Table A.2: Summary variables for the normalized elastic modulus.

	Elastic Modulus (GPa)			
Summary variables	Nylon-MMT	Pa-$CaCO_3$	SBR-MWCNT	iPP-MWCNT
Min	1.18	1.53	1.39	1.21
Q1	1.31	1.61	1.66	1.38
Median	1.54	1.75	1.85	1.84
Q3	2.29	2.30	1.93	1.94
Max	2.80	2.99	2.27	2.10

Table A.3: Comparison of the mean and the median of the normalized elastic modulus.

	Elastic modulus			
Nanocomposite	Median	IQR	Mean	SD
Nylon-MMT	1.54	0.98	1.81	0.69
Pa-CaCO3	1.75	0.69	2.01	0.58
SBR-MWCNT	1.85	0.27	1.82	0.30
iPP-MWCNT	1.84	0.56	1.70	0.38

A.3.2.1.2 Tensile strength

Table A.4 shows the five-number summary variables for the normalized tensile strength. Table A.5, shows the comparison of the mean and median results of the normalized elastic modulus. The table also provides the IQR and SD of the two analyses respectively. From both IQR and SD values it can be seen that the variations of the results from the two approaches are almost similar.

Table A.4: Summary variables for the normalized tensile strength.

	Tensile strength (GPa)			
Summary variables	Nylon-MMT	Pa-$CaCO_3$	SBR-MWCNT	iPP-MWCNT
Min	0.83	0.90	0.94	0.95
Q1	0.87	0.93	0.96	0.96
Median	0.93	0.97	0.97	0.97
Q3	0.97	0.98	0.98	0.99
Max	0.99	0.98	0.99	1.00

Table A.5: Comparison of the mean and the median of the normalized tensile strength.

	Tensile strength			
Nanocomposite	Median	IQR	Mean	SD
Nylon-MMT	0.93	0.10	0.92	0.07
Pa-CaCO3	0.97	0.05	0.96	0.03
SBR-MWCNT	0.97	0.02	0.97	0.02
iPP-MWCNT	0.97	0.03	0.97	0.03

A.3.2.2 Nanofillers thickness

Table A.6 shows the five-number summary variables for the thickness of the nanofillers. Table A.7 gives the comparison of the mean and median results of the nanofillers thickness.

Table A.6: Summary variables for thickness of nanofillers.

	Nanofiller thickness (nm)			
Summary Variables	Nylon-MMT	Pa-$CaCO_3$	SBR-MWCNT	iPP-MWCNT
Min	4.17	3.92	5.91	4.84
Q_1	4.37	6.09	5.97	6.88
Median	5.41	6.42	6.18	7.01
Q_3	6.93	6.98	7.01	7.95
Max	7.46	8.23	7.52	8.48

Table A.7: Comparison of the mean and the median of the nanofillers thickness.

	Nanofillers thickness			
Nanocomposite	Median	IQR	Mean	SD
Nylon-MMT	5.41	2.56	5.65	1.48
Pa-$CaCO_3$	6.42	0.90	6.36	1.43
SBR-MWCNT	6.18	1.05	6.5	0.71
iPP-MWCNT	7.01	1.07	7.07	1.30

A.3.2.3 Thickness of the interphase

Table A.8 shows the five-number summary variables for the thickness of the interphase. Table A.9 gives the comparison of the mean and median results of the thickness of the interphase.

Table A.8: Summary variables for the interphase thickness.

	Interphase thickness (nm)			
Summary Variables	Nylon-MMT	Pa-$CaCO_3$	SBR-MWCNT	iPP-MWCNT
Min	1.76	1.91	1.63	1.72
Q_1	2.43	1.98	1.99	2.02
Median	2.96	2.24	2.12	2.31
Q_3	6.15	3.05	2.31	2.55
Max	7.29	5.11	2.84	3.02

Table A.9: Comparison of the mean and the median of the interphase thickness.

	Interphase thickness			
Nanocomposite	Median	IQR	Mean	SD
Nylon-MMT	2.96	3.72	4.07	2.46
Pa-$CaCO_3$	2.24	1.08	2.78	1.25
SBR-MWCNT	2.12	0.31	2.17	0.41
iPP-MWCNT	2.31	0.53	2.32	0.47

A.3.2.4 Nanofillers loading

Table A.10 shows the five-number summary variables for the nanofillers loading. Table A.11 gives the comparison of the mean and median results of the loading of the nanofillers.

Table A.10: Summary variables for nanofillers loading.

	Weight fraction (wt. %)			
Summary Variables	Nylon-MMT	Pa-$CaCO_3$	SBR-MWCNT	iPP-MWCNT
Min	1.11	1.13	2.36	1.04
Q_1	1.45	4.40	4.19	1.91
Median	3.21	4.52	4.69	4.53
Q_3	4.29	4.58	4.92	4.67
Max	4.66	4.88	4.97	5.00

Table A.11: Comparison of the mean and the median of the nanofiller loading.

	Weight fraction			
Nanocomposite	Median	IQR	Mean	SD
Nylon-MMT	3.21	2.84	2.95	1.61
Pa-$CaCO_3$	4.52	0.18	4	1.42
SBR-MWCNT	4.69	0.73	4.29	1.00
iPP-MWCNT	4.53	2.76	3.47	1.88

A.3.2.5 Interphase modulus

Table A.12 shows the five-number summary variables for the modulus of the interphase. Table A.13 gives the comparison of the mean and median results of the elastic modulus of the interphase.

Table A.12: Summary variables for the interphase modulus.

	Interphase modulus (GPa)			
Summary Variables	Nylon-MMT	Pa-$CaCO_3$	SBR-MWCNT	iPP-MWCNT
Min	18.81	27.83	530.92	365.15
Q_1	19.68	28.58	538.43	453.95
Median	19.87	31.31	551.04	539.39
Q_3	19.91	33.41	636.84	561.79
Max	20.24	35.48	772.60	636.19

Table A.13: Comparison of the mean and the median of the interphase modulus.

	Interphase modulus			
Nanocomposite	Median	IQR	Mean	SD
Nylon-MMT	19.87	0.23	19.72	0.49
Pa-$CaCO_3$	31.31	4.82	31.28	3.14
SBR-MWCNT	551.04	98.42	600.88	97.24
iPP-MWCNT	539.39	107.85	512.47	98.35

A.3.2.6 Interfacial shear stress

Table A.14 shows the five-number summary variables for the interfacial shear stress. Table A.15 gives the comparison of the mean and median results of the interfacial shear stress.

Table A.14: Summary variables for the interfacial shear stress.

	Interfacial shear stress (Mpa)			
Summary Variables	Nylon-MMT	Pa-$CaCO_3$	SBR-MWCNT	iPP-MWCNT
Min	46.89	49.33	47.54	48.40
Q_1	50.05	50.27	48.75	51.74
Median	51.92	51.97	50.36	51.92
Q_3	51.97	51.99	51.80	52.00
Max	52.00	52.00	51.98	52.00

Table A.15: Comparison of the mean and the median of the interfacial shear stress.

	Interfacial shear stress			
Nanocomposite	Median	IQR	Mean	SD
Nylon-MMT	51.92	1.92	50.69	2.12
Pa-$CaCO_3$	51.97	1.72	51.16	1.28
SBR-MWCNT	50.36	3.06	50.12	1.96
iPP-MWCNT	51.92	0.26	51.32	1.44

A.3.2.7 Dispersion Parameter, B

Table A.16 shows the five-number summary variables for parameter B. Table A.17 gives the comparison of the mean and median results of the dispersion parameter.

Table A.16: Summary variables for the dispersion parameter.

Summary Variables	Nylon-MMT	Pa-$CaCO_3$	SBR-MWCNT	iPP-MWCNT
Min	3.06	2.80	4.42	3.25
Q1	3.12	2.81	4.47	3.33
Median	3.16	2.84	4.55	3.34
Q3	3.17	2.84	4.63	3.34
Max	3.17	2.84	4.64	3.34

Table A.17: Comparison of the mean and the median of the parameter B.

	Parameter B			
Nanocomposite	Median	IQR	Mean	SD
Nylon-MMT	5.41	2.56	3.14	0.05
Pa-$CaCO_3$	6.42	0.90	2.83	0.02
SBR-MWCNT	6.18	1.05	4.54	0.10
iPP-MWCNT	7.01	1.07	3.32	0.04